The relation between shallow marine chert, barite and jaspilite deposition in the 3.2 Ga Mapepe Formation of the Barberton Greenstone Belt, South Africa.

J.M.Postema
Msc thesis
Utrecht University
2019

Table of contents

1 Abstract

Normally rare barite deposits are quite common in the 3.260–3.226 Ga Fig Tree Group of the Barberton Greenstone Belt in South Africa. These barites in the Mapepe Formation of the Fig Tree Group were seemingly fed by chert dikes and are unusually rich in detrital minerals. Immediately below the barites jaspilite bands can be found containing oxidized iron. Barite is used for estimates of the atmospheric oxygen levels before 3.0 Ga and the sulphur inside the barites is extensively used to understand the sulphur cycle on the Early Earth. If the barites are to be used to answer these questions, it is paramount to understand the geological formation of the barites. The aim of this research is to determine the relationship between the barite, chert and jaspilite deposition in the Mapepe Formation and to uncover how the barite deposits formed.

Barites are inert to instruments analysing trace elements and almost no trace element data exists on barites. In this research the first relatively complete and significant trace element data on barites are presented. Samples of the barites, cherts and jaspilites were taken from the Old Mine, Barite Valley and Puddingstone Hill sites. Bulk Laser-Ablation Inductively Coupled Plasma Mass Spectrometry (LA-ICP-MS) trace element analyses were done on pearls of the barites and cherts normally used for X-Ray Fluorescence (XRF). Moreover, microanalytical trace element analyses have been done on epoxy blocks of the cherts and jaspilites. To circumvent any possible BaO interference, barium was separated from the barite samples using column separation and the residue inside the columns analysed using Solution-ICP-MS. Lastly, cathodoluminescence, back scatter and secondary imaging was done on the zircons from the barites using the Electron Mirco Probe Analyzer (EMPA) and U-Pb dating was executed on these zircons using LA-ICP-MS.

No evidence for a relation to sea water is found in the barites and the cherts. The barites show a relatively flat PAAS (Post Archean Average Shale) normalized REEY (Rare Earth Element Yttrium) pattern with small positive Eu anomalies in the Puddinstone Hill samples and some Barite Valley samples. The other Barite Valley samples and the Old Mine samples do not show a positive Eu anomaly. Similar REEY patterns can be found in the cherts with two additional types, one that is LREE depleted and one with positive REEY slope. The remaining trace elements are quite similar and demonstrate a relation between the barites and the cherts. Wall rock incorporation may have been a significant contributor of the REEY in the cherts. The observed REEY patterns for the cherts and the barites can be linked to the input of low temperature continental hydrothermal fluids and were deposited close to or on the continent. Chert dikes were likely the conduits supplying the Ba^{2+} to the surface where it reacted with photolytically produced SO_4^{2-} supplied by meteoric fluids to form the barites. The difference in size of the positive Eu anomalies, likely indicates a difference in temperature and possibly composition of the hydrothermal fluids feeding the different sites.

The U-Pb data of the zircons inside the barites is highly discordant and intersects the concordant line at ~3.25-(3.3) Ga and the origin. Only one concordant zircon with an age of 3.243 ± 0.016 Ga was found and the remaining zircons had experienced Pb loss due to recent weathering. Four other zircons deviate from the discordant line and intersect at ~3.45 Ga. The obtained ages are consistent with detrital zircons from the Fig Tree Group and had been sourced from TTG bodies from the Onverwacht Group and tuffs from the Mendon Formation and the Fig Tree Group itself. A large input of detritus to the barite deposits elevated the REEY patterns inside the barites.

The geochemistry of the jaspilites is completely unrelated to the geochemistry of the barites and the cherts. The jaspilites have a clear sea water signature with a positive PAAS normalized REEY slope and a positive Eu anomaly and positive Y anomaly. The shallow slope of the REEY may indicate that the jaspilite bands were deposited from a mixture of marine and hydrothermal fluids on the sea floor. The oxidation of the jaspilites may have occurred either by microorganisms or by free oxygen in the lower Mapepe Formation.

2 Introduction

The 3.55-3.22 Ga Barberton Greenstone Belt of the Kaapvaal Craton is one of the oldest and most well-preserved Archean rock groups in the world together with the Isua Greenstone Belt in Greenland and the Pilbara Craton in Australia. The greenstone belt documents an impressive record of Paleoarchean volcanic and sedimentary sequences of the early Earth (Drabon et al., 2019). Although much research has been done on most rock types inside the Barberton Greenstone Belt, one chemical sediment that is unusually common in the Fig Tree Group of the greenstone belt, still arises many questions and has not been as extensively researched as the other rock types. The rock type in question is barite ($BaSO_4$), a normally uncommon rock in the rock record. Barite is used for estimates of the atmospheric oxygen levels before 3.0 Ga and the sulphur inside the barites is extensively used to understand the sulphur cycle on the Early Earth. It is paramount to understand whether sulphur reduction was done by photolytic processes or done by microbial activity, which would be one of the oldest indicators of early life (Lowe et al., 2019). The formation of barite usually involves the interaction of two contrasting fluids with one containing dissolved Ba^{2+} and the other containing dissolved SO_4^{2-}. When these ions meet under normal circumstances, they immediately form the incredibly stable $BaSO_4$. In modern settings this is a common process at hydrothermal systems at the ocean floor, where Ba^{2+} from the vents meets the ocean water saturated in SO_4^{2-}. However, this cannot have happened in the Archean due to a lack of SO_4^{2-} until the Great Oxygenation Event (GOE) (Lowe et al., 2019).

The Barite deposits in the Mapepe Formation of the Fig Tree Group are associated with chert dikes. These chert dikes seem to originate from a single sandstone layer and terminate at the barite deposits. Also, immediately underneath the barite deposits are jaspilite bands containing oxidized iron. It is unknown what the relationship is between these different rock types and their components Ba, S, Si and Fe. Moreover, the barites are unusually rich in detrital minerals such as zircon (Drabon et al., 2019; Lowe et al., 2019). All these different rock types and minerals make the barite deposits quite complex. The aim of this research is to determine the relationship between the barite, chert and jaspilite deposition and determine how the barite deposits formed.

Four hypotheses exist for the formation of the barite deposits and the chert dikes: a low-temperature hydrothermal origin of the chert dykes, a high-temperature hydrothermal origin of the chert dykes, a neptunian origin of the chert dykes and a separate origin of the chert dykes and the barite deposits. To determine which of the hypotheses fits with the barite deposition, it is important to figure out the relationship between the barites and the chert dikes and if these chert dikes had fed the barite deposits chemical components via hydrothermal fluids. Moreover, it is important to estimate the temperature of the rocks and the fluids, which will indicate which geologic processes could have been active during barite deposition. It is also important to understand why there are so many detrital minerals in the rock and where the detrital minerals came from. Besides that, the role of the jaspilites in the system is unclear and what caused the iron oxidation. Were the jaspilites deposited in association with the barites and did the fluids that caused the barite deposition also cause the iron oxidation, or were they oxidized by a different process.

To understand all the different components inside the barites and how they formed, chemical analyses have been done on the barites, cherts and jaspilites focussing on the trace elements. Bulk Laser-Ablation Inductively Coupled Plasma Mass Spectrometry (LA-ICP-MS) trace element analyses have been executed on the barites and cherts. Due to the stability of barite, barely any trace element results have ever been acquired for barites (Oostingh 2011). To circumvent this, the analyses have been done on pearls normally used for X-Ray Fluorescence (XRF) analyses to gain better and more complete results. Furthermore, microanalytical trace element LA-ICP-MS analyses have been done on the cherts and jaspilites to determine the geochemical differences between the different components inside the cherts and jaspilites. To circumvent any possible BaO interference, the barites have also been analysed by Solution-ICP-MS after removing the Ba in a clean room using column separation. The last research done is U-Pb dating on the zircons inside the barites with the LA-ICP-MS, to get a better understanding of the detrital minerals inside the barites. All these analyses will be components to gain an

understanding of the relation between the barites, cherts and jaspilites and how the barite deposits formed.

3 Geological setting

The 3.55-3.22 Ga Barberton Greenstone belt is part of the Kaapvaal Craton and located in the north-eastern part of South Africa and Eswatini (Fig. 1) (Hofmann, 2005; Drabon et al., 2019; Lowe et al., 2019). The belt is characterised by NE-SW trending Archean supracrustal rocks with intrusions of granitoids, also known as the Swaziland Supergroup (Hofmann, 2005; Busigny et al., 2017; Drabon et al., 2019). The Barberton Greenstone Belt is exceptionally well preserved with predominately low-grade metamorphism and relatively low strain-intensities, which is low compared to other Archean terranes (Hofmann, 2005; Kisters et al., 2010; Satkoski et al., 2015; Busigny et al., 2017; Drabon et al., 2019). Most of the rocks have only been heated to 300-325 °C, which corresponds to lower greenschist facies, but can go up to amphibolite facies when in contact with the surrounding granitoid bodies. Although the rocks in the Barberton Greenstone belt have undergone low grade metamorphism, high grade deformation and alteration, the sedimentary structures in the rocks are still well preserved (Hofmann, 2005; Kisters et al., 2010; Drabon et al., 2019). Removal of Fe, Na, Mg and Ca, addition of Si, K and Rb and local carbonization are characteristics of the rocks in the Barberton Greenstone Belt, caused by metasomatic alteration and local to regional recrystallization (Drabon et al., 2019).

Three stratigraphic units constitute the Barberton Greenstone Belt. From base to top are the Onverwacht Group, the Fig Tree Group and Moodies Group (Fig 1A). Deformation has widely affected these units, especially in the centre of the belt. The units have been tightly folded into commonly overturned synclines and these synclines are separated from each other by sheared and faulted tight anticlines. A major structural feature in the centre of the Barberton Greenstone Belt is the Inyoka Fault, which divides the rock formations north and south of the fault in age, stratigraphy and depositional environment (Hofmann, 2005; Drabon et al., 2019). Because the geology is so different north and south of the Inyoka Fault, the fault is thought to be a tectonostratigraphic boundary. The base of the Barberton Greenstone Belt could be regarded as a set of distinct tectonostratigraphic packages, which may represent the remnants of two juxtaposed oceanic plateaus. In this case the Inyoka Fault may have been the terrane suture of the geologic system (Hofmann, 2005; Kisters et al., 2010).

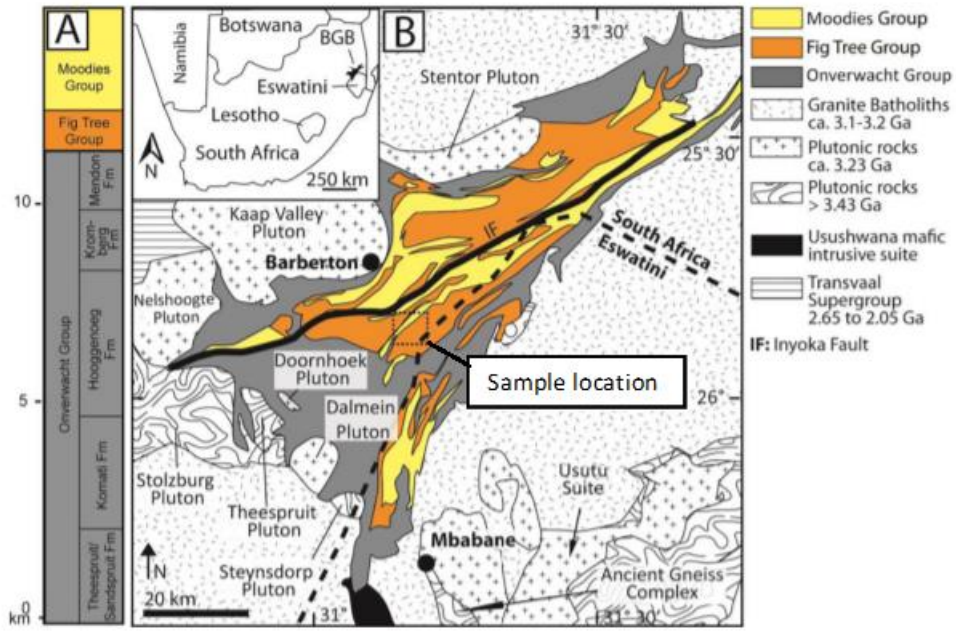

Figure 1: A) Stratigraphic column of the Barberton Supergroup. B) Geological map of the Barberton Greenstone Belt.

The 3.552–3.260 Ga Onverwacht Group contains basalts and komatiites likely deposited in a shallow to deep marine environment. These mafic and ultramafic rocks have been intruded by at least two units of felsic rhyolitic to dacitic volcanism and by co-magmatic tonalite-trondhjemite-granodiorite (TTG) plutons and shallow hypabyssal plutons (Hofmann, 2005; Kisters et al., 2010; Drabon et al., 2019). The Onverwacht Group south of the Inyoka Fault can be characterised by the Sandspruit, Theespruit, Komati, Hooggenoeg, Kromberg and Mendon geologic formations. The felsic rhyolites and dacites can be found in the Theespruit and Hooggenoeg Formations and are respectively ~3.53 and ~3.45 Ga. Other felsic volcanic rocks in the shape of dacitic tuffs and detrital zircons are found in the Kromberg and Mendon Formations with a respective age of 3.34 and 3.30-3.28 Ga. The rocks of the Onverwacht Group north of the Inyoka Fault are not subdivided in different formations and together known as the Weltevreden Formation (Hofmann, 2005; Drabon et al., 2017)

The unconformibly overlain Fig Tree and Moodies Group characterize a significant change in geologic setting. This is likely linked to uplift of the greenstone belt and the related deposition of siliciclastic and subordinate felsic volcaniclastic sediments (Kisters et al., 2010; Drabon et al., 2019). The <3.225 Ga Moodies Group is predominantly characterized by coarse and clastic quartz-rich terrigenous and arenaceous rocks and consists of the Clutha, Joe's Luck and Baviaanskop Formation (Anhaeusser, 1976; Hofmann, 2005; Kisters et al., 2010). All the formations constitute of a fining upward sequence of a basal conglomerate or pebbly sandstone, an intermediate thick sandstone unit and an upper unit of shale, siltstone and Banded Iron Formation (BIF). The rocks were deposited in a shallow-marine to fluvial environment and sediment clasts were likely derived from uplifted older greenstone and TTG terranes (Hofmann, 2005; Kisters et al., 2010).

The 3.260–3.226 Ga Fig Tree Group is composed of siliciclastic and felsic volcanic rocks. Like with the Onverwacht Group, a distinction is made between formations north and south of the Inyoka Fault. North of the fault the Ulundi, Sheba, Belvue Road, Bien Venue, and Schoongezicht Formations can be found and south of the fault the Mapepe and Auber Villiers Formations. The relationship between the formations north and south of the Inyoka Fault is still unknown (Hofmann, 2005; Satkoski et al., 2015; Drabon et al., 2019). Most of the formations north of the Inyoka Fault are characterised by clastic sediments. The Ulundi Formation consists of carbonaceous shales or mudstones and banded cherts and the overlying Sheba and Belvue Road Formations contain shales, siltstones or mudstones intercalated with turbiditic sandstone (Hofmann, 2005; Drabon et al., 2019). The previous formations are separated with the Schoongezicht Formation by a regional thrust fault and may have partially been deposited at the same time as the Sheba and Belvue Road Formations. The formation contains plagioclase-rich volcaniclastic conglomerates intercalated with volcaniclastic sandstones and grey shales or mudstones. The formation is covered by the conglomerate at the base of the Moodies Group. The Bien Venue Formation is restricted to the north-eastern part of the Barberton Greenstone Belt and constitutes predominantly of felsic and intermediate volcanic and volcaniclastic rocks with an age of 3.25 ± 0.01 and 3.259 ± 0.005 Ga. These rocks have likely been deposited under deep marine conditions (Hofmann et al., 2003; Drabon et al., 2019).

South of the Inyoka Fault the Mapepe Formation and the underlying Auber Villiers Formation are separated by a regional thrust fault. The Auber Villiers Formation is made out of dacitic, plagioclase-phyric volcaniclastic conglomerate, breccia and sandstone and has zircons dated to 3.256 ± 0.004 Ga (Hofmann, 2005; Drabon et al., 2019). The Mapepe Formation is characterized by quartz-poor siliciclastic, volcanoclastic and chemical sediments interbedded with several dacitic to rhyolitic intrusions (Hofmann, 2005; Busigny et al., 2017; Drabon et al., 2019). De sediments were derived from uplifts of the Onverwacht Group and the intruding dacitic to rhyolitic intrusions, but the source of these plutonic rock intrusions is still unknown. To understand the structural relations of the Mapepe Formation, two meteoritic spherule beds S2 and S3 have been used as regional marker beds, which have been dated to ~3.26 and ~3.24 Ga respectively (Drabon et al., 2019).

The sedimentary deposits of the Mapepe Formation are associated with deep- to shallow-water, fan delta and alluvial sedimentary environments. The earliest deposits of the Mapepe Formation were fine-grained and often iron-rich sediments containing among others several BIF's deposited in

relatively deep water. This changed to shallow water deposits next to a northeast oriented elongated area of uplift and erosion in the middle of the Mapepe Formation. The last part of the Mapepe Formation was continuously deposited under the influence of widespread uplift resulting in the formation of prograding fold-and-thrust belts an two associated northeast-trending foreland basins (Hofmann, 2005; Drabon et al., 2019). The base of the Mapepe Formation has been dated to 3.258 ± 0.003 Ga in the south-eastern area of the greenstone belt and to 3.243 ± 0.004 Ga to the south of the Inyoka Fault, while the top has been dated to 3.227 ± 0.005 Ga. Age estimates of detrital zircons and xenocrysts demonstrate peaks in age populations at 3.281 ± 0.004 and 3.484 ± 0.004 Ga (Busigny et al., 2017; Drabon et al., 2019).

In several stratigraphic levels of the Fig Tree Group barite deposits can be found and in particular the Mapepe Formation contains several well-preserved barite deposits (Heinrichs and Reimer, 1977; Hofmann, 2005; Busigny et al., 2017; Drabon et al., 2019; Lowe et al., 2019). Although initially these deposits were thought to have replaced primary gypsum, later studies demonstrated that the barite deposit were in fact primary (Lowe et al., 2019). The barite deposits show a variety of morphologies, from well developed 'cauliflower' textures in barite mounts, to layered bladed barite, to detrital barite sand (Heinrichs and Reimer, 1977; Lowe et al., 2019). The barites themselves are unusually rich in detrital minerals e.g detrital zircons (Heinrichs and Reimer, 1977; Drabon et al., 2019). In association with these barite deposits cherts dikes and faults are found which seem to originate from a sandstone layer and end at the barite deposits. Like all the rocks in the Mapepe Formation the barites and the chert dikes have been (partially) silicified, which in the case of the chert dikes must have replaced the original softer sediments that the dikes were made of (Drabon et al., 2019; Lowe et al., 2019). Immediately underneath the barite deposits jaspilite bands intercalated with chert bands can be found, containing oxidized iron in the jaspilites. The jaspilite bands and the barite deposits are separated by an erosional contact (Heinrichs and Reimer, 1977; Lowe et al., 2019).

4 Methods

4.1 LA-ICP-MS trace element analyses

Samples were taken from an area south of the town of Barberton close to the border with Eswatini. To the East of the R40 road samples were taken from Puddingstone Hill and to the West from Barite Valley and Old Mine (Fig. 2). They included barite-rich rocks, cherts, sediments and jaspilites. Fusion beads that were used for major element analyses on the samples, were also used for the bulk trace element analyses. These fusion beads were made using 0.6 g sample and 6 g of the flux material, which consisted of 66% Lithium Tetraborate ($Li_2B_4O_7$), 34% Lithium Metaborate ($LiBO_2$) and of 0.5% Lithium Iodide (LiI) (guided research report by D. Bakker). To make the fusion beads suitable for analysis, they were crushed and shards of the fusion beads of different samples taped on a thin glass plate. The trace elements in the fusion bead shards of the sample were measured using Laser-Ablation Inductively Coupled Plasma Mass Spectrometry (LA-ICP-MS) at the University of Utrecht. A crater size of 120 µm was used for the analysis to achieve a high material removal rate from the samples with a laser pulse repetition rate of 10 Hz and a fluence of ~12 J/m^2. Because the fluence meter on the instrument was broken, no exact value for the fluence could be provided. The NIST-SRM-612 was used as the calibration standard and the BCR2G as the independent secondary standard. Three repeat measurements were made of each sample.

From the remaining chert, sediment and jaspilite rock samples fresh pieces were selected for microanalysis. This included some veins and clasts included in the chert and sediment samples. Blocks of roughly 1-2 cm^2 were cut out of samples and put into epoxy mounts. The trace elements of the blocks in the epoxy mounts were measured using the LA-ICP-MS under identical conditions and using the same standards as for the bulk trace element analyses.

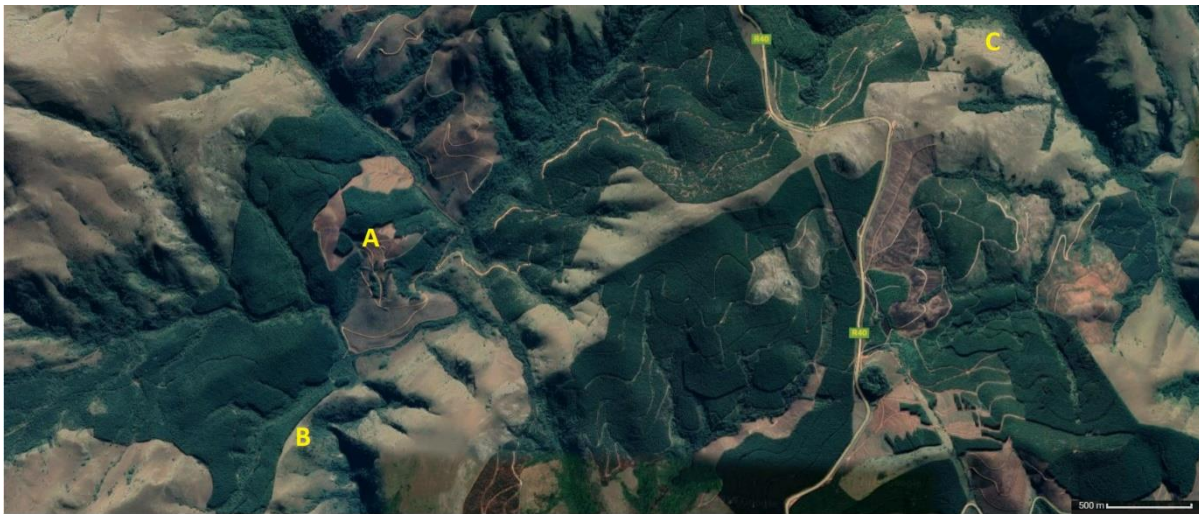

Figure 2: Satellite photo of field area with the different sample sites. A) Old Mine, B) Barite Valley and C) Puddingstone Hill.

4.2 Column separation and Solution-ICP-MS trace element analyses

To circumvent any potential barium oxide interference on europium, trace element analyses were also executed after the separation of barium and the Rare Earth Elements (REE). This was done at the Vrije Universiteit Amsterdam by column separation in the clean room. In advance 15 round bottom 7 mL beakers made of Teflon were thoroughly cleaned to prepare them for usage. Firstly, the beakers and their lids were washed with distilled water and then put in a large beaker filled with concentrated nitric acid for approximately two hours. Subsequently, the nitric acid was washed off the beakers and their lids with distilled water and then put in a large beaker filled with concentrated hydrochloric acid again for approximately 2 hours. Secondly, after washing off the hydrochloric acid with distilled water, the beakers were filled with concentred hydrochloric acid in a laminar flow room and put on the hotplate for several days. Thirdly, the hydrochloric acid was removed, and the beakers washed with milli-Q water. Subsequently, the beakers were filled with hydrofluoric acid and nitric acid in a ration 1 to 2 in the laminar flow room and put on the hot plate for several days. After removing the acids and washing the beakers with milli-Q water, they were ready for usage.

At the University of Utrecht crushed rock fragments of the samples were grinded to powder with a pulverizing mill using a tungsten carbide grinding vessel. In the clean room of the Vrije Universiteit Amsterdam roughly 10 mg of the sample was weighed and put in the cleaned beakers together with roughly 100 mg of Na_2CO_3 and 10 mL of milli-Q water. The beakers were put on a hot plate in the laminar flow room for roughly a week. Under these circumstances, the Na_2CO_3 should react with the $BaSO_4$ in the samples to form $BaCO_3$ and Na_2SO_4 (Sokolova and Povarov, 2013). The $BaCO_3$ formed an insoluble powder inside the beaker and the Na_2SO_4 remained in the liquid. The liquid and the powder inside the beakers were put into small vials and centrifuged. Inside the laminar flow room, the liquid was pipetted inside separate vials and the powder was left behind. The vials with the powder were filled with milli-Q water, put into the centrifuge again and then the liquid was removed with a pipette. This process was repeated, so that the vial with the powder had been centrifuged three times in total to make sure that what was in the liquid after the reaction, was completely removed. The samples with the $BaCO_3$ were dissolved in 1.5 mL of 5 M HNO_3 and consequently centrifuged for 5 minutes at 10000 rpm for one last time. With this last step the samples with the $BaCO_3$ were ready for column separation.

The columns contained a 100-150 µm sized resin, which had organics that could adhere the REE to certain sites in the organics under acidic circumstances. The resin used was Eichrom's TRU Resin which consisted of octylphenyl-N,N-di-isobutyl carbamoylphosphine oxide (abbreviated CMPO) dissolved in tri-n-butyl phosphate (TBP) and had a bed density of ~0.37 g/mL and a working capacity of 2 mg Am per mL or 4 mg Am per 2mL of resin pre-packed column. This resin separated the REE from the Ba,

which did not adhere to these sites. Firstly, the columns were cleaned by eluting 2.5 mL of 5 M HNO_3 and consequently 2.5 mL of milli-Q water to remove any remaining REE in the columns. This was done two times and the waste was collected in waste vials. During all the steps of the column separation pipets were used to administer the right amounts of liquid. The next step was to condition the columns to create the acidic environment required to adhere the REE the organics. This was done by eluting 1 mL of 5 M HNO_3. Subsequently, 0.5 mL of the samples could be pipetted on the columns. This included the 15 prepared samples, two standards and a blank, so 18 columns in total. The Ba was obliterated from the columns by eluting 0.5 mL of 5 M HNO_3 for three times. The REE were obtained by collecting in 0.5 mL milli-Q water that was added to the columns. This step was performed two times. Lastly, the post-fraction was collected in separate vials and obtained by eluting 1 mL of milli-Q water through the columns.

The REE abundances were consecutively measured by Solution Inductively Coupled Plasma Mass Spectrometry (Solution-ICP-MS). The instrument used was a Thermo X-Series II equipped with a SIS (Sample Introduction System; a double cyclonic spray chamber) and had a Radio Frequency (RF) power of 1200 W. Samples were analysed in 5% HNO_3 and measured with 3 replicates of 25 sweeps. The gas settings were 13.0 l/min for the cool gas, 1.18 l/min for the auxiliary gas and 0.77 l/min for the sample gas. Changes in sensitivity during the analysis were monitored and corrected for using a BCR-2 solution as a drift correction standard, which was executed after every second sample (modified after Eggins et al., 1997). After isobaric interference correction, elemental concentrations of the samples were calculated using a two-point calibration of blank and BCR-2 (about 5000 times diluted).

4.3 Zircon dating

Samples 18-BV-02a, 18-BV-02b, 18-BV-03a and 18-BV-03b were especially rich in detritus and deemed suitable for zircon dating. Crushed material of these samples was sieved, so that only the 66 to 90 and 90 to 125 µm fractions were left. Mineral separation was performed at the Vrije Universiteit of Amsterdam. Dense liquid separation was not performed, because barite and zircon have similar densities with 4.50 and 4.7-4.7 g/cm^3 respectively. The zircons were slightly magnetic, so could be separated using a Frantz isodynamic magnetic separator. Most of the zircons were present in the intermediately magnetic fraction (Frz 6 degrees to max 2 degrees) and subsequently handpicked underneath a standard binocular microscope. Subsequently, the four samples were mounted on one epoxy mount. A carbon coating was applied to the mount to make it suitable for analysis with the Electron Mirco Probe Analyzer (EMPA) at the University of Utrecht. With the EMPA back scatter, secondary and cathodoluminescence images were made of each individual zircon in the four samples. After analysis, the mount was polished to remove the carbon coating.

$^{206}Pb/^{207}Pb$ ages were measured using the LA-ICP-MS at the University of Utrecht. A crater size of 30 µm was used for the analysis and the ion beam on the sample had a fluence of ~8,8 J/m^2 and a frequency of 10 Hz initially. After measurement 18-BV-02a-2 the frequency was adjusted to 7 Hz and after measurement 18-BV-03b-19-rim-1 to 8 Hz to achieve an as high as possible measurement time without lowering the quality of the data. The calibration standard used was ZR91500.

The ages were determined using the U and Pb isotope ratios. Isotopes measured were: Z=204, 206, 207, 208, 235 and 238, where 206-208 are Pb isotopes and 235 and 238 refer to U. ^{204}Z can be a mix of ^{204}Pb and ^{204}Hg. Experience from earlier years, when control measurements of ^{200}Hg and ^{202}Hg were routinely done, has shown that ^{204}Hg is negligible in the lab at the Utrecht University, so it is assumed that all ^{204}Z is ^{204}Pb. This implies that any part of an analysis that shows high ^{204}Z is discarded on the basis that it carries a high common Pb component. Each isotope was measured 4 times per second at a specific dwell time per isotope and the signal generally lasts for 100 sec, giving 400 data points per spot analysis. Sessions start with background analyses (>20 sec), then a period of sample analysis, and, if feasible, a short second period of background at the end (Leo Kriegsman, pers. comm.).

For each spot analysis the best data window was selected using the Glitter software. A lower and an upper limit were manually chosen by visual inspection, giving a window with relatively smooth data acquisition, preferably without peaks. Glitter automatically calculated the isotope ratios and

uncertainties for each spot. Using the analyses of the zircon standard, it corrected the ratios of the unknown zircons and calculated isotope abundances and (apparent) ages and uncertainties for each of the three isotope systems. Glitter output values on the standard analyses were plotted and analysed first. They showed a good cluster with little or no instrument drift and average values close to the reference values, so it could be concluded that the LA-ICP-MS instrument operated well and the results on unknown zircons were reliable. The Glitter data on the unknown zircons were then plotted and analysed, which lead to a first assessment of the data in terms of data quality, consistency, variation, existence of separate clusters, outliers, etc. (Leo Kriegsman, pers. comm.).
Data were processed using Leo Kriegman's personal spreadsheets and the IsoPlot software (Excel plug-in) in several ways: (i) calculating weighted averages and uncertainties for each isotope ratio for all data and for selected populations; (ii) upper and lower concordia intercepts. In view of the significant data scatter and the high levels of dicordancy, selected spot analyses were restudied using the UR-ZUPPE1 spreadsheet, developed by Leo Kriegsman. For each spot analysis, the 400-point multi-isotope signal and the background data were transferred from the raw data file to a single spreadsheet, named and stored. UR-ZUPPE1 allows custom-based automatic filtering using clear criteria ($^{206}Pb/^{204}Pb$ ratio, magnitude of peaks) as well as a manual filtering after visual inspection. At every step of the process, data were visualized and the output values were shown. Based on the selection, the spreadsheet calculated a regression line, throwed away outliers >3 sigma, then recalculated a regression line and throwed away outliers >2 sigma, following the procedure in Kooijman et al. 2012 (Leo Kriegsman, pers. comm.).
Isotope ratios were calculated by time regression, using the cut-off value at the start of the signal (laser on) as the most likely value. Output values were: isotope ratios and 1σ uncertainties, apparent ages and 1σ uncertainties, and the estimated Th/U ratio at the (assumed) concordant Pb-Pb age. In addition, data quality was checked by calculating the $^{238}U/^{235}U$ ratio, which should be close to 137.88, by the % of data points remaining after filtering, and by the consistency of the three isotope ratios. Ideally, this leads to the ratios and ages with lowest 1σ uncertainties. When data showed considerable zoning as a function of measuring time, i.e. non-linear trends with time, they were split into "early" and "late" analyses. In many cases, when zircons had been polished in half, "early" analyses were representative of the zircon core, whereas "late" analyses represented the rim underneath. This revealed several cases where the core analyses gave apparent ages close to the upper intercept of the discordia line, whereas the rims showed major Pb loss and ages close to 0 (Leo Kriegsman, pers. comm.).

5 Results

5.1 Trace element analysis of bulk samples

In Fig. 3 the PAAS (Post Archean Average Shale) normalized REEY (Rare Earth Element Ytrrium) graphs of the bulk analysis are shown for the barites, cherts and sediments and in Fig. 4 the PAAS normalized remaining trace elements are shown for the same rock types. As is demonstrated in Fig. 3A most of the barite samples demonstrate a relatively flat REEY pattern with an apparent positive Eu and possibly a positive La anomaly. This positive Eu anomaly seems to increase in size when the concentration of the other REE is lowered. Also, the data gets less consistent when the concentrations of the REE are lower. A positive Y anomaly is present in the samples with the lowest concentrations. A small positive Y anomaly may be present in sample 18-BV-02b and 18-BV-14. Sample 18-BV-03c and 18-BV-21 deviate from the general trend as is shown in Fig. 1A. Sample 18-BV-03c, which is a sample of barite mixed with sandstone, shows an enrichment in LREE compared to the other REE, while sample 18-BV-21 shows the reverse with a depletion in LREE compared to the other REE. Also, sample 18-BV-21 has a clear apparent positive Y anomaly and negative Ce anomaly.
The chert samples in Fig. 3B. are not consistent compared to the barite samples and are more irregular, while the samples shown are already the samples with the least irregular data patterns. Like the barites, the cherts display a relatively flat REEY pattern with maybe only a slightly positive slope in some of the samples. There is again an apparent positive Eu anomaly present except for sample 18-

BV-15. There is an apparent negative Ce and positive La anomaly in several of the samples, but no positive Y anomalies can be distinguished. Sample 18-BV-13 shows an enrichment in MREE and HREE compared to LREE, but the Y concentration does not seem to have been affected by this enrichment. In Fig. 3C REEY patterns of the sediments are shown, but none of the samples shows the same pattern. Samples 18-BV-12 and 18-BV-20 seem to have a relatively flat REEY pattern, although there are some irregularities in the REEY of sample 18-BV-20. Both samples have an apparent negative cerium anomaly, but only sample 18-BV-20 has an apparent positive Eu anomaly. Sample 18-BV-17 is LREE depleted compared to the other REE but does not show any noticeable anomalies except for maybe a small Eu anomaly.
As is shown in Fig. 4A the barites are extremely enriched in Ba and Sr and fairly enriched in Cr when normalized to PAAS. Moreover, the elements U, Th, Hf, Zr and Ti have very variable concentrations, form enriched to depleted when normalized to PAAS. Co and Ta have similar concentrations to PAAS, and other elements are depleted compared to PAAS. In Fig. 2B and Fig. 2C it is demonstrated that the cherts and sediments are depleted in most trace elements except for Ba, Cr and Co. Except for Ti, the elements U, Th, Hf and Zr show a similar although smaller variance in concentration as in the barites. The cherts and the sediments are similar except for the sediment sample 18-BV-12, which is relatively enriched compared to the other cherts and sediments.
Closely exanimating Fig. 1 and Fig. 2 reveals that the trace elements patterns differ per location. The highest REE and other trace element concentrations for the barites are present in Old mine, where most of the samples show high concentrations in REE and the elements U, Th, Hf, Zr and Ti and the lowest concentrations of these elements in the barites are reached in Puddingstone Hill. They are more intermediate in concentration in Barite Valley, although there is some variability. The exceptions are sample 18-BV-21, which has an unique REEY pattern in the first place and sample 18-BV-03c, which is a mixture of barite and sandstone. The cherts and the sediments are generally quite depleted in trace elements in both Barite Valley and Puddingstone Hill. The exceptions are sample 18-BV-16 and 18-BV-12, which have relatively high concentrations of REEY.

In Fig. 5 the relationship between Zr and several other trace elements in the bulk samples is shown. There is a clear correlation between Zr and Ti, Cr, Nb, Hf, U and Th for the barite samples. These correlations are also shown for the cherts and sediments except for Cr, which does not show a correlation and U, which may show a correlation except for one to three samples. Lu may correlate with Zr in the barites, cherts and sediments, if some of the samples are not included, but has a much lower R^2 value compared to the other trace elements.
It is displayed in Fig. 5 that the concentrations of the trace elements are generally the highest in Old Mine, intermediate in Barite Valley and the lowest in Puddingstone Hill. Even if the samples come from different locations, most of them plot on a single line. However, there are some exceptions. In Fig. 5A in the Barite Valley and possibly Puddingstone Hill samples tend to plot at a shallower slope than the Old Mine samples. This indicates that there is relatively more Zr than Ti in the Old Mine compared to the other locations. The same trend can be seen in Fig. 5E, indicating a relatively higher concentration of Zr than Nb compared to Barite Valley and Puddingstone Hill. There may be two, possibly three different slopes for the different locations in Fig. 5M. At least there seems to be a clear difference in slope between Old Mine and Puddingstone Hill. The slope of puddingstone hill is shallow, while the slope of Old Mine is steep. This indicates a relative larger amount of Zr than Lu in the Old Mine compared to Puddingstone Hill site.

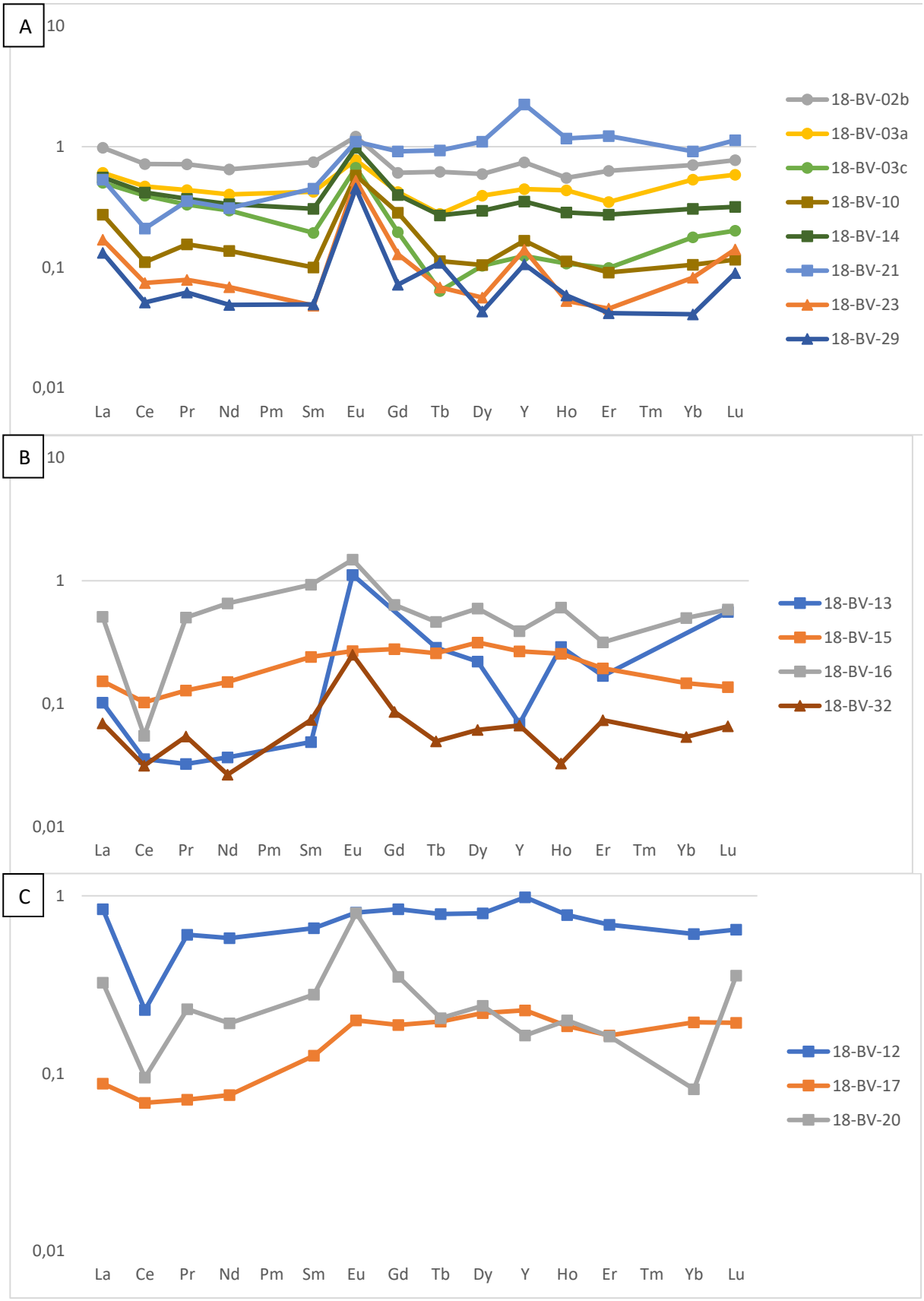

Figure 3: PAAS normalized REEY graph of bulk A) barite, B) chert and C) sediment samples. Concentrations are in ppm. Symbols annotate the location from which the samples came: Old Mine (spheres), Barite Valley (squares) and Puddingstone Hill (triangles). (PAAS values used for normalization from Hofmann (2005)).

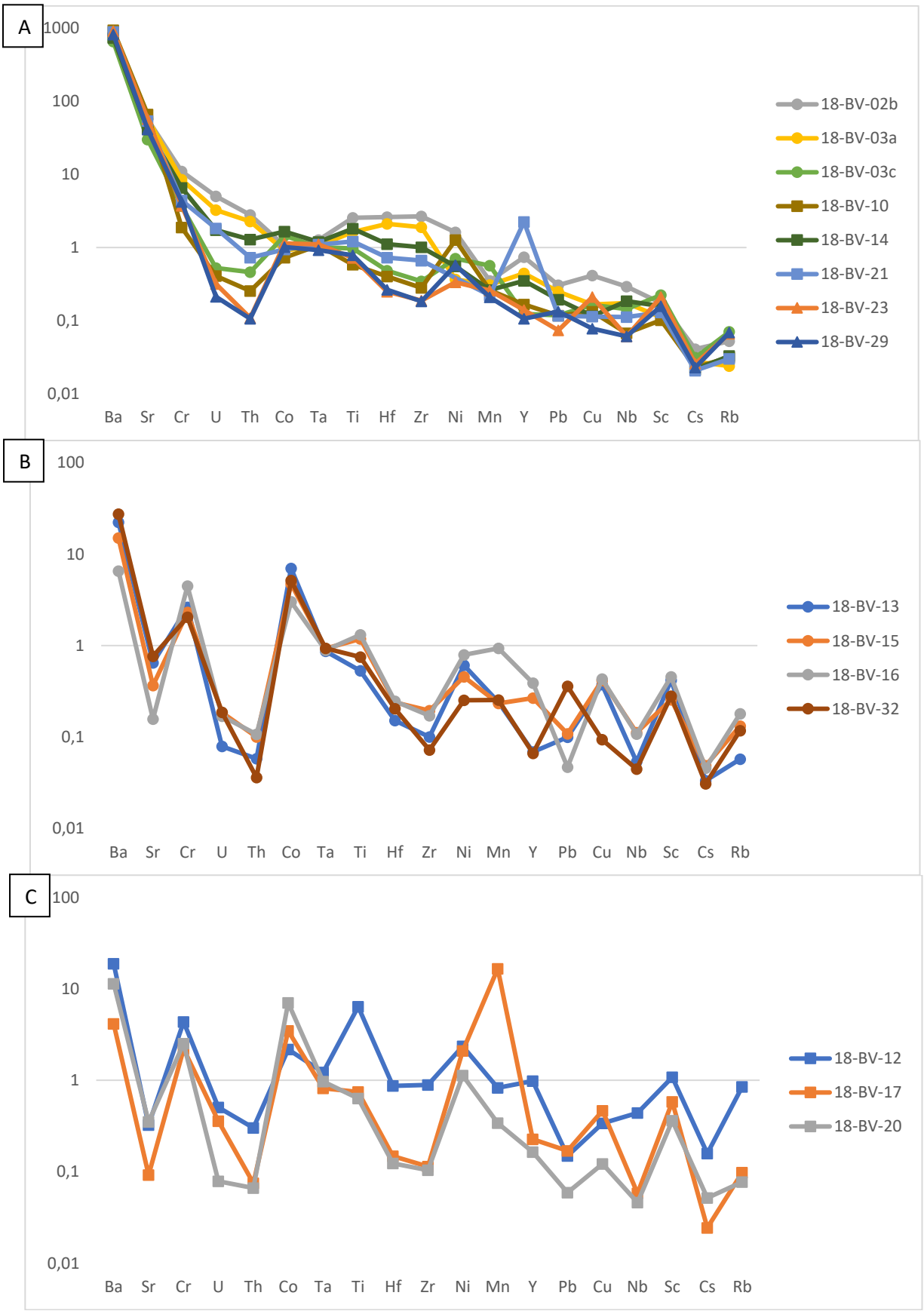

Figure 4: PAAS normalized trace element graph (excluding REE) of bulk A) barite, B) chert and C) sediment samples. Concentrations are in ppm. Symbols annotate the location from which the samples came: Old Mine (spheres), Barite Valley (squares) and Puddingstone Hill (triangles). (PAAS values used for normalization from Hofmann (2005)).

A

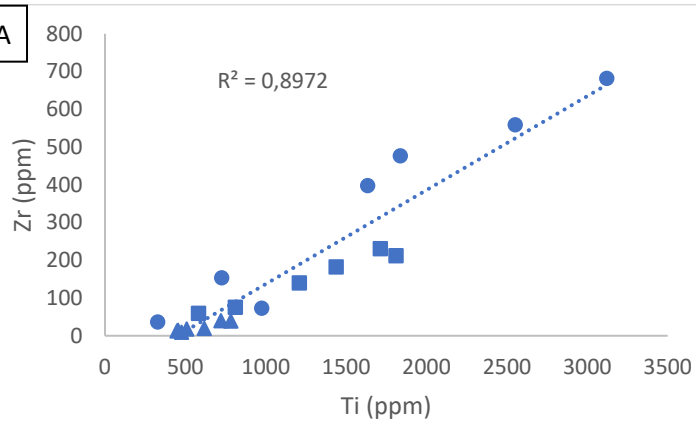
R² = 0,8972
Zr (ppm)
Ti (ppm)
0
100
200
300
400
500
600
700
800
0
500
1000
1500
2000
2500
3000
3500

B

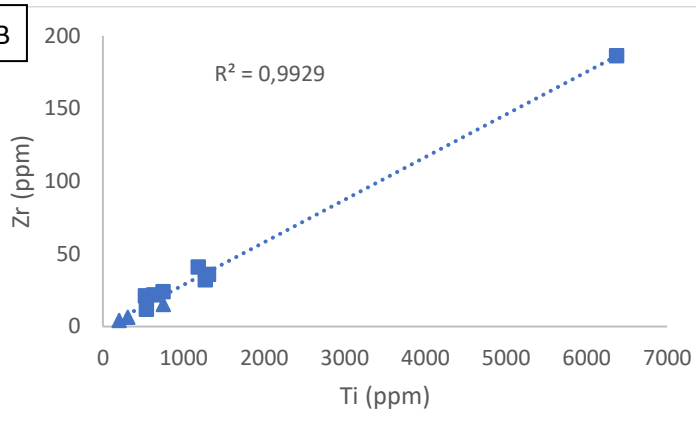
R² = 0,9929
Zr (ppm)
Ti (ppm)
0
50
100
150
200
0
1000
2000
3000
4000
5000
6000
7000

C

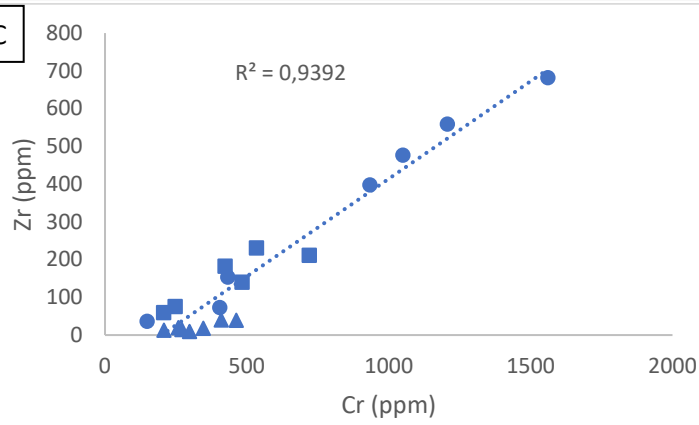
R² = 0,9392
Zr (ppm)
Cr (ppm)
0
100
200
300
400
500
600
700
800
0
500
1000
1500
2000

D

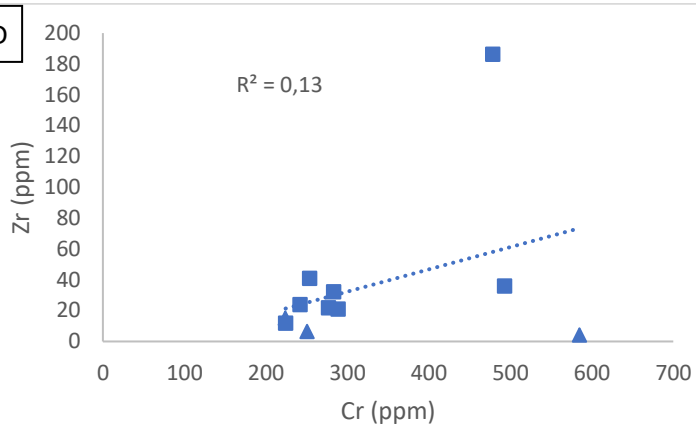
R² = 0,13
Zr (ppm)
Cr (ppm)
0
20
40
60
80
100
120
140
160
180
200
0
100
200
300
400
500
600
700

E

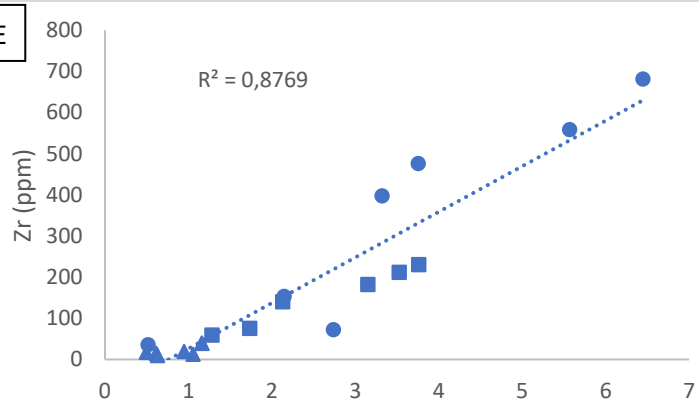
R² = 0,8769
Zr (ppm)
Nb (ppm)
0
100
200
300
400
500
600
700
800
0
1
2
3
4
5
6
7

F

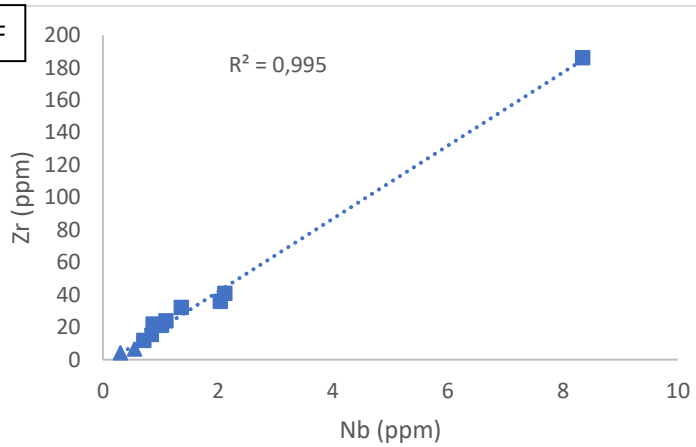
R² = 0,995
Zr (ppm)
Nb (ppm)
0
20
40
60
80
100
120
140
160
180
200
0
2
4
6
8
10

G

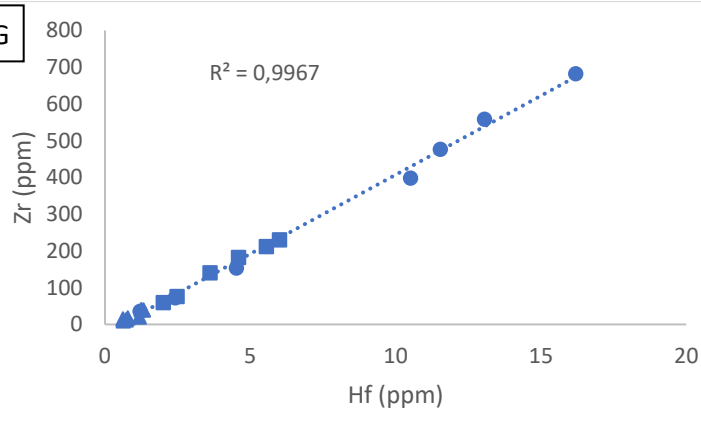
R² = 0,9967
Zr (ppm)
Hf (ppm)
0
100
200
300
400
500
600
700
800
0
5
10
15
20

H

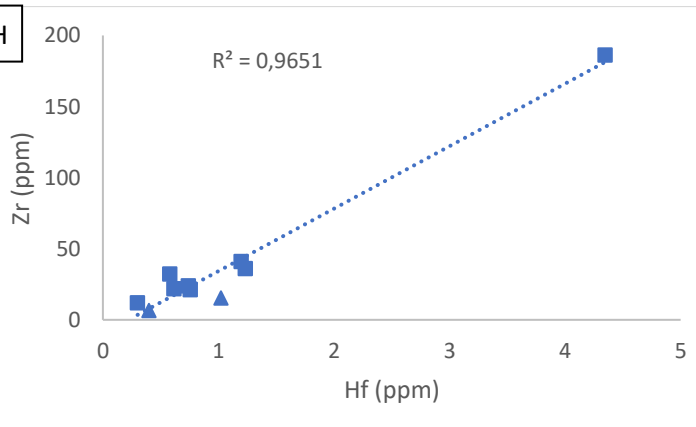
R² = 0,9651
Zr (ppm)
Hf (ppm)
0
50
100
150
200
0
1
2
3
4
5

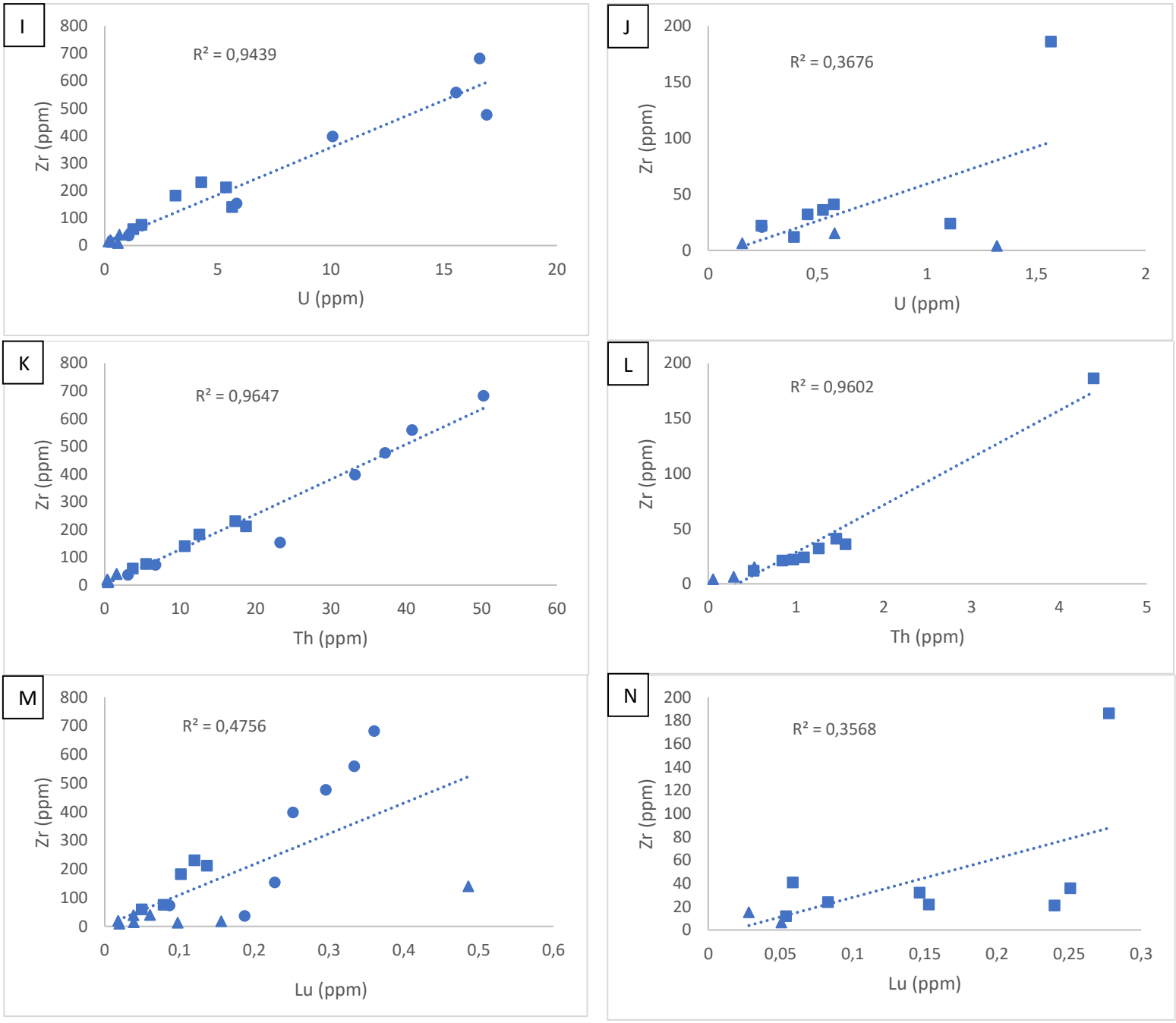

Figure 5: Zr plotted to A) Ti for barite samples, B) Ti for chert and sediments samples, C) Cr for barite samples, D) Cr for chert and sediment samples, E) Nb for barite samples, F) Nb for chert and sediments samples, G) Hf for barite samples, H) Hf for chert and sediments samples, I) U for barite samples , J) U for chert and sediments samples, K) Th for barite samples, L) Th for chert and sediments samples , M) Lu for barite samples and N) Lu for chert and sediments samples. The formula of the trendline and the R^2 value are given in the graphs. Symbols annotate the location from which the samples came: Old Mine (spheres), Barite Valley (squares) and Puddingstone Hill (triangles). Concentrations are in ppm.

5.2 Trace element analysis of epoxy blocks

In Fig. 6 graphs of the REE and other trace elements in the epoxy blocks are given, which demonstrate quite some variability between different samples. The REE patterns in Fig. 6A are mostly flat and at most the white altered cherts (orange line) may have a slightly positive slope. The fresh grey cherts show a depletion in LREE, especially compared to the other rock types. The bulk analysis does not agree well with the data and has a higher concentration of REE and seems to be enriched in MREE and HREE,

while the Y concentration has been affected less. The enrichment of the trace elements in the bulk data is also demonstrated in the remaining elements (Fig. 6B). The bulk analysis, the altered white chert (orange line) and the fresh grey chert veins have an apparent positive Eu anomaly, but the fresh grey chert and the other altered white chert (yellow line) do not. Some irregularity can be recognised in the altered white chert (orange line), but the other data are relatively consistent. Most of the remaining elements are similar for the different rock types and all show low trace elements concentrations in the chert except for Ba and Cr (Fig. 6B).

Sample 18-BV-15 in Fig. 6C shows a positive slope in the altered chert with an apparent positive Eu anomaly. However, the bulk analysis does not show such an anomaly and has elevated REE, especially in the MREE. Also, the remaining elements show an increase in concentration in the bulk analysis compared to the analysis of the altered chert (Fig. 6B).

Prominent negative Ce anomalies are present in the altered rocks and the bulk analysis in Fig. 6E. Only the fresh black chert does at most show a minor negative Ce anomaly. On the other hand, a small positive Eu anomaly seems to be present in all the analyses of sample 18-BV-16. The fresh black chert has a flat REE pattern, which is also present in the least altered sandstone and the bulk analysis. It is demonstrated in Fig. 6E that the overall REE concentration increases with an increase in alteration of the rocks, the LREE are especially enriched in the most weathered part of the epoxy block. A similar trend can be seen in the remaining elements, which also have the highest concentration in the most weathered samples (Fig. 6F). The fresh black chert has low trace element concentrations except for Ba, Cr and Ti.

In Fig. 6G the bulk analysis and the black clast of chert have flat REE patterns, although the REE pattern of the bulk analysis is somewhat irregular and has higher REE concentrations. Both analyses also seem to display a small positive Eu anomaly. The grey clast of chert demonstrated a large enrichment in MREE and HREE compared to the other two analyses. Also, the grey clast of chert shows a large enrichment in Zr, Hf and Y and to a lesser extend U and Th compared to the black clast of chert and the bulk analysis (Fig. 6H). All the other elements are low in concentration for all three analyses except for Ba, Cr and Ti.

It is demonstrated in Fig. 6I that a high enrichment in LREE and REE generally is present in the altered brown chert compared to the fresh grey and black clasts of chert. Also, an apparent negative Ce anomaly increases in size with more alteration and is only minor in the fresh clasts. The bulk analysis is intermediate in REE composition between the altered brown chert and the fresh grey and black chert. An apparent positive Eu anomaly is present in the bulk analysis and a minor one in the altered brown chert, but no positive Eu anomaly can be recognised in the grey and black clasts of chert. While the altered brown chert has a negative REE slope and the bulk analysis is flat in slope, the grey and black clasts of chert have a positive slope, with the grey clast of chert having a steeper slope. The altered brown chert has the highest concentrations of the remaining trace elements, the black clast of chert the lowest concentration of remaining trace elements and the bulk analysis is intermediate in composition between the two extremes (Fig. 6J). The grey clast is intermediate in composition for most elements except for Ba, Sr, Cr, U, Th, Cs and Rb and has remarkably high concentrations of Ti.

Although the REE patterns are quite irregular and miss data for all analyses, still some observations can be made based on Fig. 6K. The REE patterns seem to be either flat or seem to have a slightly positive slope. All the analyses have an apparent positive Eu anomaly and have relatively low REE concentrations, with the bulk analysis and the fresh grey quartz having slightly higher concentrations than the greenish quartz and the white altered vein. Moreover, the white altered vein seems to have a positive Y anomaly. The remaining elements miss quite a bit of data but show very low concentrations of most trace elements in the different rock types (Fig. 6L). The bulk analysis is enriched in Co and Ta compared to the other analyses. Large differences are present in the concentrations of the elements Ba and Sr between the different rock types. The fresh grey quartz is depleted in Ba and Sr, while the greenish quartz only has an enrichment in Ba. The white altered vein is extremely enriched in Ba and Sr and has a concentration as high as the barite samples. The bulk analysis is intermediate in Ba and Sr concentration between the fresh grey quartz and the white altered vein.

The REE pattern of the bulk analysis and the altered greenish chert in Fig. 6M are similar, although the bulk analysis has increased concentrations of REE. They show an apparent positive Eu anomaly and positive slope in the REE. Also, the bulk analysis has slightly higher concentrations of the remaining trace elements (Fig. 6N) and much higher concentrations of Co and Ta. Both analyses show generally low concentrations of trace elements, high concentrations of Ba and remarkably high concentrations of Cr.

Most of the REE patterns of the different rock types in Fig. 6O show a depletion of LREE and a slightly positive or flat slope. This includes the least and most altered jaspilite clasts, the altered white chert and the altered white chert vein. In the altered white chert vein and the most altered jaspilite clast an apparent small positive Eu anomaly seems to be present. Unfortunately, in the other two rock types Eu was below detection limit, so it cannot be confirmed whether there was a similar anomaly in these rock types. The bulk analysis is like the chert around the vein, although having slightly higher REE concentrations. Both analyses have a flat REE pattern and an apparent positive Eu anomaly, larger than the anomaly in the previous rock types. The vein itself shows a large positive Eu anomaly and positive Y anomaly and may show an enrichment in the LREE. However, the trend in the REE is difficult to distinguish due to the irregular pattern. The fresh grey vein is also distinctly different from the other analyses in the remaining trace elements (Fig. 6P) and is somewhat like the vein in Fig. 6L. There is a distinctive enrichment in Ba and Sr, but the remaining elements are depleted, especially compared to the other rock types. These rock types are still relatively enriched in Ba and Sr, but less than the vein and have relatively high concentrations of Ti. The bulk analysis shows the highest concentrations in trace elements but is intermediate in Ba and Sr between the fresh grey vein and the other rock types.

In Fig. 6Q the fresh jaspilite shows a slightly positive slope in the REE and a positive Eu and a positive Y anomaly, while the fresh black chert seems to have a positive slope with an enrichment in the MREE. The general concentrations of the REE in these two rock types are the lowest compared to the other analyses. Also, the remaining trace elements have relatively low concentrations (Fig. 6R). Also, the trace element pattern is completely different form the previous analyses, does not have high concentrations of Ba an Cr and has some of the lowest trace element concentrations measured for the other trace elements. Moreover, only Mn and Cu seem to be like PAAS, and all other elements are depleted relative to PAAS.

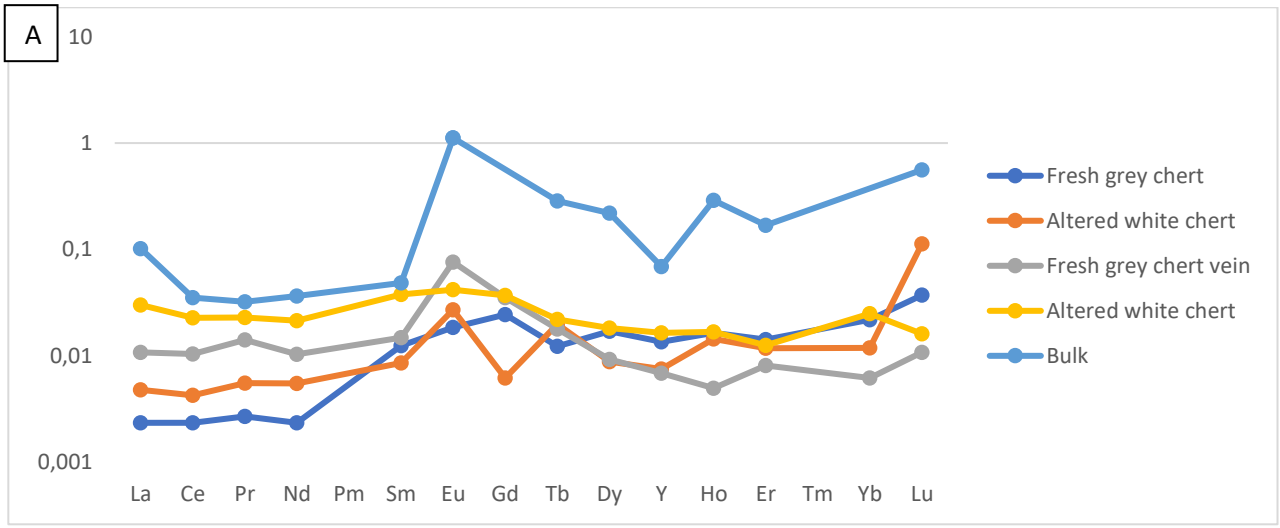

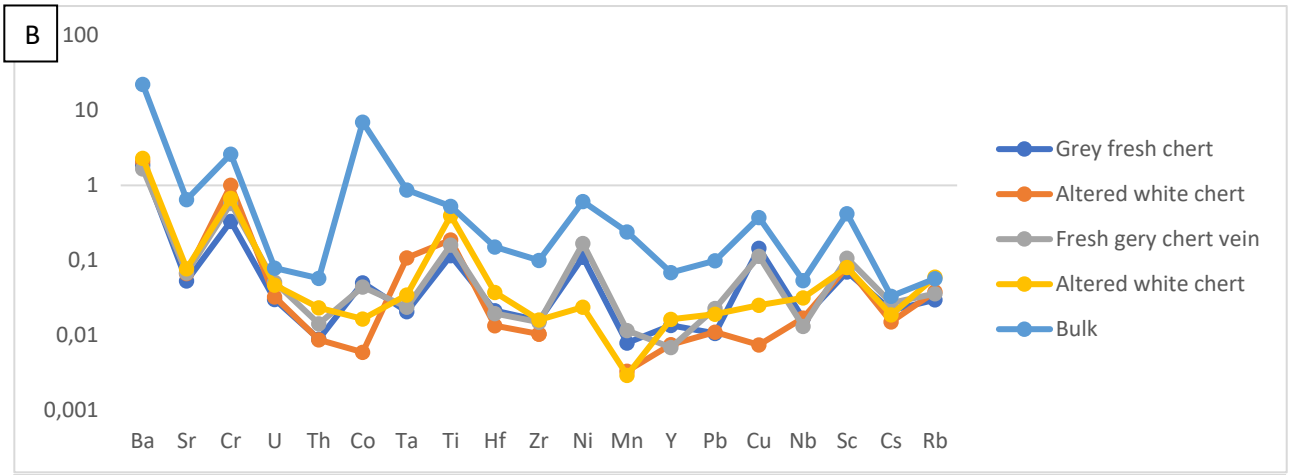
B
100
10
1
0,1
0,01
0,001
Ba Sr Cr U Th Co Ta Ti Hf Zr Ni Mn Y Pb Cu Nb Sc Cs Rb
Grey fresh chert
Altered white chert
Fresh gery chert vein
Altered white chert
Bulk

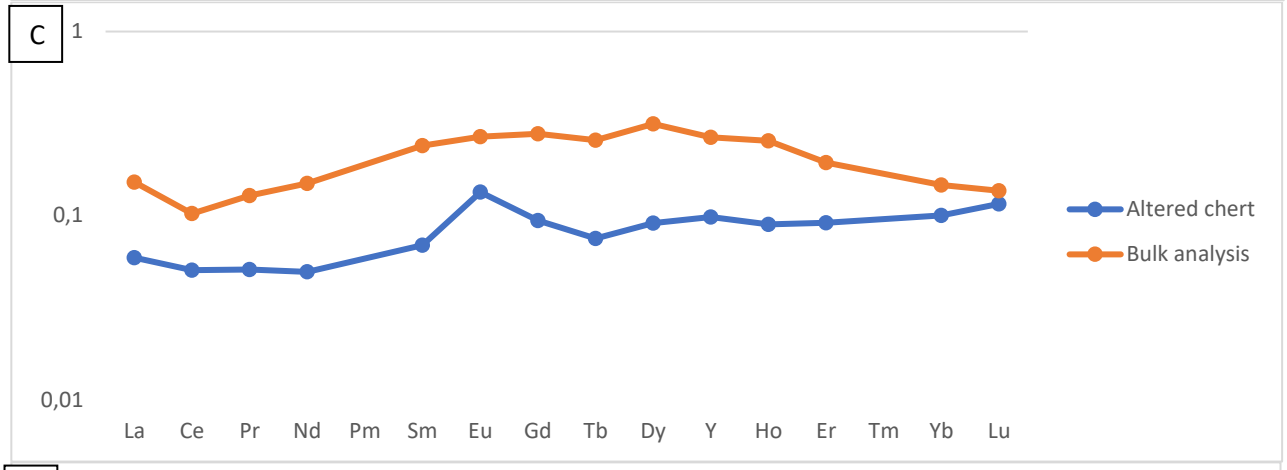
C
1
0,1
0,01
La Ce Pr Nd Pm Sm Eu Gd Tb Dy Y Ho Er Tm Yb Lu
Altered chert
Bulk analysis

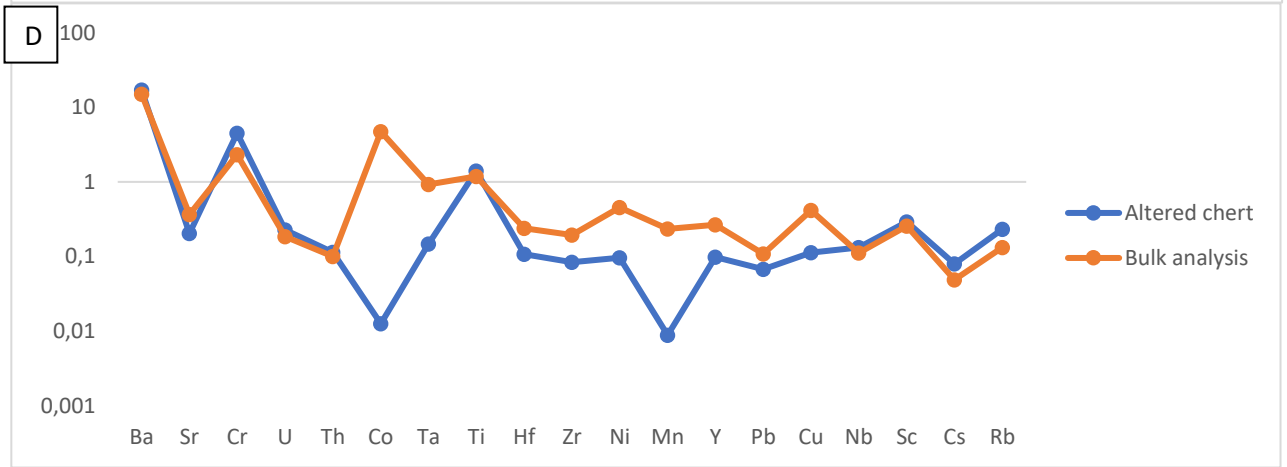
D
100
10
1
0,1
0,01
0,001
Ba Sr Cr U Th Co Ta Ti Hf Zr Ni Mn Y Pb Cu Nb Sc Cs Rb
Altered chert
Bulk analysis

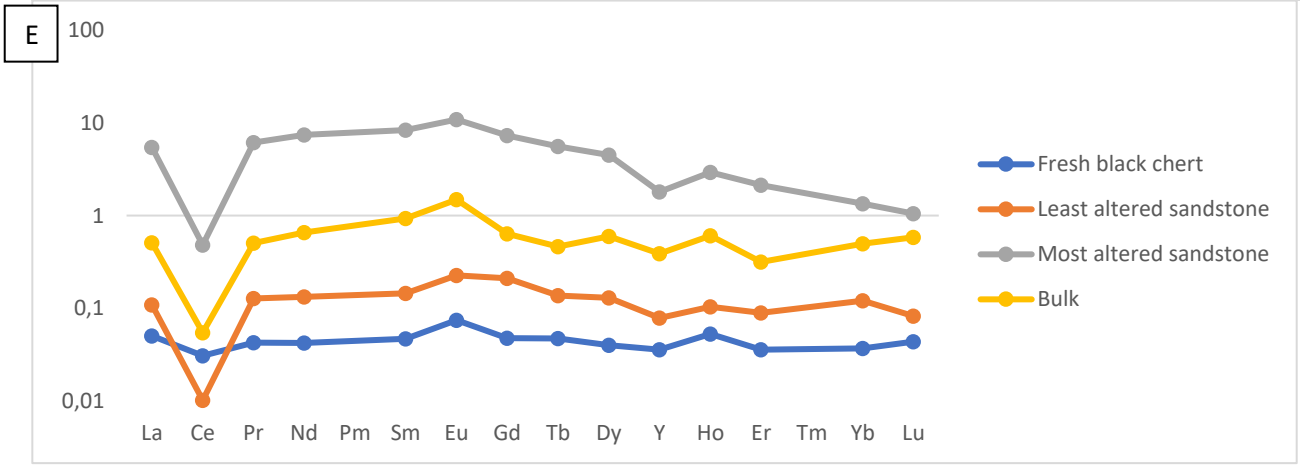
E
100
10
1
0,1
0,01
La Ce Pr Nd Pm Sm Eu Gd Tb Dy Y Ho Er Tm Yb Lu
Fresh black chert
Least altered sandstone
Most altered sandstone
Bulk

F

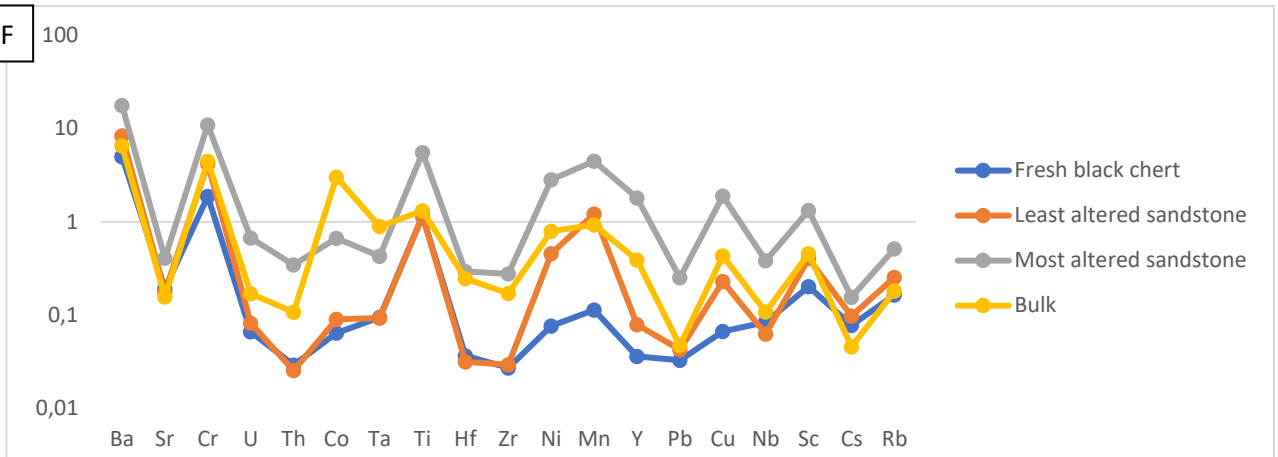
100
10
1
0,1
0,01
Ba Sr Cr U Th Co Ta Ti Hf Zr Ni Mn Y Pb Cu Nb Sc Cs Rb
Fresh black chert
Least altered sandstone
Most altered sandstone
Bulk

G

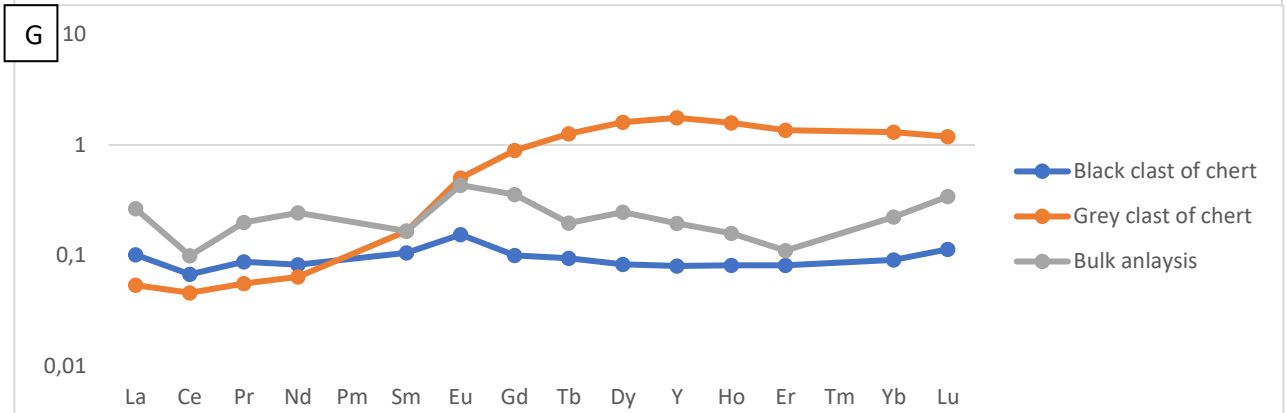
10
1
0,1
0,01
La Ce Pr Nd Pm Sm Eu Gd Tb Dy Y Ho Er Tm Yb Lu
Black clast of chert
Grey clast of chert
Bulk anlaysis

H

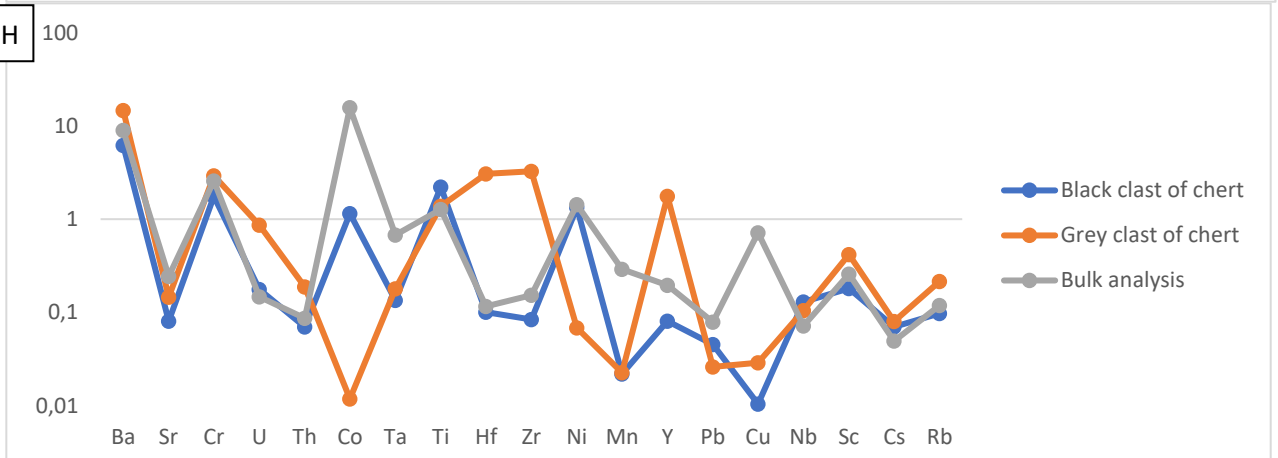
100
10
1
0,1
0,01
Ba Sr Cr U Th Co Ta Ti Hf Zr Ni Mn Y Pb Cu Nb Sc Cs Rb
Black clast of chert
Grey clast of chert
Bulk analysis

I

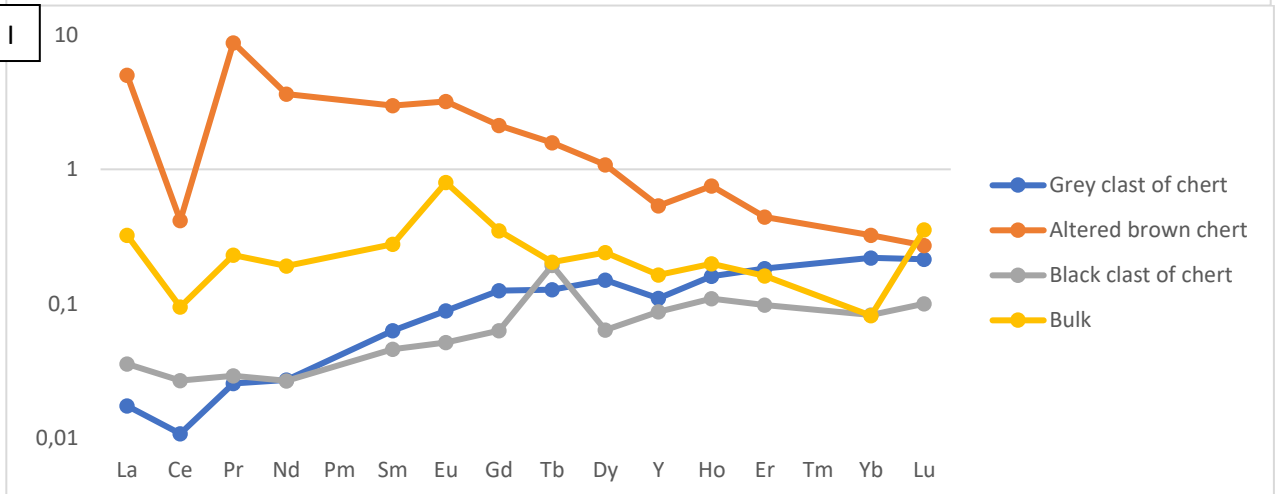
10
1
0,1
0,01
La Ce Pr Nd Pm Sm Eu Gd Tb Dy Y Ho Er Tm Yb Lu
Grey clast of chert
Altered brown chert
Black clast of chert
Bulk

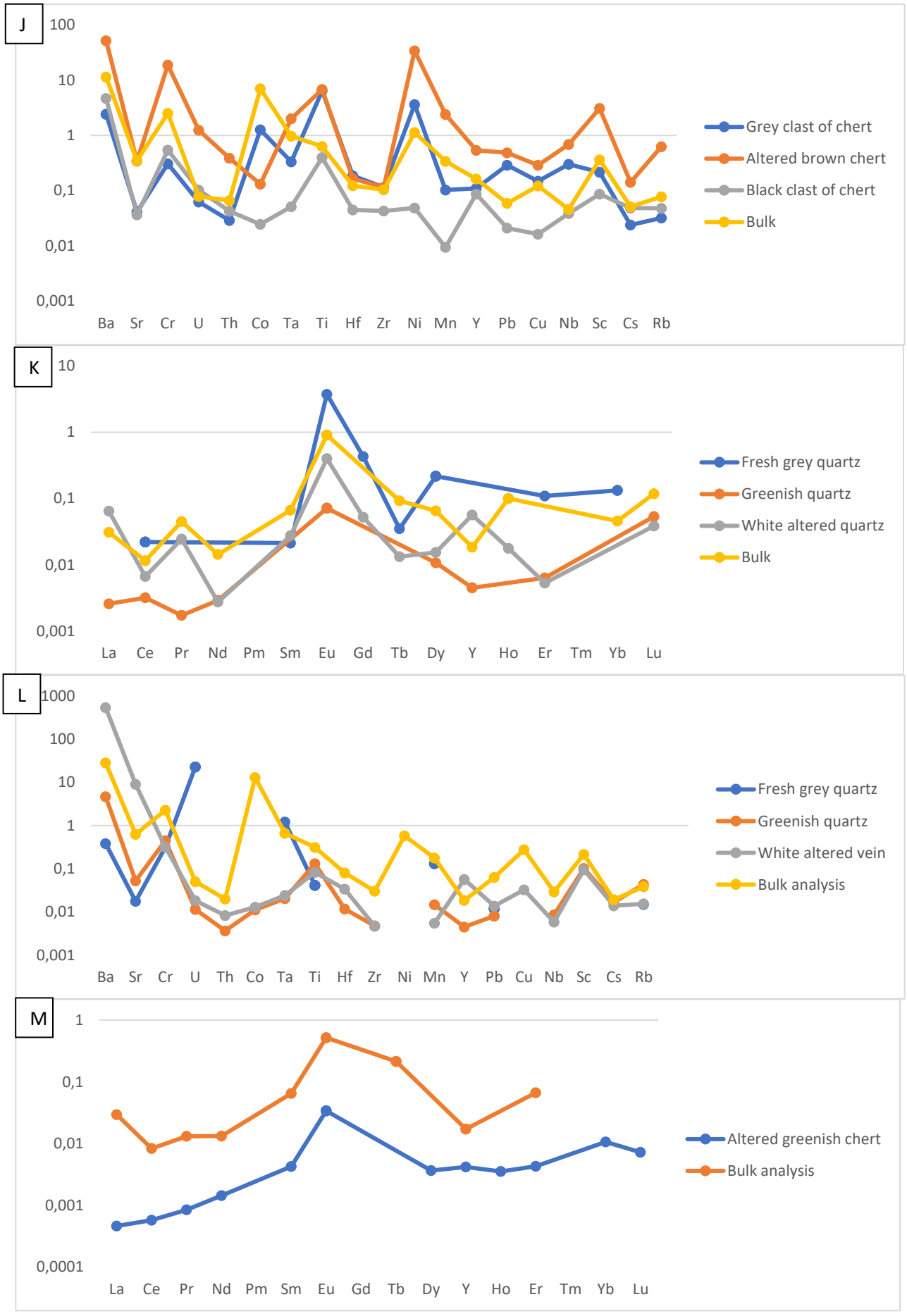
J
100
10
1
0,1
0,01
0,001
Ba Sr Cr U Th Co Ta Ti Hf Zr Ni Mn Y Pb Cu Nb Sc Cs Rb
Grey clast of chert
Altered brown chert
Black clast of chert
Bulk
K
10
1
0,1
0,01
0,001
La Ce Pr Nd Pm Sm Eu Gd Tb Dy Y Ho Er Tm Yb Lu
Fresh grey quartz
Greenish quartz
White altered quartz
Bulk
L
1000
100
10
1
0,1
0,01
0,001
Ba Sr Cr U Th Co Ta Ti Hf Zr Ni Mn Y Pb Cu Nb Sc Cs Rb
Fresh grey quartz
Greenish quartz
White altered vein
Bulk analysis
M
1
0,1
0,01
0,001
0,0001
La Ce Pr Nd Pm Sm Eu Gd Tb Dy Y Ho Er Tm Yb Lu
Altered greenish chert
Bulk analysis


N
100
10
1
0,1
0,01
0,001
Ba Sr Cr U Th Co Ta Ti Hf Zr Ni Mn Y Pb Cu Nb Sc Cs Rb
Altered greenish chert
Bulk analysis
O
1
0,1
0,01
0,001
0,0001
La Ce Pr Nd Pm Sm Eu Gd Tb Dy Y Ho Er Tm Yb Lu
White altered chert vein
Jaspilite clast least altered
Jaspilite clast most altered
Altered white chert
Grey fresh vein
Chert around vein
Bulk
P
1000
100
10
1
0,1
0,01
0,001
0,0001
0,00001
Ba Sr Cr U Th Co Ta Ti Hf Zr Ni Mn Y Pb Cu Nb Sc Cs Rb
White altered chert vein
Jaspilite clast least altered
Jaspilite clast most altered
Altered white chert
Grey fresh vein
Chert around vein
Bulk
Q
1
0,1
0,01
0,001
0,0001
La Ce Pr Nd Pm Sm Eu Gd Tb Dy Y Ho Er Tm Yb Lu
Fresh jaspilite
Fresh black chert

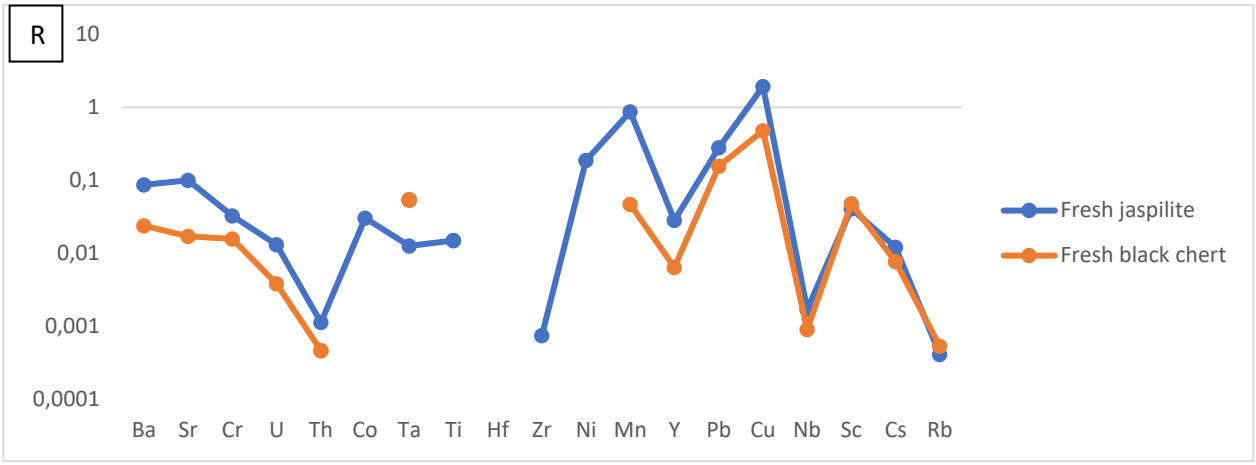

Figure 6: PAAS normalized graphs of the microanalytical trace element analyses on the chert, jaspilite and sediment epoxy blocks of A) REE in 18-BV-13, B) remaining trace elements in 18-BV-13, C) REE in 18-BV-15, D) remaining trace elements in 18-BV-15, E) REE in 18-BV-16, F) remaining trace elements in 18-BV-16, G) REE in 18-BV-18, H) remaining trace elements in 18-BV-18, I) REE in 18-BV-20, J) remaining trace elements in 18-BV-20, K) REE in 18-BV-26 , L) remaining trace elements in 18-BV-26, M) REE in 18-BV-30, N) remaining trace elements in 18-BV-30, O) REE in 18-BV-32, P) remaining trace elements in 18-BV-32, Q) REE in 18-BV-08 and R) remaining trace elements in 18-BV-08. Concentrations are in ppm and the rock types measured are given in the legend. (PAAS values used for normalization from Hofmann (2005)).

5.3 Trace element analysis after barium removal

The REEY data after the barium removal are quite consistent (Fig. 7) like the LA-ICP-MS bulk data, but there are differences between the two data sets and the general concentration of the elements is lower. Like with the LA-ICP-MS bulk data the Puddingstone Hill data have the lowest overall concentrations, but concentrations of the samples from Old Mine are overall lower than those from Barite Valley. Several of the samples show a negative REEY slope with a depletion in the HREE and Y. Moreover, most of samples show a small negative Y anomaly. Some samples, like sample 18-BV-02b, show an enrichment of the MREE compared to the other trace elements. All samples from Barite Valley and Old Mine show a negative Ce anomaly, which sometimes seems to be accompanied by a positive La anomaly. Only a few samples from Old Mine have a small positive Eu anomaly and a couple more from Barite Valley. All the samples from Puddingstone Hill have a positive Eu anomaly and those are also larger than in the other two locations.

The positive Eu anomalies are much smaller and less common than in the LA-ICP-MS bulk data. Also, in both analyses the REEY patterns are flat, except that after the barium removal, there is a depletion in the HREE and Y. Also, more negative Ce anomalies are present after the Ba removal. The results after the barium removal are generally quite consistent excluding sample 18-BV-21, which already shows deviation in the LA-ICP-MS bulk data. This sample has a large negative Ce anomaly, the only small positive Y anomaly, a depletion in LREE (or enrichment in MREE) and only a depletion in the heaviest HREE. This is like the pattern in the LA-ICP-MS bulk data except for the absence of a positive Eu anomaly and the depletion of the heaviest HREE.

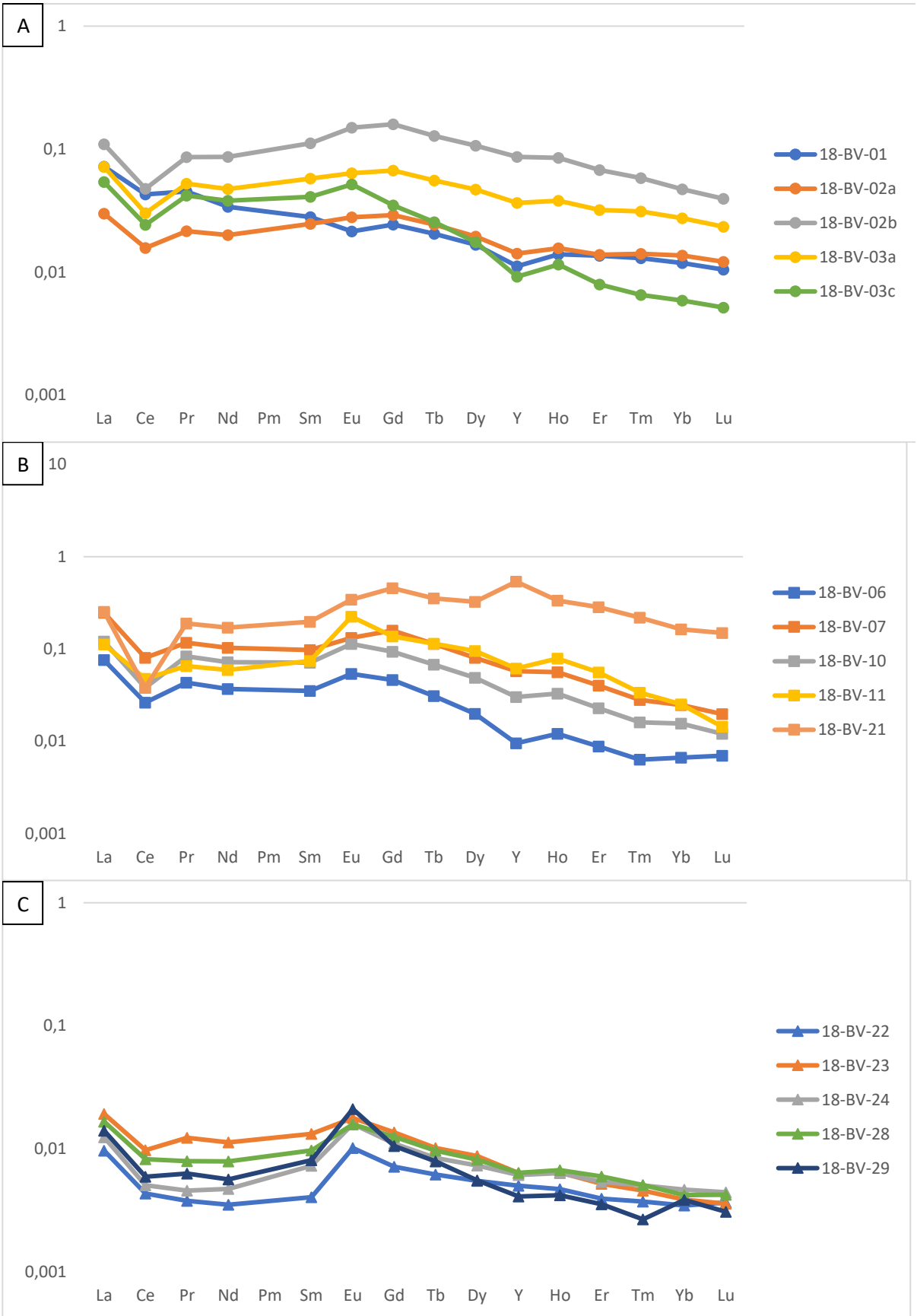

Figure 7: PAAS normalized REEY graphs of the Solution-ICP-MS barite data. A) Old mine, B) Barite Valley and C) Puddingstone Hill. Concentrations are in ppm. (PAAS values used for normalization from Hofmann (2005)).

5.4 Zircon dating

The zircons in the barite samples were predominantly transparent and brown or dark brown in colour. Some of the zircons were yellow and there might have been 1-3 transparent zircons, but the bulk was (dark) brown. Many of the zircons still had well developed crystal surfaces and the tetragonal crystal shape of zircon in both the thin section and the images from the EMPA (Fig. 8A, B and C), although many were only half or fragments of the original (Fig. 8B and C). Still, there were a large amount of complete zircon crystals. Many zircons were still quite euhedral with only smoothed crystal edges (Fig. 8A, B, C), but some were square, diamond shape or rectangular instead of tetragonal (Fig. 8D). There were also zircons that had been rounded and had become more spherical or oval (Fig. 8E). Although most zircons did not experience much rounding, the CL and backscatter images still show quite some fractures and fragmented rims in many of the zircons (Fig. 8A, B, C, D and F). Also, inclusions were quite common in the zircons (Fig. 8A, B, C and D). In general, the zircons had extremely well-developed zoning patterns, which often showed tetragonally zoned growth of the crystals (Fig. 8A, B, C and F). Although it was very rare, some zircons demonstrated entirely different cores from the rims (Fig. 8B and F).

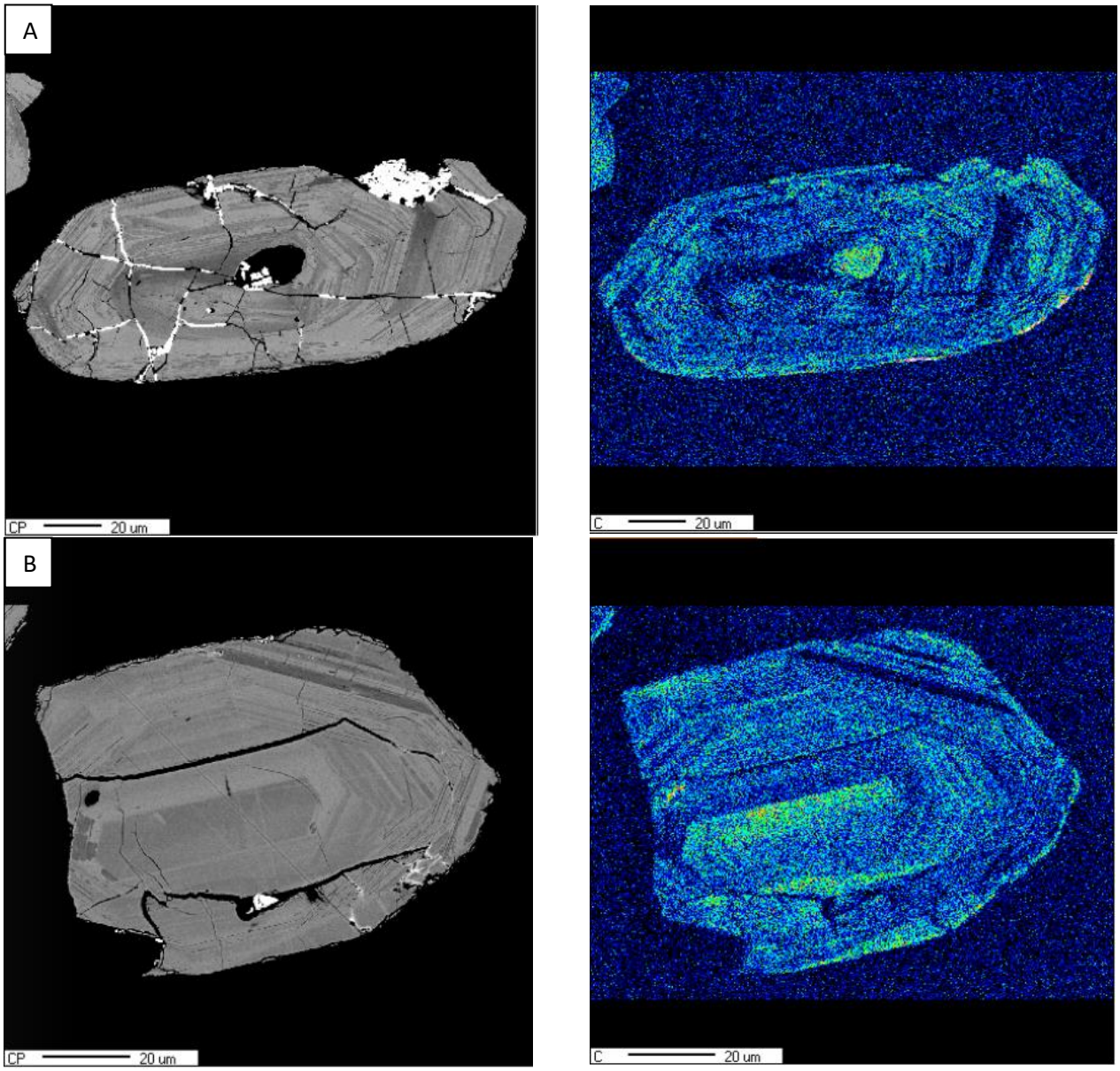

C

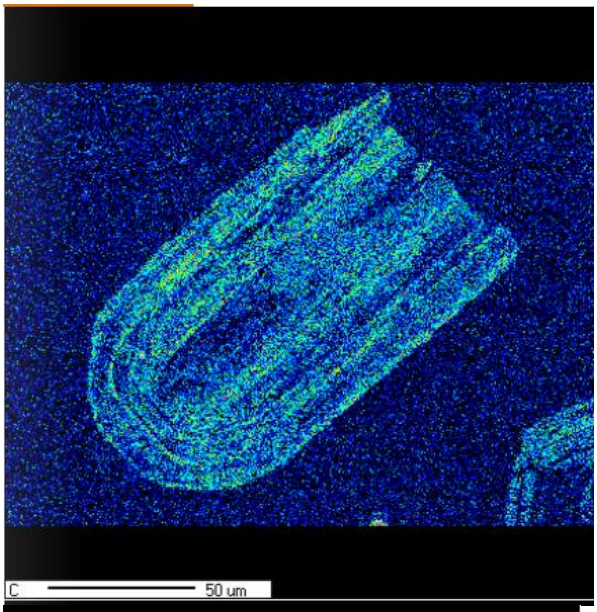

D

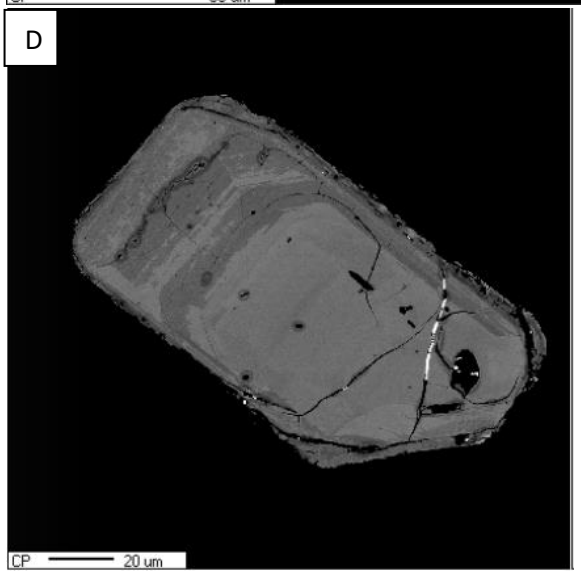

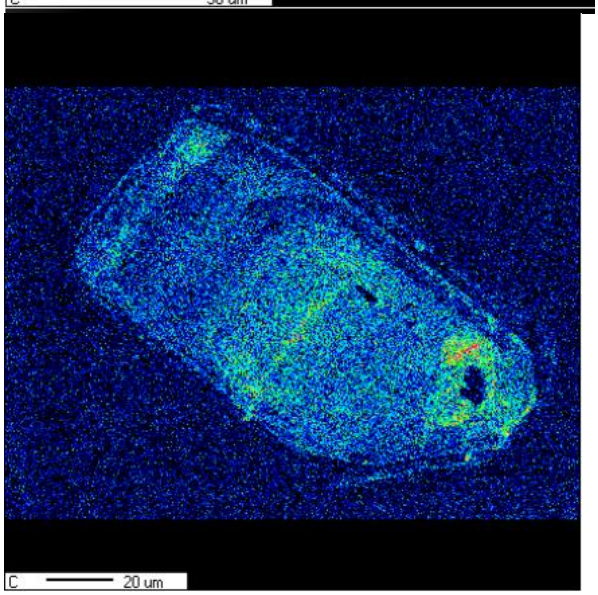

E

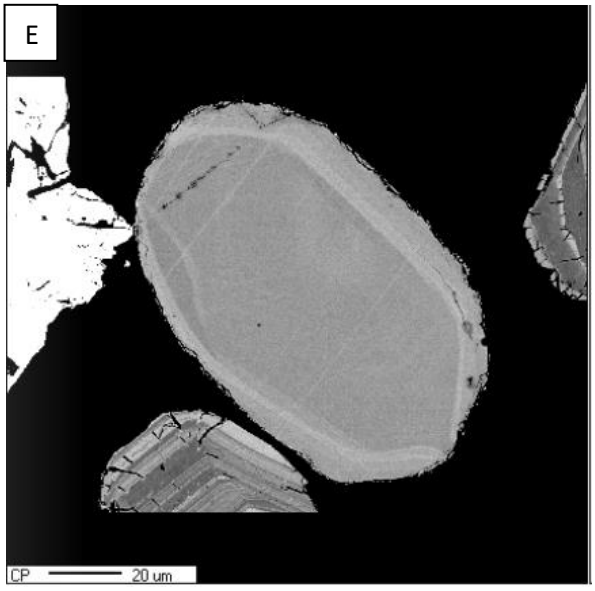

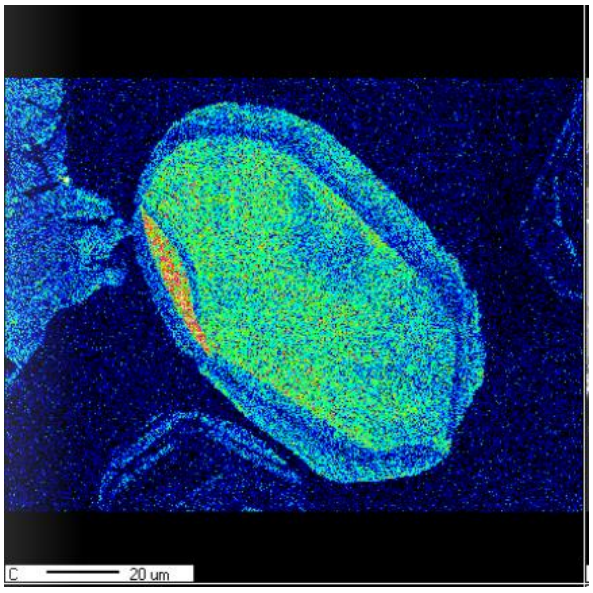

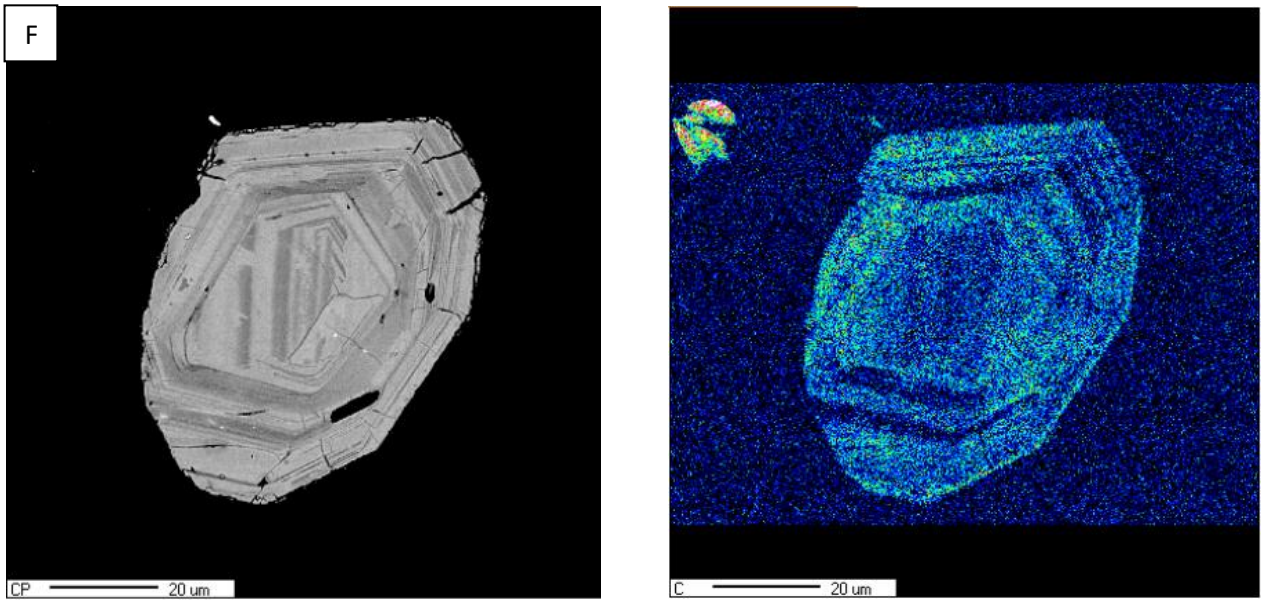

Figure 8: Several back scatter (left) and CL (right) images from zircons in sample 18-BV-03b.

In Fig. 9A it is shown that none of the zircons plot on the concordia line, but most roughly plot on a discordia line that roughly intersects the origin and the concordia at 3.265 ± 0.036 Ga (Fig. 9B). There is one concordant point with a Pb^{207}/Pb^{206} age of 3.243 ± 0.016 Ga. Most of the zircons plot at the younger part of the discordia compared to the older part. Also, when the ages become younger, more of the zircons start to plot left of the discordia line (Fig. 9A). Moreover, there are some older zircons that seem to plot to the right of the discordia line, resulting in an age of ~3.45 (3.472 ± 270) Ga when they would intercept the concordia line (Fig. 9A and C). The zircons in Fig. 8B and E are two of the four zircons that seem to have recorded an older age. Histograms featuring Pb-Pb ages of the analysed zircons show the highest abundance of zircons at ~3.25 Ga for all the zircons (Fig. 9D) and the least discordant zircons (Fig. 9E). The histogram with all the zircons shows that many of the zircons have a Pb-Pb age younger than 3.25 Ga and there are only ~15 with an older age. There are three zircons of the least discordant zircons with an age around ~3.4 Ga. The $^{207}Pb/^{206}Pb$ ages shown in Fig. 10C display a consistent value during the whole LA-ICP-MS analysis with a clear linear relationship, resulting in an age of ~3.25-3.3 Ga. The $^{206}Pb/^{238}U$ and $^{207}Pb/^{235}U$ ratios in Fig. 10A and B. do not demonstrate this relationship, but instead have low $^{206}Pb/^{238}U$ and $^{207}Pb/^{235}U$ ratios at the start and end of the measurement and have a peak plateau in between. The plateau ages determined from these $^{206}Pb/^{238}U$ and $^{207}Pb/^{235}U$ ratios are still ~3.25-3.3 Ga, but only with a larger uncertainty. In Fig. 10D it is shown that there is an increase of common Pb (Pb^{204}) with a decrease in the calibrated age of the zircon.

6 Discussion

6.1 Bulk and microanalytical trace element data of the cherts and sediments

There is a clear difference between the data obtained from the bulk trace elements analyses and from the microanalytical trace elements analyses of the cherts and the sediments. Most of the microanalytical data do not directly agree with the bulk data (Fig. 3 and 6). In most instances the bulk data is more enriched in trace elements compared to the microanalytical analyses. The exceptions are samples 18-BV-16, 18-BV-20 and 18-BV-26 and interestingly, in the first two the data is intermediate in composition between the fresh parts of the rock and the most weathered part of the rock (Fig. 6E, F, I, J, K and L). This demonstrates that due to weathering, the sediments and the cherts have gained trace elements. The most weathered samples show an increase in particular in elements such as Zr, Hf, U, Th, Ti and Cr, which are common in detrital minerals. Therefore, the weathering enriches the cherts and sediments in detrital minerals, which would also explain the elevation of the REEY

A

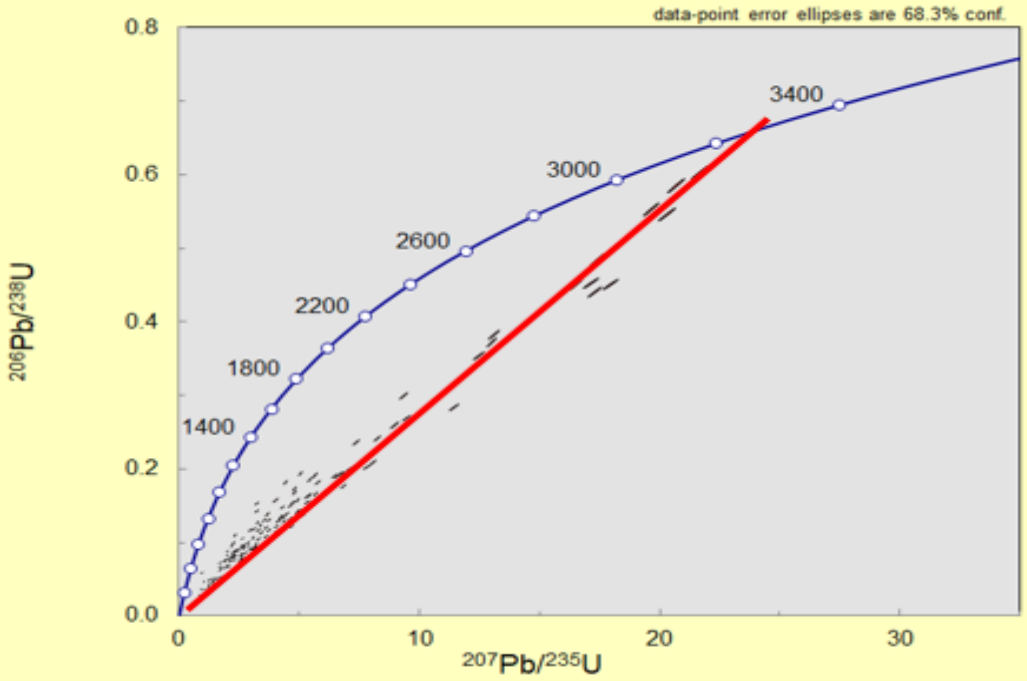
data-point error ellipses are 68.3% conf.
0.8
0.6
0.4
0.2
0.0
0
10
20
30
3400
3000
2600
2200
1800
1400
206Pb/238U
207Pb/235U

B

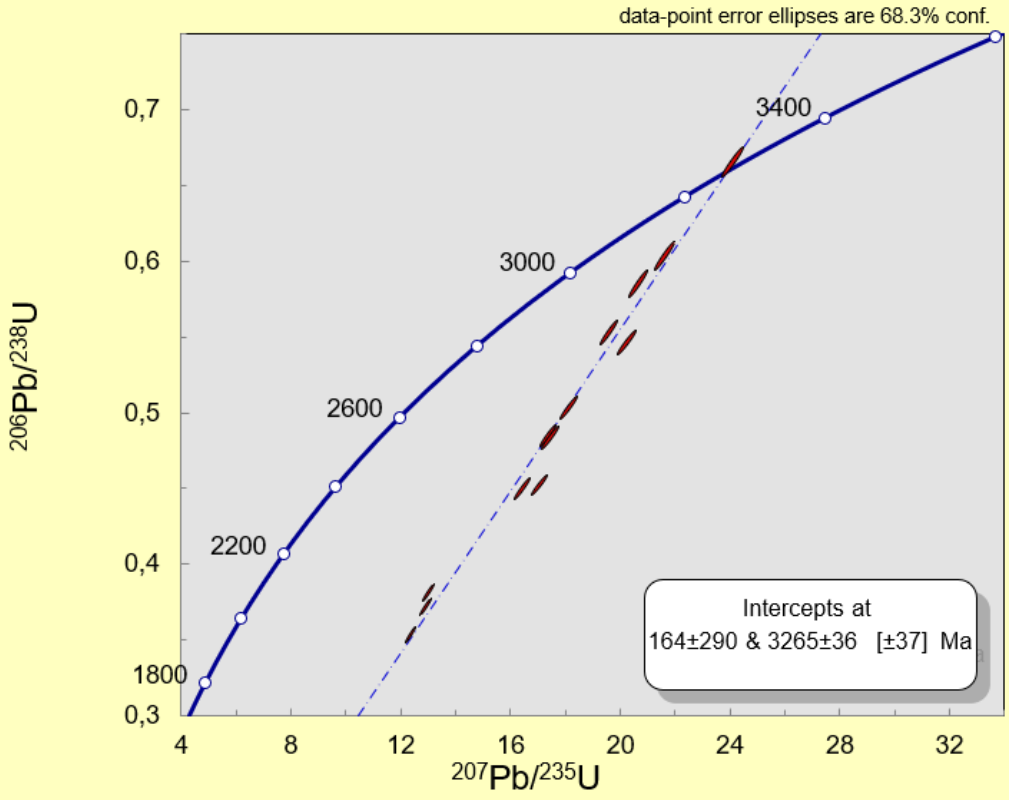
data-point error ellipses are 68.3% conf.
0,7
0,6
0,5
0,4
0,3
4
8
12
16
20
24
28
32
3400
3000
2600
2200
1800
Intercepts at
164±290 & 3265±36 [±37] Ma
206Pb/238U
207Pb/235U

C

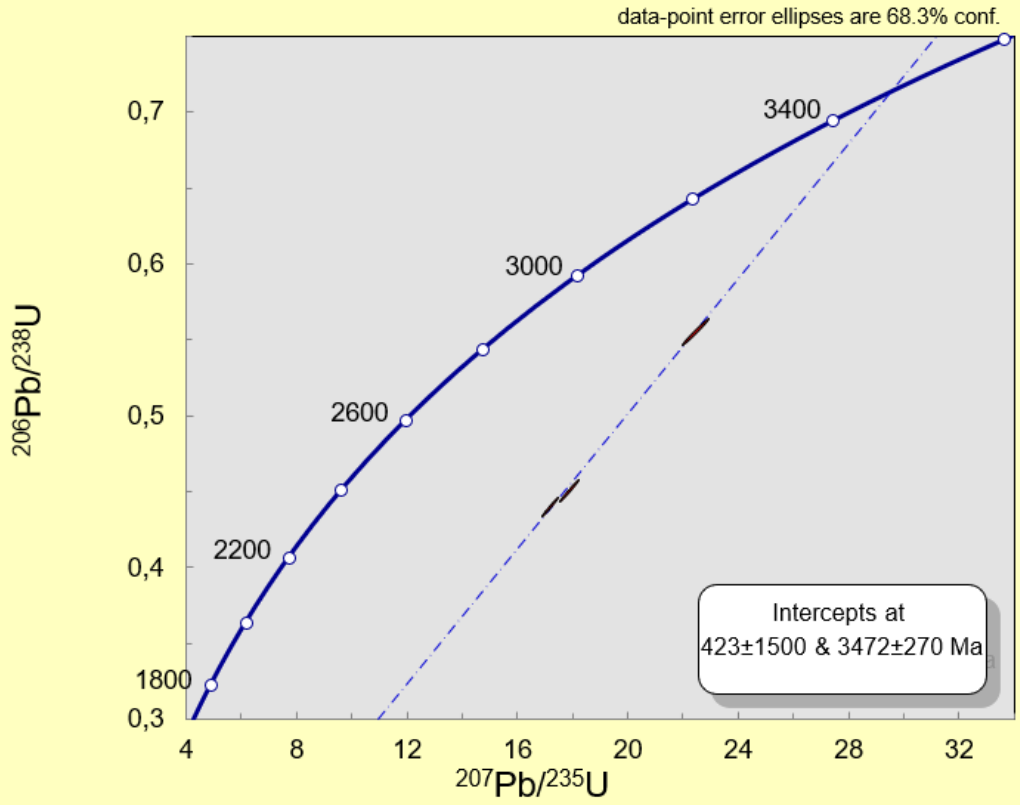
data-point error ellipses are 68.3% conf.
0,7
0,6
0,5
0,4
0,3
206Pb/238U
3400
3000
2600
2200
1800
Intercepts at
423±1500 & 3472±270 Ma
4
8
12
16
20
24
28
32
207Pb/235U

D

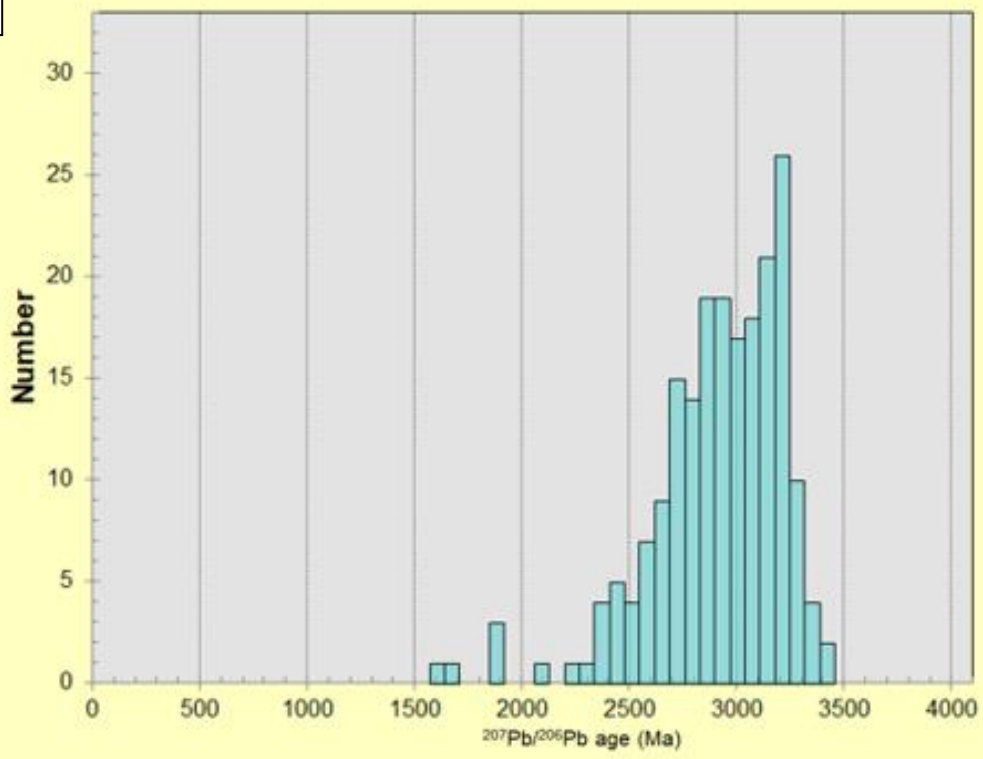
Number
30
25
20
15
10
5
0
0
500
1000
1500
2000
2500
3000
3500
4000
207Pb/206Pb age (Ma)

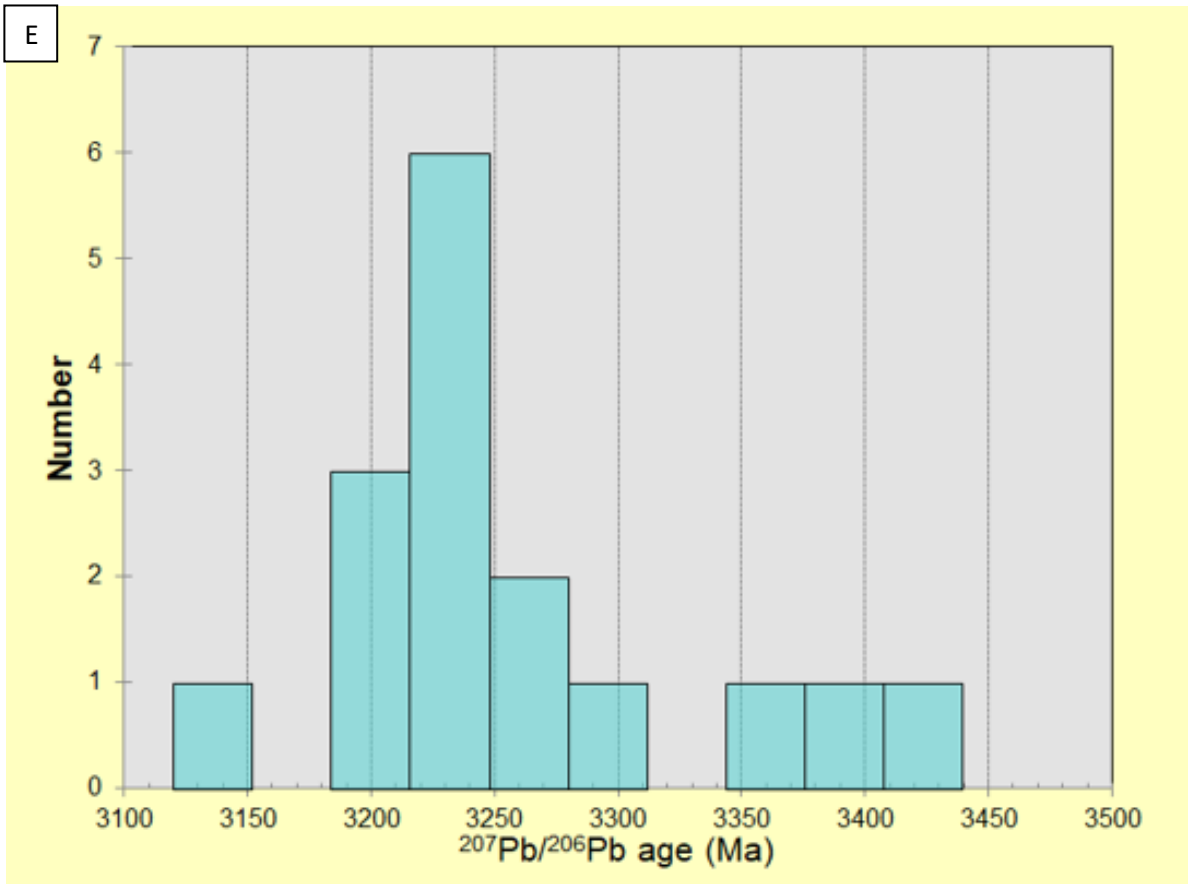

Figure 9: A) $^{206}Pb/^{238}U$-$^{207}Pb/^{235}U$ graph with a concordia based on the ZR91500 calibration standard and Pb-Pb ages of the analysed zircons (n=202). B) $^{206}Pb/^{238}U$-$^{207}Pb/^{235}U$ graph of the least discordant zircons (n=13) and the calibrated intercept with the concordia by linear regression. C) $^{206}Pb/^{238}U$-$^{207}Pb/^{235}U$ graph of the zircons right of the discordia in A and B (n=3) and the calibrated intercept with the concordia by linear regression. D) Histogram of the $^{207}Pb/^{206}Pb$ ages of the analysed zircons (n=202). E) Histogram of the $^{207}Pb/^{206}Pb$ ages of the least discordant zircons (n=16).

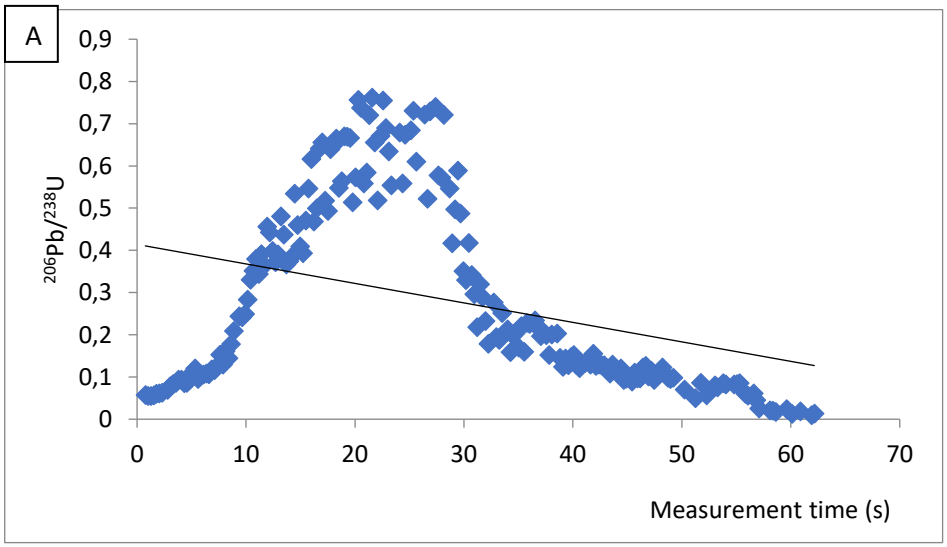

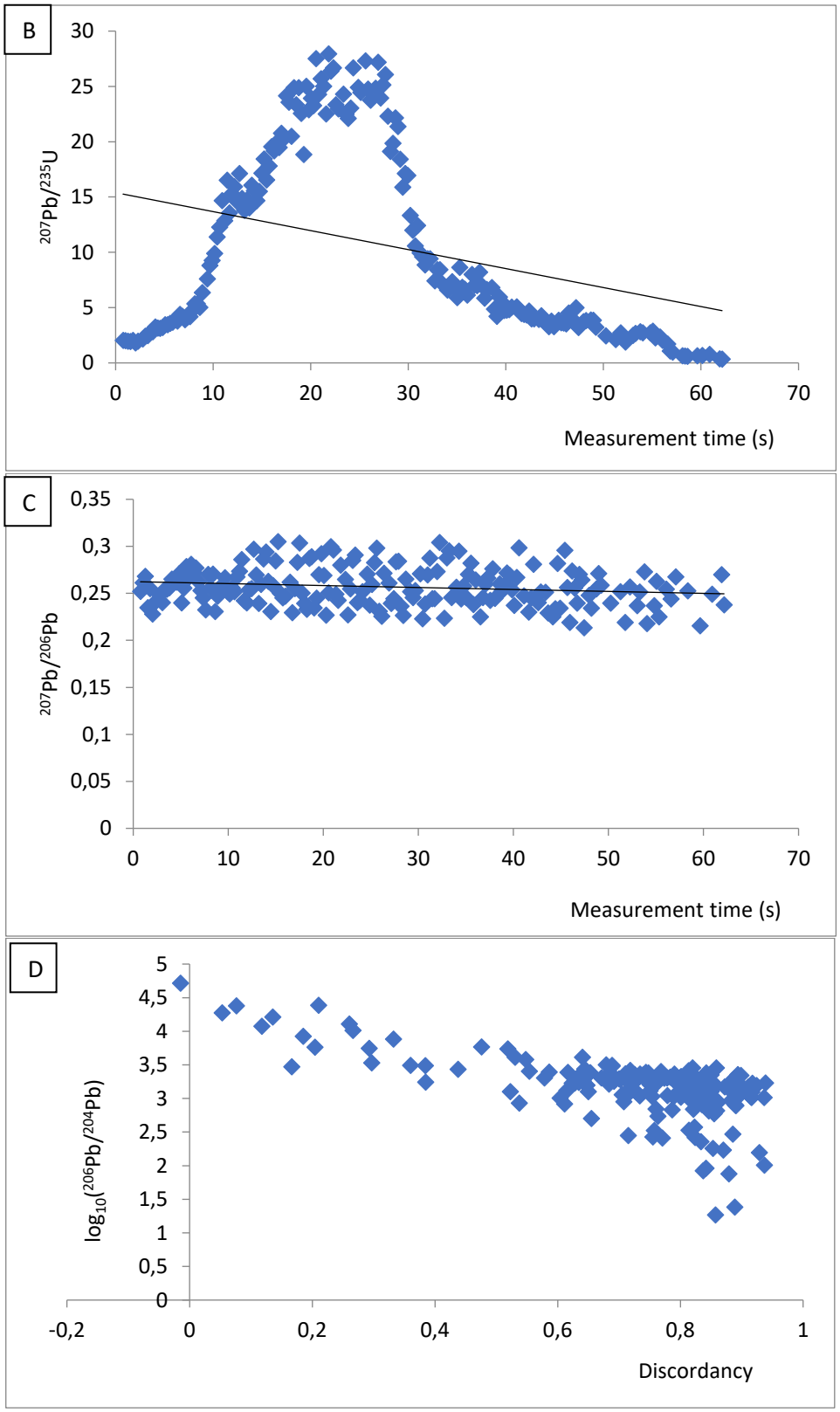

Figure 10: A) $^{206}Pb/^{238}U$ ratio against measurement time for zircon sample 18-BV-02a-07-core (4 data points per second). B) $^{205}Pb/^{235}U$ ratio against measurement time for zircon sample 18-BV-02a-07-core (4 data points per second). C) $^{207}Pb/^{206}Pb$ ratio against measurement time for zircon sample 18-BV-02a-07-core (4 data points per second). D) $Log_{10}(^{206}Pb/^{204}Pb)$ ratio against discordancy (1-(206Pb/238U age)/(207Pb/206Pb)). This graph describes the relation between the discordancy (amount of Pb loss) of the zircons and the relative amount of common Pb (^{204}Pb) in the analysed zircons. A value of 0 is no discordancy and 1 is maximum discordancy.

concentrations, because detrital minerals generally have high REEY concentrations. The exception is the grey clast of chert in Fig. 6G, which is heavily enriched in MREE and HREE. This had been caused by the analytical error of the analysis site on top of a zircon during ablation. The LREE should be more representative for the REE concentrations in the grey clast of chert, which is significantly below the concentration of the LREE in the bulk analysis. Based on the consistently higher concentration of REE in the bulk analyses and that the bulk analyses are intermediate in trace elements between the most weathered data and the fresh data in two of the samples, it can be confidently stated that all the bulk analyses of the cherts and the sediments have been affected by weathering.

Because the weathering has drastically changed the REE pattern and trace element concentrations in several samples, it is unwise to use the bulk analyses of the cherts and the sediments to determine the geological signatures in and the geological formation of the rocks. Also, the data is often quite irregular, making it difficult to convincingly recognise anomalies in some cases, if the supposed anomaly has a similar deviation range as the irregularities. However, this does not mean that the bulk analyses are unusable. Because weathering has affected the trace element concentrations in the cherts and the sediments and there is information about the most and least altered parts of the rocks, the increase in concentration per element due to weathering can be determined. In Fig. 6E and I the clearest effect is the 10-100 times higher enrichment of the LREE compared to the other REE. This is conforming with the LREE being slightly more mobile than the other REE during alteration processes. Most of the remaining elements were relatively equally enriched to 10-50 times higher concentrations. This indicates that the weathering may have not caused significant increase in trace element concentrations for any particular or couple of trace elements, even on mobile elements like Pb, Rb and Cs. Instead, the weathering increased the trace element concentrations relatively evenly by 10-50 times.

The remaining trace element data can also show the contamination of detritus in some of the rock samples. This is demonstrated in Fig. 6A and B of the sample 18-BV-13, in which the bulk analysis shows a relatively high enrichment in MREE, HREE, Hf and Zr compared to the microanalytically measured fresh and altered rock types. This trend is like the analysis of the grey clast in Fig. 6G and H, in which a zircon was measured due to an analytical error. This likely indicates that the bulk sample was contaminated by detrital minerals, which is supported by the enrichment of Cr in the sample and therefore likely chromite in the bulk sample. Ti which is commonly associated with the detrital mineral rutile (Osborne Hutton, 1950), is not enriched compared to microanalytical analyses. Moreover, in the other samples Ti is also as high or even lower in concentration compared to different rock types measured, which can be explained by the immobility of Ti during weathering.

6.2 Anomalies in the REEY of the barites, cherts and jaspilites

Several anomalies have been observed in the barites, cherts and jaspilites, namely negative Ce anomalies, positive Eu anomalies, negative Y/Ho anomalies and positive Y/Ho anomalies. These anomalies can be quite small, but because they occur in multiple samples, the actual validity of the presence of these anomalies becomes more genuine.

Some of the most pronounced anomalies are the negative Ce anomalies. The presence of a negative Ce anomaly in most of the bulk samples is confirmed in Fig. 11, although several samples have a positive La anomaly instead of a negative Ce anomaly. Especially the samples from Old Mine tend to have a positive La anomaly instead of a negative Ce anomaly. The positive La anomaly in the bulk samples is likely caused by the addition of La by the flux when creating the fusion beads. Most of the cherts and sediments have large negative Ce anomalies with only a few exceptions. Also, almost all the barites analysed after the barium removal with Solution ICP-MS show a negative Ce anomaly (Fig. 12). There are less apparent negative Ce anomalies present in Fig. 13 of the microanalytical data compared to Fig. 11 of the bulk analyses. The largest apparent negative Ce anomalies are present in the most weathered samples and in fresh grey veins that contain Ba concentrations at the level of the barites in the bulk analyses but have irregular data. Moreover, the negative Ce anomaly often increases with an

increase in weathering in the measured rock type. All the other data points plot around the field for a positive La anomaly.
The samples from puddingstone Hill clearly do not display a negative Ce anomaly except for the fresh grey veins. The Barite Valley data points more often show an apparent negative Ce anomaly, and this is often in the data points from weathered rock types. Using the microanalytical trace element data from samples 18-BV-16 and 18-BV-20 (Fig. 6E and I), it becomes clear that the negative Ce anomalies become larger in the more altered parts of the samples and are (almost) absent in the fresh parts of the samples. Also, the prominent negative Ce anomalies in the microanalytical data only occur in the most altered parts of the samples, while in the bulk data they are more common. This is a clear indication that the negative Ce anomaly in the cherts is caused by the recent weathering of samples e.g. oxidation and does not have any geological significance for the formation of the rocks. No microanalytical analyses have been done on the barites, but it can be assumed that any negative Ce anomalies in the barites have also been caused by the recent weathering.

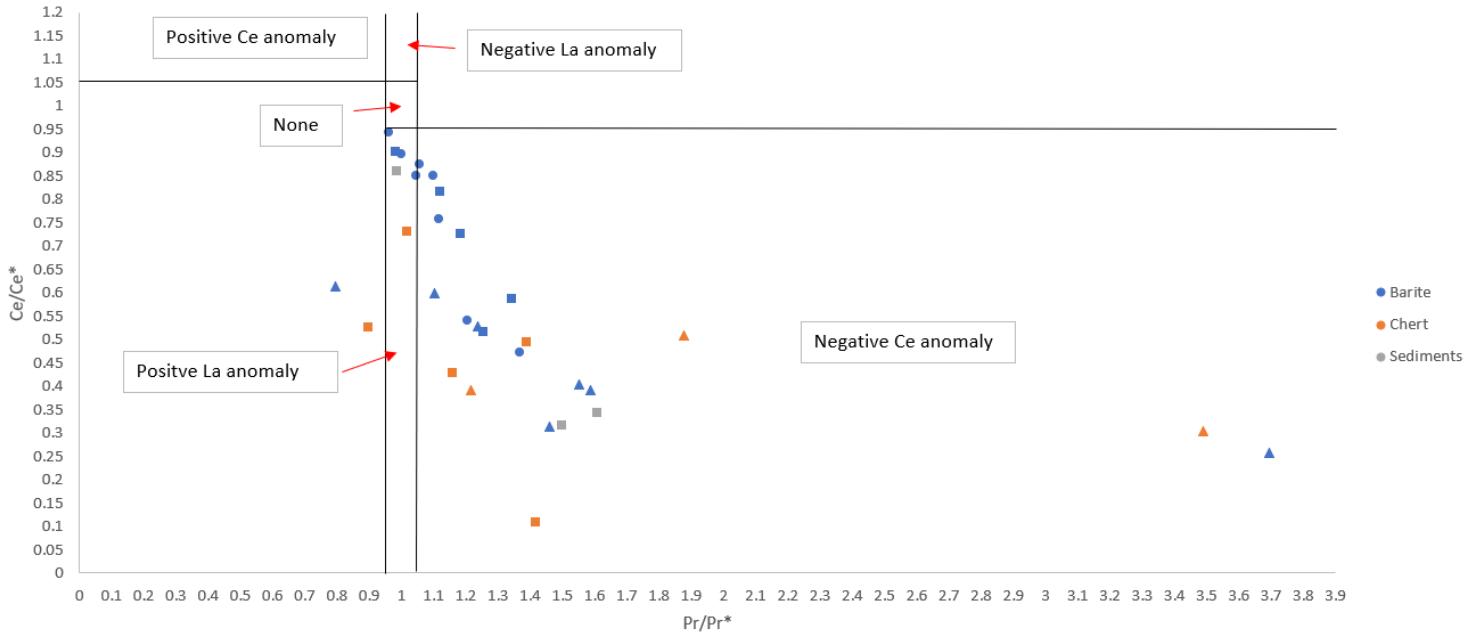

Figure 11: PAAS normalized Ce/Ce (Ce*=0.5La+0.5Pr) over Pr/Pr* (Pr*=0.5Ce+0.5Nd) graph for the bulk data. The graph describes whether there are positive or negative La or Ce anomalies in the data (based on* (Bau and Dulski, 1996). *Symbols annotate the location from which the samples came: Old Mine (spheres), Barite Valley (squares) and Puddingstone Hill (triangles).*

Many of the samples in the bulk analyses show a positive Eu anomaly, which increases with a decrease in overall REEY concentrations (Fig. 14) and the largest anomalies are present in Puddingstone Hill and the smallest in Old Mine. (Fig. 15). The barites seem to have a larger positive Eu anomaly compared to cherts and sediments with similar REE concentrations. In Fig. 16 it is shown that the positive Eu anomalies are smaller and less consistently present in the microanalytical data than in Fig. 15 of the bulk analysis. The relationship in the bulk analysis that the positive Eu anomaly seems to increase with a decreasing general concentration of REE is less conspicuous in this graph. For the Barite Valley data points, it is observable that there are two dominant groups with three outliers. One of the two groups show relatively higher general REE concentrations, but smaller or no positive Eu anomalies and the other group does show a positive Eu anomaly, but lower general REE concentrations. Two of the outliers of the Barite Valley data points show very high general REE concentrations compared to the

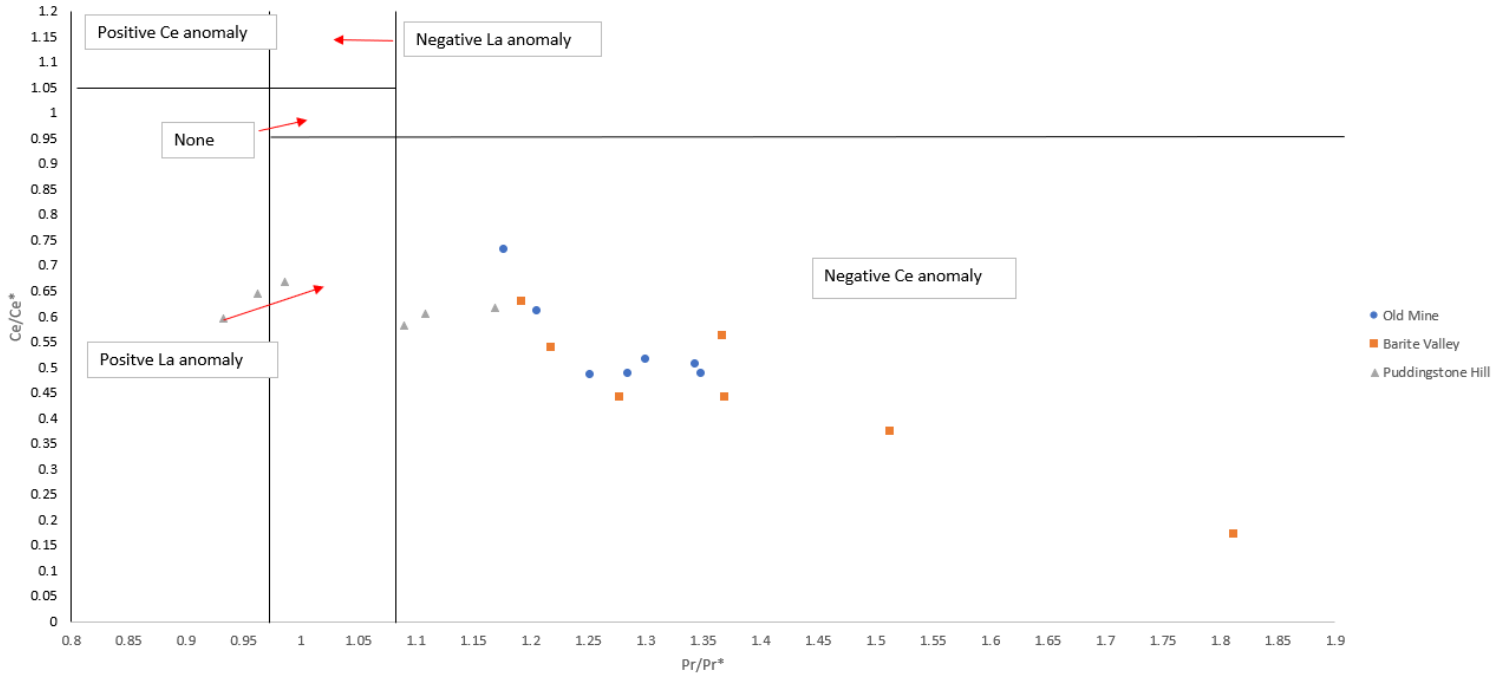

Figure: 12 PAAS normalized Ce/Ce (Ce*=0.5La+0.5Pr) over Pr/Pr* (Pr*=0.5Ce+0.5Nd) graph for the Solution ICP-MS data of the barites after the barium removal. The graph describes whether there are positive or negative La or Ce anomalies in the data (based on* (Bau and Dulski, 1996)*. Symbols annotate the location from which the samples came: Old Mine (spheres), Barite Valley (squares) and Puddingstone Hill (triangles).*

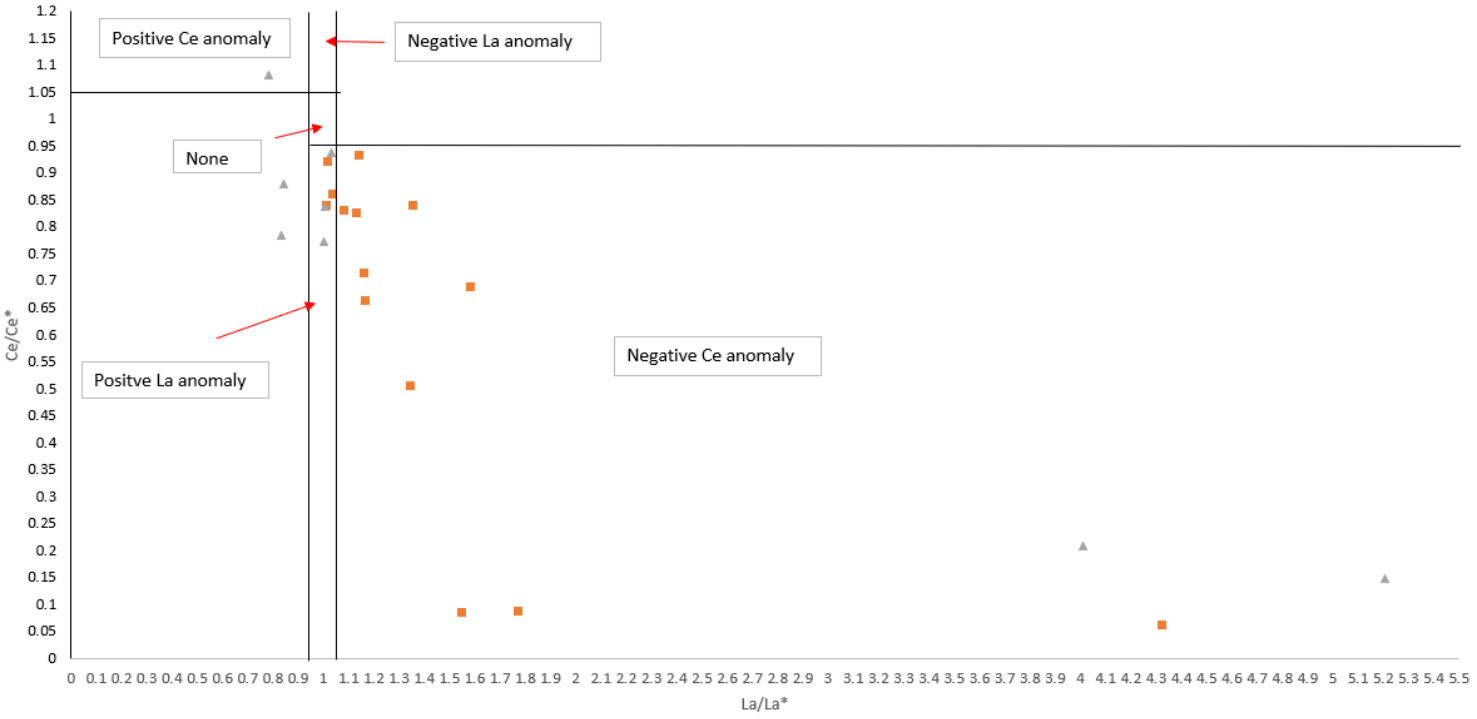

Figure 13: PAAS normalized Ce/Ce (Ce*=0.5La+0.5Pr) over Pr/Pr* (Pr*=0.5Ce+0.5Nd) graph for the epoxy block data. The graph describes whether there are positive or negative La or Ce anomalies in the data (based on* (Bau and Dulski, 1996)*. Symbols annotate the location from which the samples came: Barite Valley (squares) and Puddingstone Hill (triangles).*

other data points and are from the two most weathered samples. the other outlier shows no positive Eu anomaly and has relatively low REE concentrations compared to the other data points. This data points corresponds to the fresh grey chert measured in sample 18-BV-13. Three of the five data points

from Puddingstone Hill plot between the two dominant groups in Barite Valley with two of them having significantly lower REE concentrations than the other one. All the data points from Puddingstone Hill show a positive Eu anomaly, either small or large. The two data points with the by far largest positive Eu anomaly correspond to the fresh grey veins that contain Ba concentrations at the level of the barites in the bulk analyses.

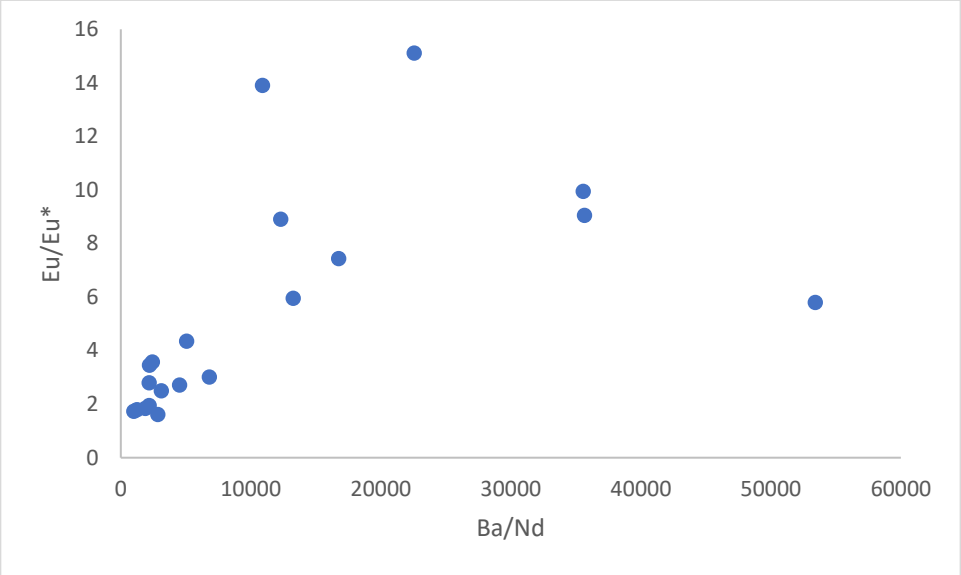

Figure 14: PAAS normalized Eu/Eu (Eu*=0.5Sm+0.5Gd) graph over Ba/Nd for the bulk analysis of the barites. Nd is used as a representation of the overall REE concentrations in a barite. The graph describes The graph describes the relationship between the size of the Eu anomaly and the overall REE concentrations of the barites.*

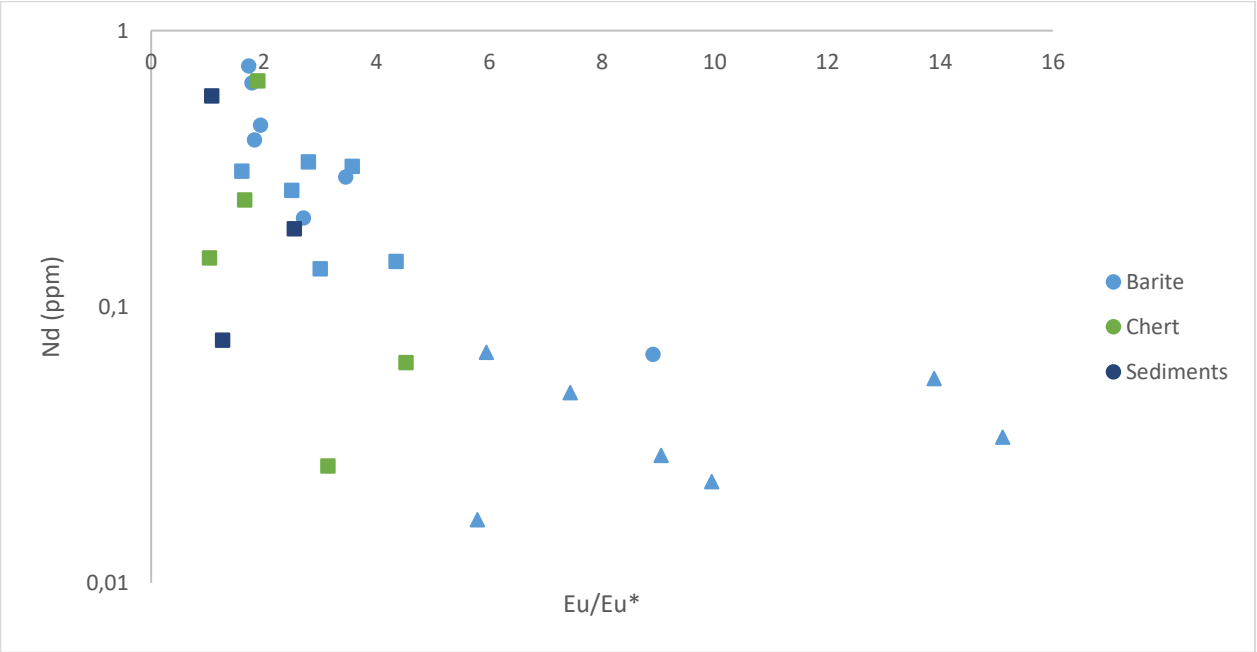

Figure 15: PAAS normalized Nd over Eu/Eu (Eu*=0.5Sm+0.5Gd) graph for the bulk data. Nd represents the overall REE concentration in the sample and the Eu/Eu* the Eu anomaly size. Symbols annotate the location from which the samples came: Old Mine (spheres), Barite Valley (squares) and Puddingstone Hill (triangles).*

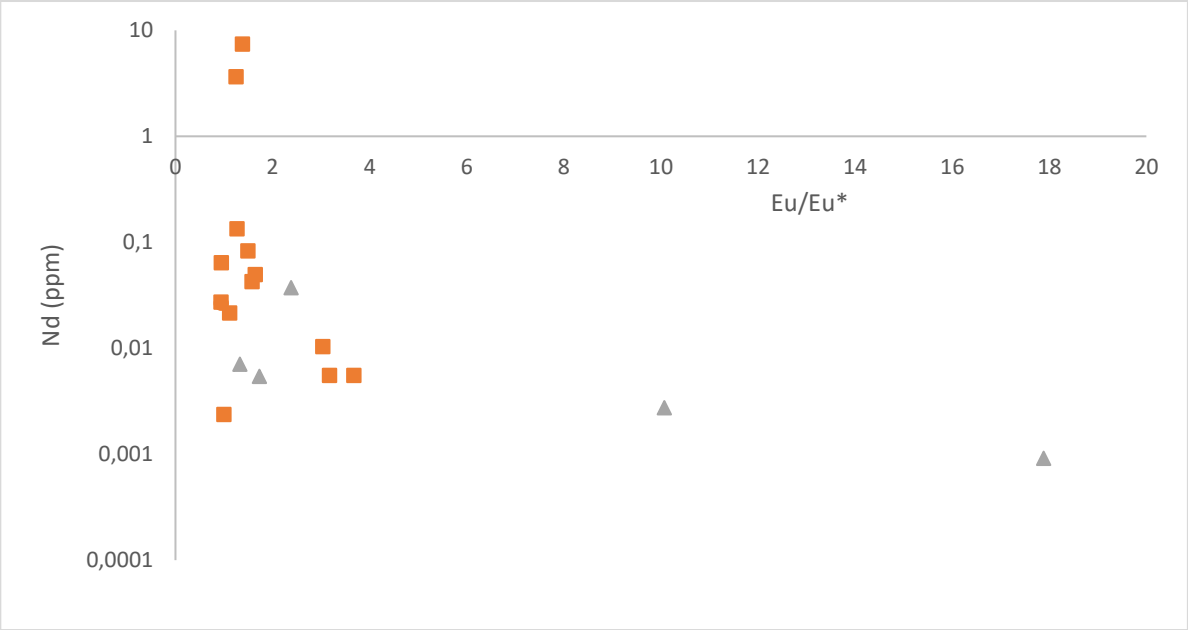

Figure 16: PAAS normalized Nd over Eu/Eu (Eu*=0.5Sm+0.5Gd) graph for the microanalytical epoxy block data. Nd represents the overall REE concentration in the sample and the Eu/Eu* the Eu anomaly size. Symbols annotate the location from which the samples came: Barite Valley (squares) and Puddingstone Hill (triangles).*

The positive Eu anomalies in the barites could be attributed to BaO interference during the analyses, especially because of the high Ba/REE ratios in the barites and the cherts. This was the reason for the barium removal analyses and the results of these analyses show a far less conspicuous presence of the positive Eu anomaly in the barites (Fig. 17). Moreover, the actual positive Eu anomalies were much smaller. The blanks in Fig. 18 show that there has been a preferential removal of the HREE and Y during the column separation, which explains the difference in REEY patterns between the bulk analyses and those after the barium removal. However, as is demonstrated in Fig. 19 the REEY in the measured standards BCR-2 and BHVO-2 agree well with the expected REEY in these standards. Therefore, despite the fractionation of the HREE and Y, the pattern of the remaining REE and remaining positive Eu anomalies should be genuine. The microanalytical analyses of the fresh pieces of chert showed no or small positive Eu anomalies and only the parts analysed around the fresh grey veins in sample 18-BV-26 and 18-BV-32, that demonstrated huge concentrations of Ba, showed large positive Eu anomalies (Fig. 16). The concentration of Ba in these veins was abnormally high, indicating that these were barite veins, so could also have experienced BaO interference. Because the positive Eu anomalies after barium removal and the fresh chert parts are small (<2.3), it is likely that all the large positive Eu anomalies in the samples (>3.0) are caused by BaO interference (Fig. 15 and 16). The remaining positive Eu anomalies (<2.3) in the cherts and barites should be geologically significant, if the barium removal was executed properly. The positive Eu anomaly in the jaspilite and possibly the black chert associated with the jaspilite is reliable, because in the jaspilite barely any Ba is present in the analysed sample (Fig. 6Q and R). Unfortunately, no Eu was measured during the analysis of the black chert, but the enrichment in Gd may be associated with a positive Eu anomaly, but this is not certain.

Anomalies of yttrium in the REEY patterns are quite common in the barites, cherts and jaspilites. Both negative and positive Y/Ho anomalies can be found in the samples, although the positive anomalies have Y/Ho ratios that go up to 35, while the negative anomalies do not become lower than ~0.65. Positive Y/Ho anomalies in the fresh pieces of the chert and jaspilite should be quite reliable, because alteration is unlikely to affect the Y/Ho significantly. Also, most of the anomalies have the right accuracy and precision, but if they are extremely small, they may only be analytical perturbations. This is especially likely when the REEY concentrations become low due to detection limits (REEY

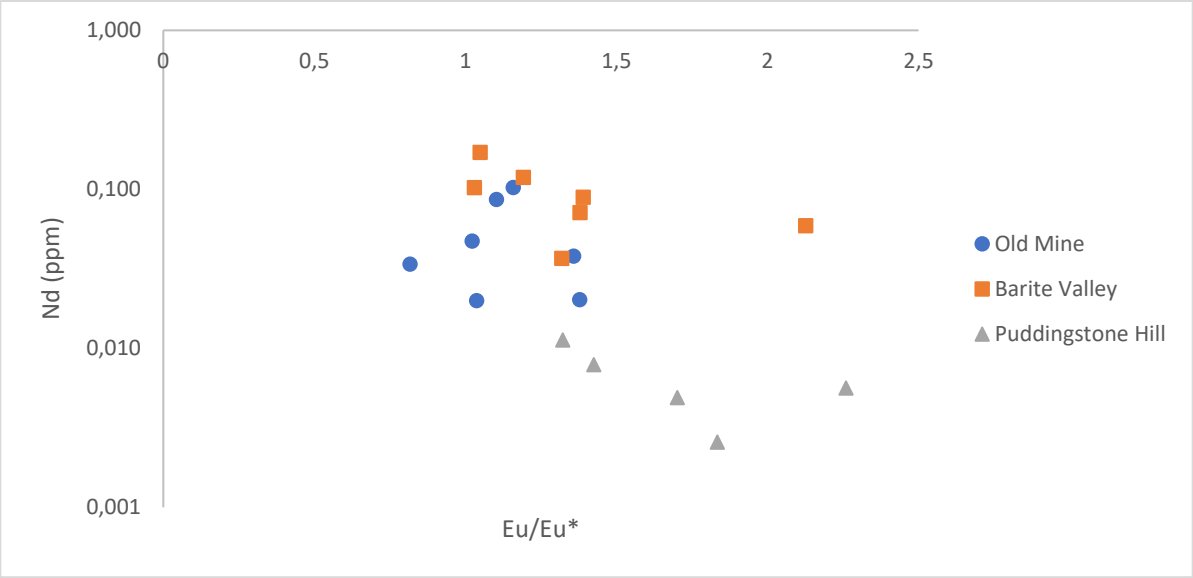

Figure 17: PAAS normalized Nd over Eu/Eu (Eu*=0.5Sm+0.5Gd) graph for the Solution ICP-MS data of the barites after the barium removal. Nd represents the overall REE concentration in the sample and the Eu/Eu* the Eu anomaly size. Symbols annotate the location from which the samples came: Old Mine (spheres), Barite Valley (squares) and Puddingstone Hill (triangles).*

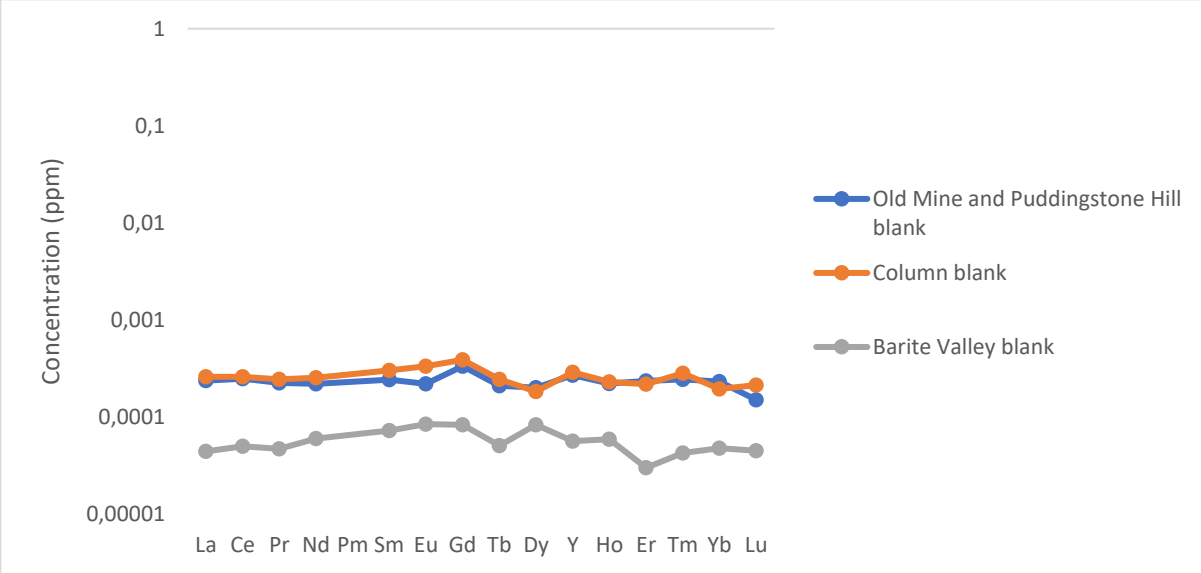

Figure 18: REEY measured on the Solution ICP-MS of blanks used in the column separation already added during sample preparation and added during the column separation. Sample preparation blanks of Old Mine and Puddingstone Hill and of Barite Valley are separate, because these samples were measured separately.

concentrations <0.05 ppm), so it cannot be confidently stated that these anomalies have geological significance. Still, Y/Ho anomalies are quite common even above 0.05 ppm, so it is likely that most of these anomalies are real. The large positive Y anomalies in the barite sample 18-BV-21, in the jaspilite sample 18-BV-08 and the in the barite veins of the samples 18-BV-26 and 18-BV-32, are real anomalies. In the bulk trace element analysis of the barites the samples show a positive Y anomaly, while these anomalies have become negative after the barium removal except for sample 18-BV-21. Because there seems to have been preferential removal of the HREE and Y (Fig. 18), it is unlikely that the negative Y anomalies in the barites are true geological signatures in the rocks and if there are any anomalies in Y, they should be positive instead.

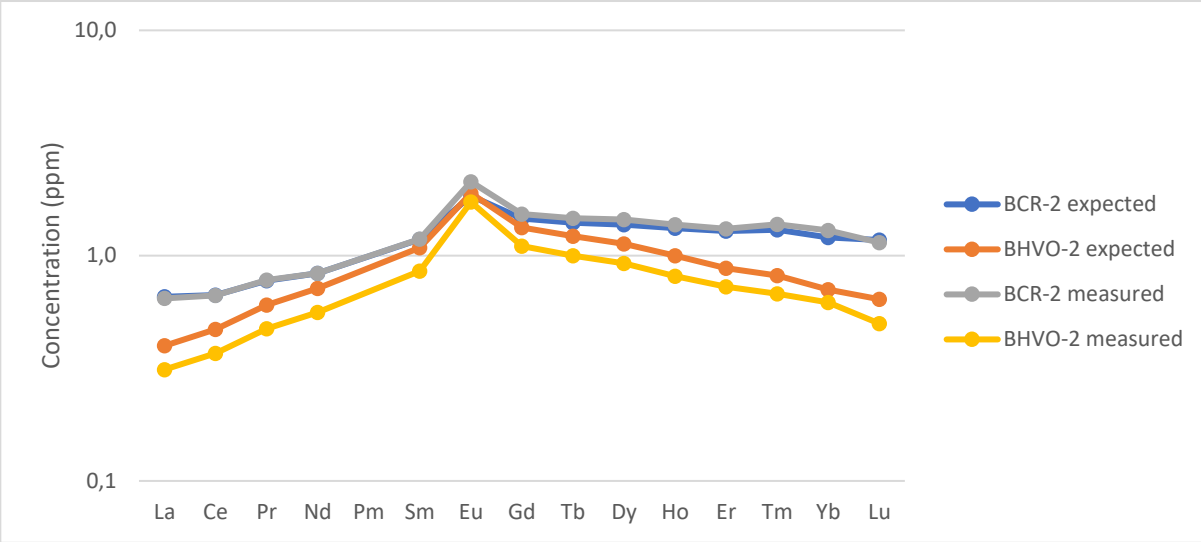

Figure 19: REEY of standards measured on the Solution ICP-MS after column separation with expected REEY and the measured REEY.

6.3 Geochemical signatures in the barites, cherts and jaspilites

The barites seem to have an overall flat REEY pattern, because the HREE and Y depletion after the barite removal seems have been caused by a preferential removal the HREE and Y by the analytical method (Fig. 18). Still, if this would have not taken place, the REEY patterns would have been flat after barium removal as well. Some of these barites seem to still have a small positive Eu anomaly after the barium removal, but they are not as prominent as in the bulk analyses of the barites.

Even if there may be a tiny positive Y anomaly in several of the barites, the REEY pattern of the barites cannot be directly linked to Archean sea water due to the flat profile for almost all the barites. Instead they show a continental relation, because they were normalised to PAAS and the flat pattern indicates a similar REEY pattern to PAAS. The only exception is sample 18-BV-21 in the bulk analysis, which is LREE depleted, has a positive Eu anomaly and a positive Y anomaly. The only problem is that after the barium removal positive Eu anomaly is not present anymore, which would suggest that the positive Eu anomaly in the bulk analysis would have been due to BaO interference. There was still solid residue left after dissolving the samples before the column separation. Because the sea water signature is most clear in the bulk sample, it might be that sea water signature was not due to barite itself, but due to the other rock components in the sample. In Fig. 2 there is no clear evidence of contamination except that the concentrations of the elements common in detrital minerals have concentrations as high as in the Old Mine site. However, these detrital minerals would not carry a sea water signature. The result of the analysis after barium removal might be a mixture between this sea water signal and the normally flat REEY patterns of the barites, either due to a mixing of rock components or by mixing of sea water and the Ba^{2+} carrying fluid when the barite formed. Although the barite itself cannot be confidently linked to sea water, some rock components inside sample 18-BV-21 seem to carry a sea water signature.

The presence of only some small positive Eu anomalies after barium removal indicates that high temperature hydrothermal fluids cannot have been responsible for the barite deposition. The rocks have only experienced up to 300-325 °C heating during peak metamorphic conditions (Hofmann, 2005; Kisters et al., 2010; Drabon et al., 2019), which indicates that no high temperature hydrothermal alteration of the rocks has taken place. However, this cannot exclude the deposition of the barites due to low temperature hydrothermal alteration. The positive Eu anomaly becomes larger with higher temperatures in hydrothermal deposits and the presence of a small positive Eu anomaly in some of the samples may be linked to hydrothermal processes. However, the temperature of the fluids was often too low to create a positive Eu anomaly in the barites. The flat profile of the barites and a small

positive Eu anomaly in several of the samples suggests a relation to low temperature continental hydrothermal processes of the barites. The difference in overall concentration of the REEY and elements common in detrital minerals such as Cr, U, Th, Hf, Zr and Ti between the different sample locations may suggest a difference fluid composition or source and detrital input between the Old Mine, Barite Valley and Puddingstone Hill sites. The fluid composition and the detrital input do not have to be linked with each other.

The REEY patterns of the cherts are more diverse than the REEY patterns of the barites. There are several rocks parts of the cherts that show a similar flat REEY pattern, but a LREE depleted variant and a REEY pattern with a positive slope are also present. Therefore, several of parts of the chert samples show a continental signature, but others show fractionation of the LREE or all the REEY compared to PAAS. The differences in the REEY patterns can occur in the same samples and in cherts and sediments inside and outside of the chert dikes, so these are not related to a difference in locations. Also, there does not seem to be significant difference between the overall REEY concentrations in the cherts from Barite Valley and Puddingstone Hill. Like with the barites, some of the rock parts of the cherts show a small positive Eu anomaly, which might be related to low temperature hydrothermal processes. The positive Eu anomalies always occur in the samples with a flat REEY pattern and can occur the LREE depleted ones and in the ones with a positive REEY slope.

Geochemically the cherts are closely related to the barite deposits. Not only do some of the parts of the cherts have similar REEY patterns to the barites, also the amount of barium in the cherts is unusually high. Moreover, most of the remaining trace elements show similar patterns between the barites and the cherts. This is especially true for the samples poor in the elements common in detrital minerals such as U, Th, Hf, Zr and Ti. Therefore, based on the geochemistry the formation of the chert dikes is likely to be related to the formation of the barites deposits.

Several of the chert and sediment samples contain distinct chert clasts with different REEY patterns, so the different REEY patterns can be explained by a different origin between chert clasts. Also, the chert dikes cut through sedimentary layers, so some of the geochemical signatures inside the sediments might have been inherited into the chert samples. In Fig. 20 the relationship between elements common in detrital minerals and the REEY is shown for the cherts and the barites. There is a strong correlation between the overall REEY concentration and elements commo in detrital minerals for the barites and a weaker correlation for the cherts (Fig. 20 A, B, C and D). However, the slope of the REE are not related to the elements common in detrital minerals (Fig. 20 E and F). This indicates that the chert dikes will likely have incorporated parts of the wall rock, which will have affected the overall REE concentrations in the cherts, but not the REEY patterns itself. For the barites it is near impossible that the wall rock was incorporated into the barites, because they formed on the sea floor or continental shelf as barite mounts by the interaction on Ba^{2+}-rich fluids and SO_4^{2-}rich fluids (Lowe et al., 2019) which should not have interacted with the wall rock.

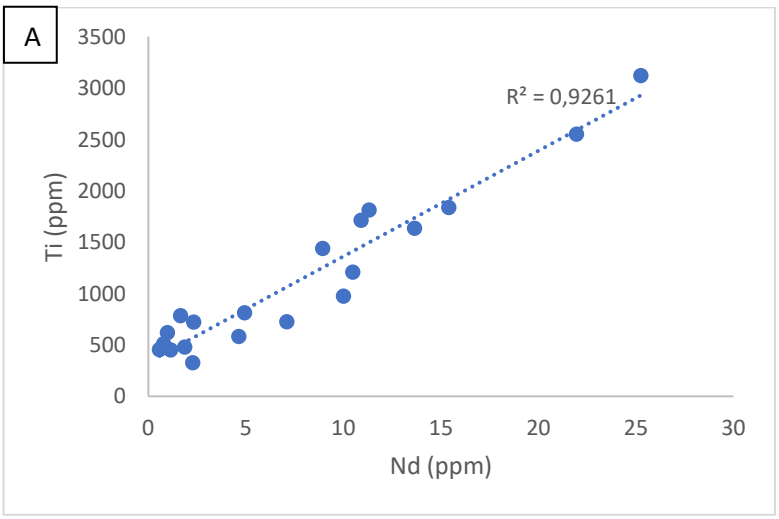

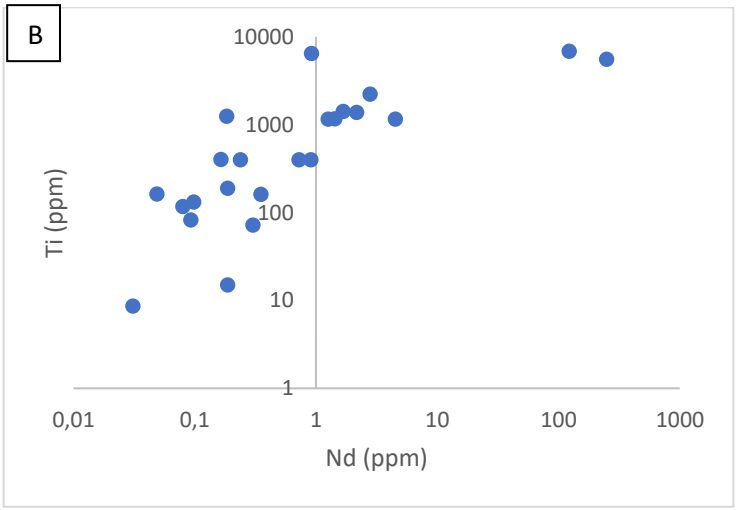

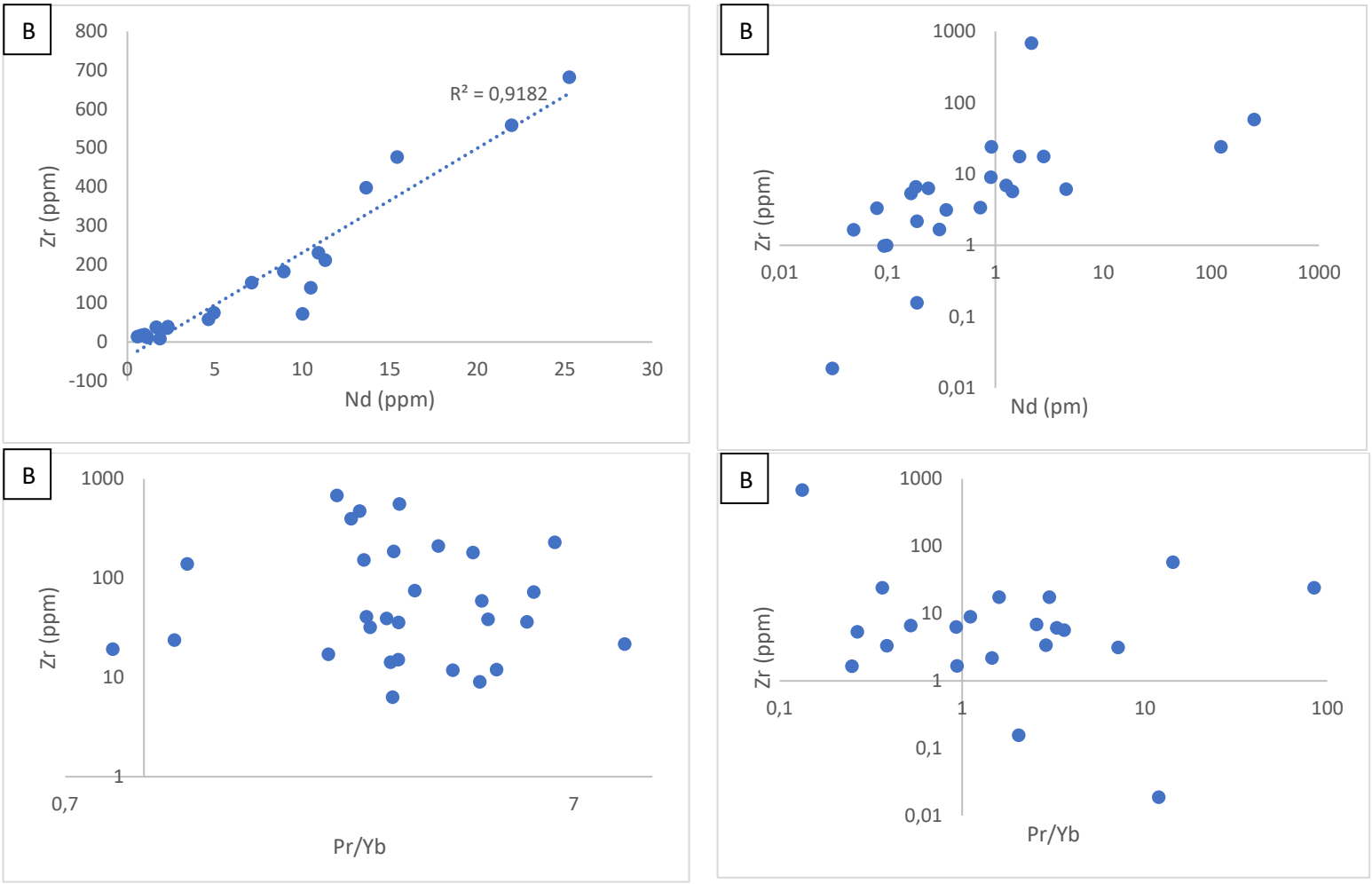

Figure 20: Graphs describing the relationship between elements common in detrital minerals and the REEY. Relationship between Ti and Nd in the A) Barites and B) cherts. Relationship between Zr and Nd in the C) Barites and D) cherts. Relationship between Zr and the REE slope in the E) Barites and F) cherts. Nd represents the overall REE concentration in the sample.

To confirm whether wall rock incorporation is a major contributor to the REEY patterns, in Fig. 21 several PAAS normalized REEY patterns are plotted from the BARB5 drill core which sampled sediments from Barite Valley close to the stratigraphic level of the barite deposits of Barite Valley in the Mapepe Formation (Drabon et al., 2019). Both the flat REEY patterns with a small positive Eu anomaly and the LREE depleted patterns are present among the sediments from the BARB5 drill core. This makes it possible that these REEY patterns have only been derived from wall rock incorporation. Only the REEY pattern with the positive slope is not present, which makes it possible that these REEY patterns are related to a different REEY source. Still, the REEY of the Barites also show a flat patterns with a sometimes a small positive Eu anomaly, but the barites cannot have incorporated wall rock and these patterns should be derived from a different source. This means that the same flat REEY pattern in the cherts does not need to be related to wall rock incorporation, but it is definitely a possibility. Therefore, the REEY patterns of the cherts should be interpreted with caution.

Although the geological signatures in the barites and the cherts are more ambiguous, the geological signature inside the jaspilites is very clear. The jaspilite in sample 18-BV-08 is LREE depleted, has a positive Eu anomaly and a positive Y/Ho anomaly. Although the REEY profile is not as steep as common sea water profiles, these three attributes inside the jaspilites are characteristic for sea water. The black chert associated with the jaspilite does not show the same REEY pattern, but many elements were below detection limit, which makes extracting the geological signatures from the REEY data inside the black chert difficult. A surprising result of the trace elements analyses on sample 18-BV-08 is the

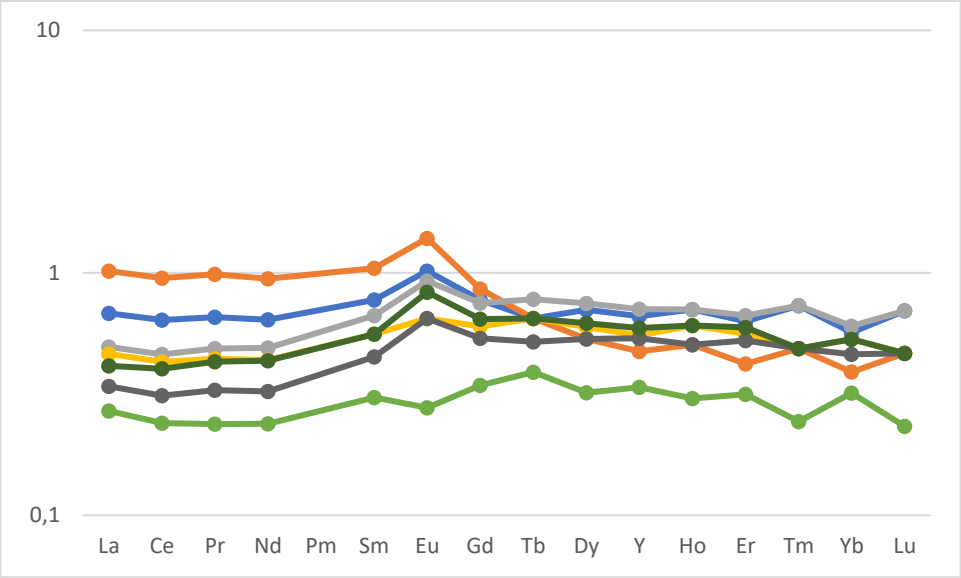

Figure 21: PAAS normalized REEY patterns of sediments in the BARB5 drill core from the Mapepe Formation (after Drabon et al. 2019)

completely different trace element concentrations of the remaining elements inside the jaspilite and the associated black chert compared to the barites, cherts and sediments. Also, the jaspilite and the associated black chert are the only rocks in the area without high barium concentrations. This is convincing evidence that the jaspilite and the associated black chert are not chemically related to the barites, cherts and sediments. This means that these rocks cannot have formed by the same process and at the same time as the barite deposits and the chert dikes based on the geochemical data. The jaspilite clast in sample 18-BV-32 from Puddingstone Hill does not show the same geochemical signatures as the fresh jaspilite in sample 18-BV-08 from Barite Valley. Actually, the REEY pattern and trace element concentrations of the remaining elements are like those in the cherts. This indicates that the process forming the chert dikes can incorporate clasts of the jaspilite layer, but the process forming the cherts dikes will completely reset the geochemical signatures inside the jaspilite clast assuming the jaspilite clast is similar to the jaspilite in Barite Valley. If this is not true, then the difference in geochemistry can also be caused by a difference in site for the jaspilite clast.

6.4 The geochemical signatures compared with literature

There is a lack of trace element data in the literature for barite due to the fact that it is challenging to digest using standard acid attack procedures that are typically used for silicate rocks (Oostingh 2011). This study produced the first complete trace element data sets for the Mapepe Formation barites from the Old Mine, Barite Valley and Puddingstone Hill locations. These are also the first data produced for any Precambrian barite. This means that no direct comparisons were possible with existing literature data for the barites, so a different approach was necessary. Modern-day barite deposits are associated with hydrothermal systems (Lowe et al., 2019), so it is common to associate barite deposits in the rock record with hydrothermal processes, but due to the vastly different environment in the Archean this should not be immediately assumed. Busigny et al. (2017) found that their samples had experienced pervasive hydrothermal alteration and that their research on iron and sulphur isotopes is consistent with global anoxic conditions in the sedimentary deposits 3.2 Ga. This would imply that the SO_4^{2-} inside barite deposits should originate from the atmospheric photolysis of S-bearing gases released by large subaerial volcanic events and possibly by the magmatic disproportionation of SO_2 by hydrothermal processes.

Sedimentological work done by Lowe et al. (2019) on the Mapepe Formation at Barite Valley opposes the view that the barite deposits are related to hydrothermal processes. They argue that the sedimentary deposits associated with the barites show evidence that these rocks have been deposited in intertidal, fan delta and shallow water to subaerial settings. Moreover, they argue that cool barium-baring, shallow subsurface fluids reached the surface via impact induced fractures and faults at cool springs and reacted with photolytically produced SO_4^{2-} from meteoric fluids e.g. rainwater. This would immediately trigger barite deposition. Busigny et al. (2017) and Lowe et al. (2019) both argue that the SO_4^{2-} had been provided by photolytic processes, but they do not agree about the fluids that supplied the barium for the barite deposits with Busigny et al. (2017) favouring hydrothermal processes and Lowe et al. (2019) favouring neptunian processes by e.g. meteorite impacts.

The barite data produced in this thesis is consistent with input of fluids from a deep reservoir that was in chemical equilibrium with average continental sediments based on the flat PAAS normalized REEY graphs. Although most low temperature hydrothermal aquifer-like fluids have a positive REEY slope and are particularly LREE depleted (Johannesson et al., 1999; Johannesson et al., 2005; Linhua et al., 2011), it is not impossible to get flat PAAS normalized REEY patterns with a small positive Eu anomaly from these fluids (Linhua et al., 2011). The role of sea water was minor for all the barites except sample 18-BV-21, which has likely been mixed with rock material containing a sea water signature as previously explained. This agrees well with the idea that the SO_4^{2-} was likely provided by photolytically produced SO_4^{2-} from meteoric fluids. However, the presence of a positive Eu anomaly in the Puddingstone Hill samples and several of the Barite Valley samples does not agree with cool continental fluids to have provided the barium as stated by Lowe et al. (2019) and supports the idea that relatively higher-temperature hydrothermal processes have a played an important role in the barite deposition. A positive Eu anomaly cannot be produced by cool continental fluids and in the absence of a sea water signature in the barites, should be linked to hydrothermal processes. The difference in size and presence or absence of the positive Eu anomalies may suggest a difference in temperature of the feeder fluids of the barites, but they should all still be hydrothermal fluids.

More research has been done on Archean cherts, jaspilites and Banded Iron Formations (BIF's), so the chert and jaspilite data can more easily be compared to the literature. The sea water signature often found in Archean cherts and BIF's (Hofmann, 2005; Allwood et al., 2010; Planavsky et al., 2010; Lantink et al., 2018) is not present in the cherts associated with the barites based on the data. The cherts and sediments with flat PAAS normalized REEY patterns and a small positive Eu anomaly are like carbonaceous cherts at the base of the Fig Tree Group investigated by Hofmann (2005). He attributed the flat profiles to detrital input and associated it with carbonaceous sediments that were silicified by low temperature hydrothermal fluids on the seafloor. The link to low temperature hydrothermal fluids fits well the data obtained in this research. However, the flat profiles can also suggest a continental signature, so it is not certain whether the hydrothermal fluids were derived from the continent or the sea floor. Alternatively, the pattern can also be affected by wall rock incorporation as was explained in the previous section (Fig. 21).

The cherts that are LREE depleted, but besides that still have a relatively flat REEY pattern are like black laminated cherts found by Allwood et al. (2010). Some of these cherts formed by the intrusion of hydrothermal silica along the laminae in the black chert replacing the carbonate originally present in the rocks. The other black cherts had been formed by dissolution and recrystallization of Si and O of the original rocks during diagenesis. The cherts associated with the barites in this research are thought to be primary deposits (Lowe et al., 2019), so it is unlikely that that they formed by diagenetic processes. Alternatively, wall rock incorporation may have also affected the REEY pattern as was explained in the previous section (Fig. 21). Therefore, the LREE depleted cherts support the theory that the cherts are related to hydrothermal processes, unless wall rock incorporation was the dominant source of the REEY.

The cherts and sediments demonstrating a positive REEY slope, but having no notable anomalies are not like many of the investigated cherts and BIF's in the literature. The cherts and BIF's with a positive slope do appear in literature, but they contain a positive Eu and Y anomaly, indicating that they are related to sea water (Hofmann, 2005; Allwood et al., 2010; Planavsky et al., 2010; Lantink et al., 2018).

The lack of anomalies in the sediments and cherts in the data of this research indicates that they cannot be related to sea water. Because the analyses on the cherts are microanalytical analyses, it is unlikely that the observed REEY patterns are a mixture between for example sea water and something else. At least they have experienced some type of PAAS normalized REEY fractionation, so it is unlikely that this occurred by fluvial processes. REEY fractionation is often limited in a fluvial environment and is restricted to fractionation of the LREE. REEY fractionation in fluvial systems of the MREE and the HREE depends on the source of the sediments (Xu and Han, 2009; Bayon et al., 2015). PAAS normalized fractionation of the MREE and HREE is limited or absent if the sources of the sediments are igneous (and metamorphic) bodies (Xu and Han, 2009; Bayon et al., 2015) which is the major constitution of the Onverwacht Group that was the sedimentary source of the Mapepe Formation. Therefore, it is more likely that the REEY pattern with a positive slope is associated hydrothermal processes, which can fractionate the MREE and the HREE. In fact, the pattern is similar to low temperature (hydrothermal) aquifer-like fluids (Johannesson et al., 1999; Johannesson et al., 2005; Linhua et al., 2011) and especially because this pattern is among others found in the sandstone layer from which the chert dikes originate, does this pattern support a low temperature hydrothermal origin of the chert dikes.

The jaspilite can be easily linked to BIF's and cherts deposited on the sea floor, because the jaspilite has a similar PAAS normalized REEY pattern and positive Eu and Y anomalies as these BIF's and cherts (Hofmann, 2005; Allwood et al., 2010; Planavsky et al., 2010; Lantink et al., 2018). There is quite some variation in the slope of the REEY in these rock types and the jaspilite investigated in this research has quite a shallow positive slope, especially between the MREE and the HREE. The slope is much more shallow than the slope of jaspilitic BIF's previously found in the Fig Tree Group (Hofmann, 2005). They are more similar to cherts and BIF's that are formed by deposition from a mixture of marine and hydrothermal fluids (Allwood et al., 2010; Lantink et al., 2018). However, they are also similar to certain Archean BIF's investigated by Planavsky et al. (2010) and they argue that the decrease in slope between Archean and Proterozoic BIF's is because of less fractionation of the REEY before the Great Oxygenation event due to a lack of oxygen in the oceans. Both are possible, but the presence of BIF's with steeper slopes in the Fig Tree Group (Hofmann, 2005), makes it more likely that the shallowing of the slope is caused by mixing of the marine and hydrothermal fluids.

Lowe et al. (2019) argue that the jasperlites below the barites in the Mapepe Formation have been produced due to the oxidation of sedimentary siderite and pyrite by photolytically produced oxidants like H_2O_2 and O_2 in meteoric fluids. However, based on the geochemical data acquired in this research that is unlikely. The jasperlites show a sea water signature, possible mixed with a hydrothermal fluid which is more consistent with deposition on the seafloor. Also, based on the geochemistry of the remaining trace elements, there is no relationship between the barites (and the cherts) and the jaspilites. There is an unconformity between the barites and the jaspilite bands (Lowe et al., 2019) and it is impossible to know how much time has passed between the deposition of the barites and the jaspilites. Therefore, it is likely pure coincidence that the jaspilite bands are immediately underneath the barites. Normally, the absence of oxygen in the Archean oceans, would rule out jaspilites deposition by the oxidation of iron by free oxygen. However, Satkoski et al. (2015) argue that free oxygen existed during the deposition of the lower part of the Mapepe Formation and that caused the deposition of the 3.23 Ga Manzimnyama BIF. Alternatively, microorganisms could have been responsible for the oxidation of the Archean jaspilites as argued by Planavsky et al. (2010).

Around the North Pole granitoid dome of the Pilbara craton in Western Australia Archean barite deposits can also be found. These deposits are widespread over a much larger area and at larger scale than the barite deposits in the Mapepe Formation, but they are also seemingly fed by chert dikes (Nijman et al., 1998). In the case of the North Pole deposits, these were deposited on the sea floor and seem to have been formed by hydrothermal processes (Nijman et al., 1998). This is like what the data of this research suggests for the barites, but the scale of the Australian deposits is much larger. The cherts, sediments and jaspilites show similar REEY patterns to Archean cherts and carbonates from the Pilbara Craton, although these come from the Strelley Pool Formation and not the North Pole Dome (Allwood et al., 2010). There are some similarities between the deposits from the Pilbara Craton and

from the Barberton Greenstone Belt, which may suggest that the barites in the Mapepe Formation may have also formed by hydrothermal processes. Perhaps a difference in environment is the main cause for the difference in size of the two barite deposits. The rocks and fluids should have been heated by contact metamorphism to much higher temperatures in the Pilbara craton due to the proximity of the North Pole granitoid dome. In the Fig Tree Group and the Mapepe Formation there is no evidence for any contemporary large and proximate magmatic bodies (Drabon et al., 2019; Lowe et al., 2019). Therefore, the temperature of the fluids and the rocks must have been much lower than in the Pilbara Craton. Also, it has already been demonstrated that there are differences between the size of the positive Eu anomaly between the different sites. This likely indicates that there has also been a difference in temperature and perhaps composition for fluids responsible for the Old Mine, Barite Valley and Puddingstone Hill deposits.

6.5 Detrital zircons ages

The zircons seem to have experienced quite some weathering based on the disintegrating rims and the amount of fractures inside zircons. Still, the zircons seem to be still quite primary and have only experienced limited rounding. This indicates that the zircons have not experienced much reworking before being incorporated inside the barites. The weathering is likely more recent, otherwise the outer appearance of the zircons should not have been as euhedral as it is. The zircons cannot have been transported over large distances and the source should have been in relative proximity of the barite deposits. The amount of fractures and the disintegrated rims make Pb loss quite likely. The cores of the zircons could be more primary, but due to the small size of the zircons, the amount of weathering and inclusions, it was often impossible to sample only the core of the zircon.

The age of ~3.25(-3.3) Ga for the zircons is reliably supported by a discordia line with few irregularities, one concordant point and the zircon population histograms (Fig. 9). Also, the $^{207}Pb/^{206}Pb$ ages show a linear trend and can be regarded as reliable measurements with a low error. Even the plateau ages of the $^{206}Pb/^{238}U$ and $^{207}Pb/^{235}U$ ratios are ~3.25 Ga, while there is no linear relationship in the continuous measurement of the ratios on the same zircons for a certain time interval. There is a large group of zircons that plot to the left of the discordia line where the calibrated ages of the zircons are younger (Fig. 9A). These are probably irregularities in the measurements. Even if these measurements were significant and a strong linear regression could be executed on these zircons, the intersection with the concordia would be around ~2.6 Ga. The Mapepe Formation in the Fig Tree Group from which the rocks and the zircons in the rock come is 3.28–3.23 Ga and it is highly unlikely to find zircons in the rocks much younger than the rocks itself with no evidence of later high grade metamorphism (Hofmann, 2005; Kisters et al., 2010; Drabon et al., 2019). If they would be present, that should indicate that the cause is weathering, Pb loss or contamination of the rocks and not that there are truly ~2.6 Ga zircons in the rocks of the Mapepe Formation. More interesting are the four zircons that plot to the right of the discordia line, because they suggest an older age of ~3.45 Ga (Fig. 9C and E). Four zircon measurements among the over 200 zircons measurements makes it impossible to fit a good linear regression for the data points, but it is entirely possible and not unlikely that older zircons have survived. One of these zircons seems to have a different core (Fig. 10B), which may suggest a ~3.3 Ga rim that grew around an older ~3.45 Ga core. However, the other three zircons do not show a distinctively different core, so that may just be a coincidence.

The fact that the zircons plot on a discordia line intersecting roughly with the origin and not on the concordia line, suggests a significant loss of Pb due to recent processes. This was likely due to weathering and possibly combined with extensive lightning strikes and forest fires in the field area. This is also displayed in the individual measurement with low $^{206}Pb/^{238}U$ and $^{207}Pb/^{235}U$ ratios at the start and the end of the analyses. Moreover, the more Pb lost or discordant the zircon measurements are, the higher the amount of common Pb in the zircons (Fig. 10D). Therefore, the Pb loss in the zircons due to recent processes are accompanied by a relative increase of common Pb compared to the

radioactive Pb isotopes. Most of the zircons, (but not all), that are the least discordant, have a low amount of (large) fractures inside the zircons according to the CL and back scatter images. This is logical, because fracturing of the zircon crystal would result in Pb loss. However, Most of these zircons are not fractureless, which explains the presence of only one concordant zircon inside a data set of 202 data points.

The ages obtained for the zircons inside the barite deposits of the Mapepe Formation fit well with previous work done on detrital zircon ages in the Barberton Greenstone Belt (Drabon et al., 2017). Zircon age populations inside the Fig Tree Group have been found to peak at 3.274 ± 0.006 Ga or 3.242 ± 0.010 Ga depending on the stratigraphy or at ~3.45 Ga. There are some smaller additional population peaks, but the previous ones are the two major populations (Drabon et al., 2017). This fits well with the ~3.25 Ga and ~3.45 Ga ages calibrated from the zircons inside the barites. Especially the one concordant zircon with an age of 3.243 ± 0.016 Ga fits well with the 3.242 ± 0.010 Ga of one of the major population peaks. No surprising or smaller populations have been found in the zircons inside the barites, but this may also have been obscured due to the highly discordant nature of the zircons. The age of ~3.45 Ga can be linked to TTG terrains of a similar age inside the Onverwacht Group and the zircons with an age of ~3.30-3.28 Ga fit with felsic tuffs deposited inside the Mendon Formation of the Onverwacht Group (Drabon et al., 2017). However, most of the zircons and the concordant zircon have an age of ~3.25 Ga which indicates that many of the zircons originated from tuffs deposited inside the Mapepe Formation itself. Especially considering that the age coincides with the age of the spherule bed S3 inside the Mapepe Formation that has an age of ~3.24 Ga. However, due to the discordant nature of the data it will be difficult to state with certainty that no zircons from the Mendon Formation are present inside the barites.

6.6 Formation of the barite deposits, chert dikes and jaspilites

Based on the data presented in this research it is likely that the barites were deposited in a shallow, low-temperature hydrothermal system. The individual pieces of evidence are not enough to support a hydrothermal origin of the barites, but the multitude of data acquired for the barites and the geochemically closely related cherts, suggest a hydrothermal origin for the barites. However, these hydrothermal deposits did not form under the conventional modern-day circumstances. In the first place, they seem to have formed with a strong input of continental fluid on or close to the continent as is demonstrated by flat PAAS normalized REEY patterns for the barites and several of the cherts. There is clearly no relationship to sea water for the barites and cherts, which also supports the continental setting of the deposits. Secondly, the hydrothermal fluids were relatively low temperature and may have had a different temperature and possibly composition for the Old Mine, Barite Valley and Puddingstone Hill sites as is evident for the only small and sometimes absence of a positive Eu anomaly. Lastly, instead of the ocean providing the SO_4^{2-} for the barite deposition, the SO_4^{2-} was likely produced by photolytic processes and added to the hydrothermal system by meteoric fluids. The Ba^{2+} was provided by relatively low temperature hydrothermal fluids through the chert dikes.

The detrital minerals in the barites had been sourced from TTG terrains inside the Onverwacht Group and tuffs from the Mendon Formation and possibly the Fig Tree Group itself. The uplift of the granitoid bodies must have caused weathering and transport of the detrital minerals to lower areas where the barites were deposited in a hydrothermal system. The absence of a high concentration of elements common in detrital minerals in the cherts, indicates that the detritus was only transported to the upper lying barite deposits. However, this was dependant on site, because the Old Mine had a high supply of detritus, barite Valley an intermediate supply of detritus and Puddingstone Hill no or almost no supply of detritus. The input of detritus severely affected the REEY patterns of the, raising the REEY concentrations in sites with a large input of detritus. The fact that most of the zircons were not severely rounded and still had a distinct crystallographic shape and that most had a similar age to the Fig Tree Group/Mapepe Formation, indicates that there was proximate source for the zircons. This agrees well

with the sampling of the zircons from the nearby TTG bodies in the Onverwacht Group and tuffs from the Mendon Formation and the Fig Tree Group.
It is clear from the jaspilite data that the jaspilite bands immediately underneath the barites were deposited on the sea floor, most likely from a mixture of marine and hydrothermal fluids. These jaspilite bands have no clear chemical relationship to the barites and the cherts. They were deposited from a different fluid source, the barites from the continent and the jaspilite bands from the sea. The unconformity between the jaspilite bands and the barite deposits and different depositional setting can indicate that there was quite some time between the deposition of the two rock types. The oxidation of the jaspilites can either have been done by microorganisms or by free oxygen in the lower part of the Mapepe Formation.
This is the first research presenting relatively complete and significant trace element data on barites. In the future more trace element data can be acquired using similar methods as used in this research. Still, improvements must be made for the column separation of the barites to circumvent the preferential fractionation of the HREE and Y on the columns. The zircon data was highly discordant but seemed to become less discordant if there were less fractures in the zircons. It is possible that if the fractureless parts of the zircon would be analysed, that more concordant zircon data points can be acquired. This cannot be done with the LA-ICP-MS however, because the crater size is too large to analyse the fractureless parts of the zircons. In the future alternative dating instruments should be used on these zircons that are more precise and do not require as large an area on the zircon for analysis. Future trace element research on different locations with Archean barite deposits including the Pilbara Craton should be executed, to see whether the data from this research agrees with barite deposits of a similar age or if there are differences in geochemistry. Furthermore, a more detailed analysis should be made for the role of wall rock incorporation and mixing of different fluid sources for the formation of the REEY patterns in the cherts and barites and the formation of the barite deposits.

7 Conclusion

In the Mapepe Formation of the Fig Tree Group of the Barberton Greenstone Belt barite deposits can be found that are seemingly fed by cherts dikes. These Barite deposits are rich in detrital minerals like zircon and immediately underneath the barite deposits, jaspilite bands are present. This research presents the first relatively complete and significant trace element data for barites. The PAAS normalized REEY patterns of the barites in the Mapepe Formation are relatively flat and show small positive Eu anomalies in all the Puddingstone Hill samples and some of the Barite Valley samples. However, there was no positive Eu anomaly in the other Barite Valley samples and the Old mine samples. The associated cherts show three different patterns. A flat PAAS normalized REEY pattern with a small positive Eu anomaly like the patterns observed in the barites, a LREE depleted REEY pattern and a REEY pattern with a positive slope. No evidence for a sea water signature has been found in the barites and the cherts, which are geochemically quite similar for the remaining trace elements. Wall rock incorporation may have been a significant source of the REEY in the cherts. The observed REEY patterns suggest that the barites were deposited by relatively low temperature continental hydrothermal fluids close to or on the continent. The hydrothermal fluids supplied the Ba^{2+} via the chert dikes to the surface, where these ions reacted with photolytically produced SO_4^{2-} supplied by meteoric waters. The difference in positive Eu anomaly size indicates that the temperature and possibly composition was different of the hydrothermal fluids responsible for the barite deposition in Old Mine, Barite Valley and Puddingstone Hill.
The U-Pb dating of the zircons inside the barites gave a highly discordant result, intersecting the concordant line at ~3.25-(3.3) Ga and the origin. There was only one concordant zircon with an age of 3.243 ± 0.016 Ga. Four other zircons deviated from the general trend and would have crossed the discordant line at ~3.45 Ga. The discordant nature of the data set indicates that the zircons have experienced severe Pb loss due to recent weathering. The dated ages fit well with other detrital zircons from the Fig Tree Group and indicate that they were sourced from TTG bodies from the Onverwacht

Group and from tuffs in the Mendon Formation and the Fig Tree Group itself. Uplift in the area caused weathering of these formations and the transport of the zircons to the lower lying hydrothermal systems where the barites were deposited. The highest supply of detrital minerals was to the Old Mine side, an intermediate supply to the Barite Valley site and the lowest or no supply to the Puddingstone Hill site. Elevation of the REEY in the barites was caused by a high supply of detritus to the barite deposits.
The jaspilite bands immediately underneath the barites were deposited on the seas floor and likely precipitated from a mixture of marine and hydrothermal fluids. They have no geochemical relation to the barites and the cherts and were deposited in different environment. Oxidation of the jaspilites could have been caused by either microorganisms or free ozygen in the lower Mapepe Formation. Future research can be done on barites using similar methods used in this research, but improvements must be made on the column separation of the barites. Using more precise instruments and those that need less area on the samples for analysis, less discordant U-Pb data may be acquired from the zircons in the Mapepe Formation.

8 Acknowledgements

Firstly, I want to thank Paul Mason (UU) for his supervision during my master thesis. I am thankful to Leonard Bik (UU) for helping me with the sample preparation. I want to thank Helen de Waard (UU) for helping me with the LA-ICP-MS measurements and Tilly van Bouten (UU) for assisting me with the EMPA. I am thankful to Jan van Tongeren (UU) for helping me with the powder grinding of the samples. I want to thank Boris Versteegh (VU) for helping me with the sample preparation for the column separation and Kirsten van Zuilen (VU) for assisting me in the column separation and doing the measurements on the Solution ICP-MS. I want to thank Roel van Elsas (VU) for assisting with the Zircon separation and Bouke Lacet (VU) for making the zircon mounts. Finally I am thankful to Leo Kriegsman (Naturalis) for determining the U-Pb ages in the zircons based on the LA-ICP-MS measurements.

9 References

Allwood A. C., Kamber B. S., Walter M. R., Burch I. W. and Kanik I. (2010) Trace elements record depositional history of an Early Archean stromatolitic carbonate platform. *Chem. Geol.* **270**, 146-163.

Anhaeusser C. R. (1976) The geology of the sheba hills area of the barberton mountain land, south africa, with particular reference to the eureka syncline. *South African Journal of Geology* **79, no., 2** 253-280.

Bakker B. (2019) Geochemical study of Archean bedded barites from the Barberton Greenstone belt: implications for a possible chert dyke hydrothermal feeder system. Guided research report.

Bau M. and Dulski P. (1996) Distribution of yttrium and rare-earth elements in the Penge and Kuruman iron-formations, Transvaal Supergroup, South Africa. *Precambrian Res.* **79**, 37–55.

Bayon G., Toucanne S., Skonieczny C., André L., Bermell S., Cheron S., Dennielou B., Etoubleau J., Freslon N., Gauchery T., Germain Y., Jorry S. J., Ménot G., Monin L., Ponzevera E., Rouget M.-L., Tachikawa K. and Barrat J. A. (2015) Rare earth elements and neodymium isotopes in world river sediments revisited. *Geochim. Cosmochim. Acta* **170**, 17–38.

Busigny V., Marin-Carbonne J., Muller E., Cartigny P., Rollion-Bard C., Assayag N. and Philippot P. (2017) Iron and sulfur isotope constraints on redox conditions associated with the 3.2 Ga barite deposits of the Mapepe Formation (Barberton Greenstone Belt, South Africa). *Geochim. Cosmochim. Acta*. **210**, 247-266.

Drabon N., Galić A., Mason P. R. D. and Lowe D. R. (2019) Provenance and tectonic implications of the 3.28–3.23 Ga Fig Tree Group, central Barberton greenstone belt, South Africa. *Precambrian Res.* **325**, 1-19.

Drabon N., Lowe D. R., Byerly G. R. and Harrington J. A. (2017) Detrital zircon geochronology of sandstones of the 3.6-3.2 Ga Barberton greenstone belt: No evidence for older continental crust. *Geology*. **45 no., 9**, 803-806.

Eggins S. M., Woodhead J. D., Kinsley L. P. J., Mortimer G. E., Sylvester P., McCulloch M. T., Hergt J. M. and Handler M. R. (1997) A simple method for the precise determination of ≥ 40 trace elements in geological samples by ICPMS using enriched isotope internal standardisation. *Chem. Geol.* **134**, 311-326.

Heinrichs T. K. and Reimer T. (1977) A sedimentary barite deposit from the Archean Fig Tree Group of the Barberton Mountain Land (South Africa). *Econ. Geol.* **72**, 1426–1441.

Hofmann A. (2005) The geochemistry of sedimentary rocks from the Fig Tree Group, Barberton greenstone belt: Implications for tectonic, hydrothermal and surface processes during mid-Archaean times. *Precambrian Res.* **143**, 23-49.

Hofmann A., Bolhar R., Dirks P. and Jelsma H. (2003) The Geochemistry of Archean shales derived from a mafic volcanic sequence, Belingwe greenstone belt, Zimbabwe: Provenance, source area unroofing and submarine versus subaerial weathering. *Geochim. Cosmochim. Acta*. **67 no., 3**, 421-440.

Johannesson K. H., Alfredo Ramos-Leal J., Durazo J., Cortés A., Alfredo Ramos Leal J. and Ramírez A. G. (2005) Geochemistry of rare earth elements in groundwaters from a rhyolite aquifer, central méxico chapter 8 geochemistry of rare earth elements in groundwaters from a rhyolite aquifer, central méxico. *Springer, Dordrecht*, 187-222.

Johannesson K. H., Farnham I. M., Guo C. and Stetzenbach K. J. (1999) Rare earth element fractionation and concentration variations along a groundwater flow path within a shallow, basin-fill aquifer, southern Nevada, USA. *Geochim. Cosmochim. Acta*. **63 no., 18**, 2697–2708.

Kisters A. F. M., Belcher R. W., Poujol M. and Dziggel A. (2010) Continental growth and convergence-related arc plutonism in the Mesoarchaean: Evidence from the Barberton granitoid-greenstone terrain, South Africa. *Precambrian Res.* **178**, 15-26.

Kooijman E., Berndt J. and Mezger K. (2012) U-Pb dating of zircon by laser ablation ICP-MS: Recent improvements and new insights. *Eur. J. Mineral.* **24**, 5–21.

Lantink M. L., Oonk P. B. H., Floor G. H., Tsikos H. and Mason P. R. D. (2018) Fe isotopes of a 2.4 Ga hematite-rich IF constrain marine redox conditions around the GOE. *Precambrian Res.* **305**, 218-235.

Linhua S., Herong G. and Song C. (2011) Rare earth element geochemistry of groundwaters from coal bearing aquifer in Renlou coal mine, northern Anhui Province, China. *J. RARE EARTHS* **29**, 185.

Lowe D. R., Drabon N. and Byerly G. R. (2019) Crustal fracturing, unconformities, and barite deposition, 3.26–3.23 Ga, Barberton Greenstone Belt, South Africa. *Precambrian Res.* **327**, 34-46.

Nijman W., de Bruijne K. (C.)H. and Valkering M. E. (1998) Growth fault control of Early Archaean cherts, barite mounds and chert-barite veins, North Pole Dome, Eastern Pilbara, Western Australia. *Precambrian Res.* **88**, 25–52.

Oostingh, K. (2011), Analysis of Rare Earth Element concentrations in barite (BaSO4). Msc thesis.

Osborne Hutton C. (1950) Studies of heavy detrital minerals. *Bull. Geol. Soc. Am.* **61**, 635–710.

Planavsky N., Bekker A., Rouxel O. J., Kamber B., Hofmann A., Knudsen A. and Lyons T. W. (2010) Rare Earth Element and yttrium compositions of Archean and Paleoproterozoic Fe formations revisited: New perspectives on the significance and mechanisms of deposition. *Geochim. Cosmochim. Acta*. **74**, 6387–6405.

Satkoski A. M., Beukes N. J., Li W., Beard B. L. and Johnson C. M. (2015) A redox-stratified ocean 3.2 billion years ago. *Earth Planet. Sci. Lett.* **430**, 43-53.

Sokolova O. B. and Povarov V. G. (2013) Equilibrium composition and initial rate of the reversible solid phase reaction in the system Na2CO3-BaSO4-Na 2SO4-BaCO3. *Russ. J. Gen. Chem.* **83**, 409–414.

Xu Z. and Han G. (2009) Rare earth elements (REE) of dissolved and suspended loads in the Xijiang River, South China. *Appl. Geochemistry* **24**, 1803–1816.